NATIONAL POLAR-ORBITING OPERATIONAL ENVIRONMENTAL SATELLITE SYSTEM (NPOESS)

VIIRS NET HEAT FLUX (NHF) ENVIRONMENTAL DATA RECORD (EDR) AND OCEAN SURFACE ALBEDO INTERMEDIATE PRODUCT (IP) ATBD (D43762 Rev A)

CDRL No. A032

Northrop Grumman Space & Mission Systems Corporation
One Space Park
Redondo Beach, California 90278

Copyright © 2004-2009
Northrop Grumman Corporation and Raytheon Company
Unpublished Work
ALL RIGHTS RESERVED

Portions of this work are the copyrighted work of Northrop Grumman and Raytheon. However, other entities may own copyrights in this work.

This documentation/technical data was developed pursuant to Contract Number F04701-02-C-0502 with the US Government. The US Government's rights in and to this copyrighted data are as specified in DFAR 252.227-7013, which was made part of the above contract.

This document has been identified per the NPOESS Common Data Format Control Book – External Volume 5 Metadata, D34862-05, Appendix B as a document to be provided to the NOAA Comprehensive Large Array-data Stewardship System (CLASS) via the delivery of NPOESS Document Release Packages to CLASS.

The information provided herein does not contain technical data as defined in the International Traffic in Arms Regulations (ITAR) 22 CFR 120.10.

This document has been approved by the Unites States Government for public release in accordance with NOAA NPOESS Integrated Program Office.

Distribution: Statement A: Approved for public release; distribution is unlimited.

D43762, A. PDMO Released: 2009-09-28 (VERIFY REVISION STATUS)
PDMO

NATIONAL POLAR-ORBITING OPERATIONAL ENVIRONMENTAL SATELLITE SYSTEM (NPOESS)

VIIRS NET HEAT FLUX (NHF) ENVIRONMENTAL DATA RECORD (EDR) AND OCEAN SURFACE ALBEDO INTERMEDIATE PRODUCT (IP) ATBD (D43762 Rev A)

PREPARED BY:

Merit Shoucri Date

ELECTRONIC APPROVAL SIGNATURES:

Roy Tsugawa Date
Algorithm & Data Processing IPT Lead &
Algorithm Change Control Board Chairperson

Gerald J. Mulvey Date
Senior Systems Engineer

D43762, A. PDMO Released: 2009-09-28 (VERIFY REVISION STATUS)
PDMO

Revision/Change Record

Document Number D43762

Revision	Document Date	Revision/Change Description	Pages Affected
---	01/26/2007	Initial PCIM Release to bring document into Matrix Accountability. Reference original document number: P1187-TR-I-003 delivered in 2006 This document replaces Raytheon document Y2407 which is obsolete.)\	All
A	02/18/2009	Updated according to CSR RFA SY_151 with NGST SPCR ALG00001365 under ECR A-202. Approved for Public Release per Contracts Letter 090903-01.	All

D43762, A. PDMO Released: 2009-09-28 (VERIFY REVISION STATUS)
PDMO

Table of Contents

Table of Contents i
List of Tables iii
List of Figures iv
1. Introduction 1
1.1. Overview 1
1.2. Scope 2
1.3. Applicable Documents 2
1.4. Relationship to Prior Work 3
2. Net Heat Flux Requirements 3
2.1. EDR NHF Requirements 3
2.2. Instrument Characteristics 6
3. Algorithm Description 6
3.1. Theoretical Description 6
3.1.1. Radiative Fluxes 7
3.1.2. Turbulent Fluxes 8
3.1.3. Ocean Surface Albedo (Input Into Radiative Flux Algorithm) 10
3.2. Mathematical Description 12
3.2.1. Radiative Transfer Equations 12
3.2.2. Turbulent Flux Equations 13
3.2.3. Ocean Surface Albedo Mathematical Description 16
3.3. Algorithm Processing Flow 18
3.3.1. Input Data 21
3.3.2. Output Data 22
3.3.3. Internal Data, Look-up Tables, Etc. 24
4. Algorithm Testing and Performance 25
4.1. Overall Approach 25
4.2. Real Data Scene-Based Testing with Proxy Sensor/Product Input Data 25
4.3. Performance Testing with Simulated Data 39
4.3.1. Methodology 39
4.3.2. Specification Errors 41
4.3.3. Sensitivity Analysis 51
4.3.4. Ocean Surface Albedo Errors 58
4.3.5. Model Error 59
4.4. EDR Performance Summary for Net Heat Flux 62
4.4.1. EDR Performance Summary for Ocean Surface Albedo 63
5. Practical Considerations 63

D43762, A. PDMO Released: 2009-09-28 (VERIFY REVISION STATUS)
PDMO

5.1. Numerical Computing Considerations 63
5.2. Programming Considerations 64
5.3. Computer Hardware/Software Requirements 64
5.4. Quality Control and Diagnostics 65
5.5. Exception and Error Handling 65
5.6. Special Database Requirements 65
5.7. Archival Requirements 65
6. List of References 66
7. Appendix A – Sea Surface Emissivity in the Long-Wave Infrared 68
8. Appendix B – Construction of Net Heat Flux Horizontal Cells (HCs) 73

D43762, A. PDMO Released: 2009-09-28 (VERIFY REVISION STATUS)
PDMO

List of Tables

Table 1-1 – Relevant Specifications....2
Table 2-1 – Preamble text and interpretation for the Net Heat EDR....4
Table 2-3 – EDR Attribute Table for Net Heat Flux....6
Table 3-1 – Aerodynamic Roughness as a Function of Ice Age....16
Table 3-3 – Summary of Atmospheric/Surface State Variables Relevant to NHF EDR Their Sources and Applicability to Ice or Water Conditions....21
Table 3-5 – Net Heat Flux Output Product Summary....22
Table 3-7 – Ocean Surface Albedo Output Product Summary....24
Table 3-9 – Summary of Key Internal Data (Static) Used by the Algorithm....24
Table 4-1 – Test Scenes for Real Data Testing....25
Table 4-3 – Data Sources of Key Input Variables for Real data Testing....25
Table 4-5 – Input parameter error specification for synthetic scenes....40
Table 4-7 – Uncertainties in net heat flux and its components for each error scenario....42
Table 4-9: Uncertainty in heat flux components due to error in input parameters....51
Table 4-11 – Heat Flux Model Component Errors....60
Table 4-13 – Daytime net heat flux errors due input specification errors with and without model error....60
Table 4-15 – Accuracy and Precision: Requirement versus simulated performance for three cases including model errors....62
Table 4-17 – Ocean Surface Albedo IP Performance Summary....63
Table 5-1 – NHF Processing Time Benchmark....64
Table 7-1 – LW Fluxes Calculated with Hemispherically Varying Emissivity (No Averaging) and a Hemispherically Averaged Emissivity....69
Table 7-2 – Hemispherically and Spectrally Averaged Emissivities as a Function of Wind Speed....69

D43762, A. PDMO Released: 2009-09-28 (VERIFY REVISION STATUS)
PDMO

List of Figures

Figure 3-1 – Net Heat Flux Algorithm Functional Flow....20
Figure 4-1 – Fluxes and SST over the Indian Ocean (October 2003)....27
Figure 4-3 – Fluxes vs input parameters over the Indian Ocean (October 2003)....28
Figure 4-5 – SST and Heat Fluxes over the Tropical Pacific (December 2003)....29
Figure 4-7 – Input Parameters and Heat Fluxes over the Tropical Pacific (December 2003)....30
Figure 4-9 – SST and Heat Fluxes over the North Atlantic (August 2003)....31
Figure 4-11 – Input Parameters and Heat Fluxes over the North Atlantic (August 2003)....32
Figure 4-13 – Nighttime SST and Fluxes over the Tropical Atlantic (July 2003)....33
Figure 4-15 – Nighttime Input Parameters and Heat Fluxes over the Tropical Atlantic (July 2003)....34
Figure 4-17 – IST and Heat Fluxes in the Hudson Bay Area (May 2003)....35
Figure 4-19 – Heat Fluxes vs Input Parameters in the Hudson Bay Area (May 2003)....36
Figure 4-21 – Ocean Surface Albedo Product (left) and Chlorophyll Input (right). Upper two images are entire North Atlantic Scene (R3); lower two images are zooms of area marked in red. Albedo units are fraction. Chlorophyll units are mg/cm^3....37
Figure 4-23 – Scatter plots corresponding to Figure 4-21. Albedo is the final corrected product that is the deliver IP. Raw albedo is the direct output of the COART LUTs. Chlorophyll units are g/cm^3. Aerosol is the optical depth (unitless).....38
Figure 4-25 – Errors in Longwave Flux Due to Errors in VIIRS Parameters Only (SST). 42
Figure 4-14 – Errors in Latent Heat Flux Due to Errors in VIIRS Parameters Only (SST). 43
Figure 4-15 – Errors in Sensible Heat Flux Due to Errors in VIIRS Parameters Only (SST).....43
Figure 4-16 – Errors in Net Heat Flux Due to Errors in VIIRS Parameters Only (SST).....44
Figure 4-17 – Error in Shortwave Flux over Water Due to Aerosol Error (AOT and Model). 44
Figure 4-31 – Errors in Daytime Net Heat Flux Due to VIIRS Input Errors (SST and Aerosol AOT and Model). 45
Figure 4-20 – Errors in Nighttime Longwave Flux Due to Reduced Errors in All Input Parameters.45
Figure 4-20 – Errors in Nighttime Latent Heat Flux Due to Reduced Errors in All Input Parameters. 46
Figure 4-21 – Errors in Nighttime Sensible Heat Flux Due to Reduced Errors in All Input Parameters 46
Figure 4-22 – Errors in Nighttime Net Heat Flux Due to Reduced Errors in All Input Parameters ...47
Figure 4-23 – Errors in Shortwave Flux Due to Reduced Errors in All Input Parameters. 47
Figure 4-26 – Errors in Daytime Net Heat Flux Due to Reduced Errors in All Input Parameters. 48
Figure 4-28 – Errors in Nighttime Longwave Flux over Water Due to Baseline Errors in All Input Parameters. 48
Figure 4-26 – Errors in Nighttime Latent Heat Flux Due to Baseline Errors in All Input Parameters. 49
Figure 4-27 – Errors in Nighttime Sensible Heat Flux over Water Due to Baseline Errors in All Input Parameters. 49

D43762, A. PDMO Released: 2009-09-28 (VERIFY REVISION STATUS)
PDMO

Figure 4-28 – Errors in Nighttime Net Heat Flux Due to Baseline Errors in All Input Parameters. ..50
Figure 4-29 – Error in Shortwave Flux Due to Baseline Errors in All Input Parameters. 50
Figure 4-34 – Errors in Daytime Net Heat Flux Due to Baseline Errors in All Input Parameters.....51
Figure 4-31 – Longwave Flux vs Air Temperature at 2m 53
Figure 4-32 – Latent Heat Flux vs Air Temperature at 2m.....53
Figure 4-34 – Sensible Heat Flux vs Air Temperature at 2m 54
Figure 4-36 – Latent Heat Flux vs Water Mixing Ratio at 2m 54
Figure 4-38 – Sensible Heat Flux vs Water Mixing Ratio at 2m.....55
Figure 4-40 – Longwave Flux vs SST 55
Figure 4-42 – Latent Heat Flux vs SST.....56
Figure 4-44 – Sensible Heat Flux vs SST 56
Figure 4-46 – Latent Heat Flux vs Wind Speed at 10 m.....57
Figure 4-48 – Sensible Heat Flux vs Wind Speed at 10 m.....57
Figure 4-42 – Shortwave Flux vs AOT at 550 nm (Aerosol Model Also Varied).....58
Figure 4-51 – Ocean Surface Albedo Errors.....59
Figure 4-53 – Specification and Model Error in Net Heat Flux Due to VIIRS Input Errors Only.....61
Figure 4-55 – Specification and Model Error in Net Heat Flux Due to Reduced Baseline Input Errors 61
Figure 4-57 – Specification and Model Error in Net Heat Flux Due to Baseline Input Errors 62
Figure 7-1: Sea Surface Emissivity.....68

D43762, A. PDMO Released: 2009-09-28 (VERIFY REVISION STATUS)
PDMO

1. Introduction

1.1. Overview

Understanding the global energy balance is essential to understanding the Earth's weather and climate. The National Polar Orbiting Satellite Systems (NPOESS) comprehensively addresses the Earth energy balance with two interrelated Environmental Data Records (numbers refer to the NPOESS System Specification paragraph number of Appendix D): Albedo (Surface) [40.5.2] and Net Heat Flux [40.7.5].

This document describes the algorithm to compute Net Heat Flux (NHF) and an associated algorithm that determines the albedo over ocean surfaces. NHF is the NPOESS EDR that quantifies energy fluxes at the water surface of the Earth. NHF is defined as the sum of four individual flux components at the air-sea boundary: long-wave radiation, short-wave radiation, latent heat, and sensible heat. It is required only for clear conditions over water- or ice-covered oceans. It is an allocated requirement of the Visible and Infrared Imaging Radiometer Suite (VIIRS) sensor, although it uses data from other NPOESS sensors (when available) and from external ancillary data sources as well. One of the key input variables is ocean surface wind speed. For the NPOESS Era, the preferred source of ocean surface wind speed is Microwave Imager Sounder (MIS) that is being developed for NPOESS C2. During the NPOESS Preparatory Project (NPP) and NPOESS C1 Era, when MIS is not available, ocean wind speed is from numerical weather prediction model inputs.

The albedo at the surface is a driving boundary condition for the NHF EDR. Over water-covered ocean, look-up tables (LUT) are used to compute the albedo with wind speed and chlorophyll concentration the primary inputs. Over ice, two options are supported to define the surface albedo boundary condition: (a) assign an albedo based on the Sea Ice Age EDR; and (b) use an external estimate from a separate sea ice albedo EDR algorithm.

Quantification of the energy flux at the air-sea boundary has broad ranging and important applications in climate, weather, and oceanography. Energy transfer at the air-sea boundary is an important driver of atmospheric and ocean circulation systems at both short and long time scales. One such interaction that affects seasonal to inter-annual weather is the El Nino/Southern Oscillation (ENSO) – a multi-year cyclical variation of tropical sea surface temperatures. For another application consider the North Atlantic Thermohaline Circulation of which the Gulf Stream is the most prominent observable feature. Long term trends in heat transfer are one driver of variations in the Atlantic Thermohaline circulation. These trends affect climate on decadal and longer time scales. More generally, oceanic heat flux is related to the water cycle and green house gas forcing (CO2 uptake/release) with diverse impacts on the climate.

The NPOESS NHF algorithm is built around two well-validated, community standard models for calculating the individual flux components: the Rapid Radiative Transfer Model (RRTM) for computing the radiative fluxes and the COARE Model for computing the turbulent fluxes (latent and sensible heat). The albedo over ocean-water conditions uses COART-derived look-up tables that were originally developed as part of the CERES Project for use in the Surface and Atmospheric Radiation Budget (SARB) Algorithm

D43762, A. PDMO Released: 2009-09-28 (VERIFY REVISION STATUS)
PDMO

component. These models have been subjected to extensive peer-level theoretical review in the published literature and comprehensive validation. They are actively maintained with updates freely provided to the community as warranted by continuing theoretical developments and validation programs. Use of these community standard models provides substantial benefits to NPOESS by simplifying the process of maintaining currency with the state of the art and leveraging community-wide model science developments.

1.2. Scope

This document presents the scientific background, algorithm design and algorithm performance of the Net Heat Flux (NHF) Environmental Data Record (EDR) Algorithm and the Surface Albedo IP for ocean water conditions. These algorithms are part of the National Polar Orbiting Environmental Satellite System (NPOESS) and will be implemented in the Integrated Data Processing Subsystem (IDPS). The Net Heat Flux Algorithm derives the heat flux transferred between the surface to the atmosphere for clear regions over water- and ice-covered oceans. It ingests derived EDRs and IPs from VIIRS as well as data from other ancillary and auxiliary data sources. Atmospheric and Environmental Research (AER), Inc. performed this work under contract to the Northrop Grumman Space Technology NPOESS Project Office.

The NHF algorithm computes the total flux as the primary EDR output that is computed for each horizontal cell plus basic quality control information. In addition, the NHF algorithm outputs the four individual components of the flux (separately for the water and ice portions of each cell). The albedo internally computed used by the algorithm is also output.

The algorithm described here has been implemented and tested as an integrated software product, written in a combination of Fortran 90 and C++. A companion document (P1187-SW-I-004, AER, Inc., Net Heat Flux Software Description) to this ATBD describes the software design and implementation, including formats and interfaces.

1.3. Applicable Documents

Table 1-1 lists relevant specifications guiding the NHF algorithm development.

Table 1-1 – Relevant Specifications

Organization	Document	Application
Northrop Grumman Space Technology	National Polar Orbiting Environmental Satellite System (NPOESS) System Specification (12 September 2008), SY15-007, Rev N	Source of System Requirements, including EDR performance

This report assumes that the VIIRS EDRs used from the VIIRS sensor meet their respective EDR requirements listed in the NPOESS System Specification. No direct sensor data (i.e., Sensor Data Records) are used by the algorithm.

D43762, A. PDMO Released: 2009-09-28 (VERIFY REVISION STATUS)
PDMO

1.4. Relationship to Prior Work

The algorithm described here is based on an approach previously developed by AER for the NPOESS VIIRS Risk Reduction Phase and reported in the document: Cady-Pereira, K., 2000: VIIRS Algorithm Theoretical Basis Document for the Net Heat Flux EDR, Version 1.3, May 2003, AER Inc. Both the current algorithm and the algorithm described in the earlier ATBD employ the same underlying models for calculating the turbulent and radiative fluxes (COARE and RRTM respectively). The current ATBD uses updated versions of those models. It also computes the Ocean Surface Albedo IP.

Descriptions of the science and underlying mathematics presented in this document are borrowed extensively from the previous ATBD. Validation and testing are entirely new in this document. The resulting software being released along with this ATBD has also been completely updated from the version delivered along with the previous ATBD.

2. Net Heat Flux Requirements

2.1. EDR NHF Requirements

Interpretation of the preamble test for Net Heat Flux EDR in the NPOESS System Specification, Appendix D, 40.7.5 is given in Table 2-1.

D43762, A. PDMO Released: 2009-09-28 (VERIFY REVISION STATUS)
PDMO

Table 2-1 – Preamble text and interpretation for the Net Heat EDR

Specification	Interpretation
Net heat flux refers to net surface flux over oceans (including ice covered).	Applies over ocean including ice covered ocean Requires ice mask input
Components are long-wave and short-wave radiation, latent heat flux and sensible heat flux	All four components must be computed and totaled
The requirements below apply only when at least 80% of the cloud mask elements on a Net Heat Flux horizontal cell are "confidently clear".	Requires VCM as input. Need to compute fraction over the applicable horizontal cell.
<Implied>	Applies both day and night (but see below, terminator orbit excluded)

We adopt the convention that heat flux is defined as positive for a net transfer of heat from the ocean (or ice) to the atmosphere.

D43762, A. PDMO Released: 2009-09-28 (VERIFY REVISION STATUS)
PDMO

Table 2-2 lists the EDR attributes and their interpretation for the Net Heat Flux EDR. We interpret HCS as the maximum cell size allowed. As highlighted in Appendix B, we choose an aggregation method that results in nearly constant spatial resolution cells across a scan. These parameters are controlled by an externally specified look-up table. We have been unable to acquire test data covering the full specified dynamic range, although the delivered NHF algorithm would support such measurements should they occur. Our test data occupy about half the specified –2000 to +2,000 W/m^2 measurement range.

The Maximum Local Average Revisit Time (MLART) is based on a swath width corresponding to ~1,700 km. This swath corresponds to the required swath for VIIRS SST. In practice, the algorithm can derive an EDR over the full VIIRS swath (~3,000 km) by using NWP data for the ocean wind speed inputs.

This document does not directly concern itself with the latency. Algorithm computation speed benchmarks are given in Section 5.3.

Measurement exclusions are derived from exclusions for VIIRS EDRs (SST, Ocean Color, and aerosol optical thickness) used in computing the heat flux. The VIIRS sensor provides input atmospheric/surface state variables (in the form of EDRs or intermediate products) that are used to derive the various components of net heat flux.

D43762, A. PDMO Released: 2009-09-28 (VERIFY REVISION STATUS)
PDMO

Table 2-2 – EDR Attribute Table for Net Heat Flux

Paragraph	Subject	Specified Value	Interpretation
40.7.5-1	a. Horizontal Cell Size	20 km	Maximum horizontal cell
40.7.5-2	b. Horizontal Reporting Interval	HCS	
40.7.5-3	c. Horizontal Coverage	Oceans	Includes ice covered ocean, not required for inland water/ lakes
40.7.5-4	d. Measurement Range	-2000 to +2000 W/m^2	Actual range is likely smaller
40.7.5-7	g. Mapping Uncertainty, 3 Sigma	1.5 km	VIIRS Mapping uncertainty specification
40.7.5-8	h. Maximum Local Average Revisit Time [No Terminator Orbit VIIRS Data]	17.1 hr	Requires swath width of ~ 1700 km
40.7.5-10	i. Latency	NPP – 150 min NPOESS – 24 hr	Latency is not covered in this ATBD
	j. Measurement Exclusion Conditions		
40.7.5-11a	1. Sun Glint < 36 deg		Exclude glint conditions where VIIRS aerosol optical depth and particle size parameter cannot be determined
40.7.5-11b	2. Wind Speed > 25 m/sec		Wind speed exclusion
40.7.5-11c	3. Orbit Other Than Nominal 1330 Orbit		Excludes terminator orbit (where aerosol optical depth is not derived by VIIRS)
40.7.5-11d	4. Aerosol Optical Thickness > 1.0		Excludes high optical depth conditions where SST is degraded or not available

. For NPP/NPOESS, data can be provided for these exclusions by using NWP data as a fall-back when MIS data is not valid.

2.2. Instrument Characteristics

Net Heat Flux does not directly employ any NPOESS sensor data (i.e., the Sensor Data Records), but rather uses EDRs and intermediate products derived by these sensors as inputs. The algorithm requires EDR inputs from VIIRS and may use inputs from the MIS when available. The specific characteristics of the SDRs are not directly relevant to this EDR.

3. Algorithm Description

3.1. Theoretical Description

The Net Heat Flux algorithm strategy is to compute each individual component using appropriate models for the relevant physical processes. The physical processes are:

- Turbulent fluxes: Latent and sensible heat

D43762, A. PDMO Released: 2009-09-28 (VERIFY REVISION STATUS)
PDMO

- Radiative fluxes: long-wave and short-wave

Sections 3.1.1 and 3.1.2 describe the theoretical basis for these calculations. The ocean surface albedo is an important input boundary condition for the short-wave radiative flux calculations. Section 3.1.3 describes the theoretical basis for determining this quantity.

3.1.1. Radiative Fluxes

The radiative transfer model chosen is RRTM (Rapid Radiative Transfer Model, Mlawer et al, 1997), which was developed at AER by the Radiation and Climate Group. RRTM is a correlated-k broadband radiative transfer model . The band parameters were derived by LBLRTM (Line By Line Radiative Transfer Model), (Clough et Iacono, 1995) a line-by-line code also developed at AER. The accuracy of LBLRTM has been established by numerous validations with measurements, especially from the ARM (Atmospheric Radiation and Measurement) program (Stokes and Schwartz, 1994). The accuracy of RRTM has been validated against LBLRTM, with errors smaller than 2 W/m^2. RRTM is currently under testing to determine if it should be incorporated into the NCAR GCM, CCM3. (Iacono et al, 1999). The version of RRTM used here employs a two stream multiple scattering model. As part of the NPOESS-VIIRS project, the RRTM interface was redesigned, allowing the user complete control over the selection of scatterers and their optical properties, including spectral dependence.

Given satellite measurements, radiative fluxes at the surface can basically be determined by two approaches:

a) using a parametric relationship between measured TOA radiances and net surface fluxes (REF); this relationship must be determined a priori and is usually valid only over the region of the globe for which it was derived

b) running a radiative transfer model whose inputs are parameters retrieved from satellite measurements; this approach requires more inputs, demands longer processing times but is globally applicable.

In view of the requirement for a globally valid operational algorithm, we have chosen the (b), the radiative transfer model approach. To minimize computational time of the RT model we have selected RRTM, that utilizes the k-correlated method for calculating fluxes, an approximate technique with accuracy comparable to line-by-line methods, but which offers an extreme reduction (by a factor of 10,000) in the number of RT operations, and thus in processing time. The RRTM version chosen uses a two-stream scattering model, offering substantial speed improvements over n-stream versions coupled to DISORT.

Absorption coefficients vary irregularly with wavenumber; thus it is difficult to determine representative values in wavenumber space. However, if the wavenumbers are rearranged with absorption coefficients in ascending order, a smooth function can be generated, from which characteristic values are easily obtained. This is done by dividing the spectrum into a number of pre-defined bands, sorting the line-by-line absorption coefficients in each band by value rather than by wavenumber, partitioning these remapped coefficients into a fixed number (16) of subintervals, then selecting a characteristic value k_j for the absorption coefficients in the subinterval. Effectively this is

D43762, A. PDMO Released: 2009-09-28 (VERIFY REVISION STATUS)
PDMO

a remapping from wavenumber to a cumulative probability space. The accuracy of this approach in inhomogeneous atmospheres depends on the correlation between the k distributions in adjacent layers.

These characteristic k_j values are then used in layer-by-layer radiative transfer calculations. RRTM does not determine the k_j values at run time. These calculations are performed on the output of a line-by-line model (LBLRTM – Clough and Iacono, 1995**)** and stored for a range of pressures, temperatures and relative species abundance. RRTM linearly interpolates from the pre-stored values to find the appropriate absorption coefficients for the given atmospheric conditions. Details regarding the choice of bands, subintervals and species, the handling of subintervals with more than one key species, and a discussion of validations can be found in Mlawer et al, (1997).

Aerosol scattering is crucial for accurate short-wave flux calculations. For the shortwave portion of the spectrum, we employ a version RRTM which calculates the optical depths and scattering coefficients as described above, but then passes this information into a two-stream multiple scattering model to perform the radiative transfer calculations with scattering. The phase function is calculated as a weighted average of the Rayleigh phase function for the molecular scattering and the Henyey-Greenstein function for aerosol scatterers. The optical depth of the scatterers and their spectrally dependent optical properties are determined by the VIIRS Aerosol EDR algorithm.

See Appendix C for additional details on the specific implementation of RRTM used here.

3.1.2. Turbulent Fluxes

The turbulent flux model selected for VIIRS is the flux code written for the TOGA COARE **(**Fairall et al, 1996) (Tropical Ocean – Global Atmosphere Coupled Ocean-Atmosphere Response Experiment). This code incorporates Monin-Obukhov stability theory, with modifications for the convective limit, surface roughness/stress formulations based on the work of Charnock (1955) and the LKB (Liu, Katsaros and Businger, 1979) model for scalar roughness. The model also calculates the cool skin and warm layer corrections, which relate the surface skin temperature to the bulk temperature measured at some small depth near the surface. In order to meet the TOGA COARE goal of an uncertainty smaller than 10 W/m^2 in the total net heat flux, physical constants were chosen very carefully, and the temperature dependency of L_e was included. The code was validated against measurements made from the RV Moana Wave from November 1992 to February 1993 in the Central Tropical Pacific.

Turbulent fluxes at the air-sea interface are, in general, well-described by Monin-Obukhov stability theory (MOS), which hypothesizes that above a viscous sub-layer dominated by molecular processes, there is a constant stress layer governed by turbulent exchanges of momentum, heat, water vapor and other scalar variables. In this layer physical quantities are assumed to be a function of height, potential temperature, eddy heat transport, and surface stress. These variables can be combined into a parameter known as the Obukhov length, L, which is a measure of the thickness of the layer dominated by shear driven turbulence; at heights greater than L, buoyancy effects become the principal sources of turbulent energy and classical MOS breaks down. The

D43762, A. PDMO Released: 2009-09-28 (VERIFY REVISION STATUS)
D43762

non-dimensional gradients of wind, temperature and water vapor can be written as functions of z/L, then integrated to yield vertical profiles of these variables. The functions of z/L must be empirically derived (Businger et al, 1971), but within the constraints of MOS theory are valid generally.

The profiles of wind speed, temperature and water vapor are functions of the surface roughness and of the fluxes of momentum, heat and water vapor. Given surface values and measurements at some specified height, these equations are solved iteratively to yield the fluxes. Alternatively, the fluxes can be written as the product of a transfer coefficient and the measured variables (e.g., Large and Pond, 1982), the bulk formulation. These transfer coefficients must obviously be determined empirically and thus are truly only valid for a limited set of conditions. This led us to choose the more complex but more general and complete approach of solving the profile equations, which provides an internally consistent set of fluxes and allows the determination of parameters of interest to other EDRs, such as a bulk-skin temperature difference for SST and the temperature 2m above the ice surface for IST.

We have adapted the TOGA COARE flux code (Fairall et al, 1996) for the NPOESS-VIIRS project. This code uses the iterative solution approach to determine the fluxes in the boundary layer. It was selected because it was written to meet the stringent requirement of the TOGA COARE program (uncertainties less than 10 W/m^2 in heat flux). In order to achieve this objective, a model was developed which would apply under a wide range of conditions, even in the limit of free convection, where many dynamical variables behave asymptotically in the MOS framework. Every effort was made to use the most accurate value available of the necessary geophysical constants, and latent heat of evaporation and kinematic viscosity are written as functions of temperature. Several small corrections to the net heat flux are available in the model: the Webb effect (Webb et al, 1980), sensible heat flux due to precipitation (Gosnell et al, 1995), cool skin and warm layer effects (Fairall et al, 1996). Due to the constraints on available inputs to NPOESS-VIIRS, only the cool skin and the Webb effect have been implemented for the baseline net heat flux algorithm.

As stated above, the profiles of wind speed, temperature and humidity are functions of the surface roughness (see section 4.2.1.2). Mathematically, the roughness length is the fictitious height z above the surface at which the profiles extrapolate to the surface value. The value of z is fictitious because these profiles are not valid so close to the surface. The roughness length for wind speed is directly related to the size of the surface roughness elements, such as surface waves on the ocean. Charnock (1955) proposed a widely used relationship between oceanic roughness and surface stress:

$$z_0 = \alpha u_*^2 / g$$

α is the Charnock constant, usually set to 0.01, but for which values as large as 0.035 have been reported. This relationship does not hold in the free convective limit, where the surface stress is small and the surface becomes aerodynamically smooth. Under these

D43762, A. PDMO Released: 2009-09-28 (VERIFY REVISION STATUS)
PDMO

conditions, the following equation has been derived theoretically and verified experimentally (Kraus and Businger, 1994)

$$z_0 = 0.11\nu / u_*$$

The TOGA COARE model combines both the above equations to yield a velocity roughness length valid over a wide range of conditions.

The roughness lengths for the temperature and humidity profiles, also known as the kinematic roughness lengths, are calculated using the model of Liu et al (1979, hereafter LKB). LKB applied a surface renewal model to determine profiles of momentum, temperature, and humidity, which would hold in the viscous sublayer (or interfacial layer), but which would also match the MOS profiles at some undetermined height. This also forces the profiles to match yielded curves of temperature and humidity surface roughness as functions of the roughness Reynolds number. These curves were fitted with polynomials, whose coefficients are easily stored and reused to quickly generate kinematic roughness values, once the roughness of the flow has been determined.

Obviously over ice the surface roughness is not a function of wind speed. It must be estimated and input to the code. The scalar roughness is determined in a manner similar to that for flow over ice, but using polynomial coefficients derived by Andreas (1987).

Two additions to the usual MOS framework are included in the TOGA COARE model to enable calculations even in the free convection regime. First, the wind speed used throughout the iterative procedure in the model is a RMS of the mean surface wind speed and the convective scaling velocity, which allows for turbulent transfer, carried out by convective eddies, even at low horizontal wind speeds. Second, the empirically derived MOS functions are actually a blend of the standard Kansas functions (Businger et al, 1971) and of a different function valid in the free convective limit (Fairall et al, 1996).

3.1.3. Ocean Surface Albedo (Input Into Radiative Flux Algorithm)

The key boundary condition for the short-wave radiative flux calculation is the surface albedo. An input albedo is required over both water-covered ocean and ice-covered ocean.

For ice, we assume that ultimately the albedo will be derived externally and input to the NHF algorithm. Such an ice albedo product was not available at the time this algorithm was developed. Thus, as a temporary measure to support testing we used the following method to estimate ice albedo: set the ice albedo to a fixed value depending on the ice age estimate (new, first-year, multi-year ice).

For water-covered ocean we adopted the same method used by the CERES for the Surface and Atmospheric Radiation Budget (SARB) algorithm (Charlock, et al, 1997). The method is not presented in SARB ATBD but is given in Jin and Charlock (2001).

For specifying the ocean surface albedo, we used a set of look-up tables produced by the Coupled Ocean Atmosphere Radiative Transfer (COART) Model

D43762, A. PDMO Released: 2009-09-28 (VERIFY REVISION STATUS)
PDMO

(http://snowdog.larc.nasa.gov/jin/rtnote.html). The model is described in detail in Jin, Charlock and Rutledge (2002). Its key features are:

- discrete ordinate multiple scattering method based on DISORT including coupled atmosphere-ocean scattering
- atmospheric absorption using 26-band k-distribution from HITRAN-2000 database
- surface boundary condition from the Cox and Monk surface reflection slope distribution from Cox and Monk (1954) as described in Jin and Simpson (1999)
- ocean water absorption/ scattering based on chlorophyll content and dissolved organic matter (DOM); DOM is parameterized with chlorophyll concentration from Morel (1991)

This model is not run in real time but is used to pre-compute look up tables for ocean surface albedo dependent on solar zenith angle (SZA), aerosol optical thickness (AOT), wind speed (U), and chlorophyll concentration (CHL). We refer to these tables as the COART-LUTs, and they are described in Jin, Charlock, Smith, and Rutledge (2004).

For a given pixel level input of SZA, AOT, U, and CHL, n-dimensional linear interpolation (with n = 4) is used to compute the ocean surface reflectivity at several wavelengths in the visible through SWIR. This reflectivity is aggregated onto the horizontal cell and is input into the RRTM shortwave model.

D43762, A. PDMO Released: 2009-09-28 (VERIFY REVISION STATUS)
PDMO

3.2. Mathematical Description

The net heat flux for a horizontal cell is given by:

$$F_{total} = f_w(R_{lw}^w + R_{sw}^w + H^w + E^w) + f_i(R_{lw}^i + R_{sw}^i + H^i + E^i)$$

where

F_{total} is the net heat flux for the cell

the superscripts *w* and *i* refer to the water and ice portions of the cell

$R_{lw}$and R_{sw} are the long-wave and short-wave surface radiative fluxes respectively

H and E are the sensible and latent heat fluxes respectively

$f_w = N_{w,c} / N_c$ and $f_i = N_{i,c} / N_c$

N_c , $N_{w,c}$, $N_{i,c}$ are the number of VIIRS pixels in the horizontal cell

that are clear, water & clear, ice & clear, respectively

The flux components are computed based on the atmospheric/surface state variables for the clear/water and clear/ice portions of the horizontal cell. The mathematical form of the radiative flux calculations is given in Section 3.2.1. For a mathematical description of the turbulent flux equations, see 3.2.2.

3.2.1. Radiative Transfer Equations

RRTM is fundamentally an accelerated radiative transfer model. Thus the fundamental equation is the standard formulation for radiative transfer in a plane-parallel non-scattering atmospheric layer, modified to accommodate the reordering of the absorption coefficients k and the partitioning into subintervals described in section 4.1.1.1:

$$R_{\nu 1,\nu 2} = \sum_j W_j [B_{eff,j} + (R_{0j} - B_{eff,j}) \exp(-\kappa_j \frac{\rho \Delta z}{\cos \phi})]$$

where

$R_{\nu 1, \nu 2}$ = average outgoing layer radiance in the band between ν1 and ν2

j = subinterval index

W_j = size of subinterval j

$B_{eff,j}$ = effective Planck function for the layer and subinterval

$R_{0,j}$ = incoming layer radiance in the subinterval j

κ_j = characteristic value of the absorption coefficient for the subinterval and layer

Δz = thickness of the layer

ϕ = optical path angle

D43762, A. PDMO Released: 2009-09-28 (VERIFY REVISION STATUS)
PDMO

The surface boundary condition for the long-wave is the effective surface emissivity. A fixed surface emissivity is used, nominally 0.97. See Appendix A for details.

The surface boundary condition for the short-wave is given by the ocean surface albedo. See Section 3.2.3.

3.2.2. Turbulent Flux Equations

The turbulent flux code iteratively solves the MOS profile equations for water conditions:

$$(U - U_s) = u_*(\ln(z / z_0) - \Psi_u(z / L))/\kappa$$
$$(T - T_s) = t_*(\ln(z / z_t) - \Psi_t(z / L))/\kappa$$
$$(Q - Q_s) = q_*(\ln(z / z_q) - \Psi_q(z / L))/\kappa$$

where

z = measurement height (10m)
u = wind speed at z
T = air temperature at z
T_s = air temperature at the sea surface (assume equal to skin temperature)
Q = specific humidity at z
Q_s = saturation specific humidity (function of the sea surface temperature)
z_0, z_t, z_q = roughness lengths for velocity, temperature, and humidity
Re = roughness Reynolds number
κ = von Karman's constant : 0.4

L is the Monin-Obukhov length discussed in 4.1.1.2, and given by

$$L = -u_*^3\theta / g < w'\theta' >$$

where

θ = potential temperature at height z
θ' = eddy potential temperature
w' = eddy vertical velocity

<w'θ'> corresponds directly to the eddy sensible heat flux.

u_*, t_*, and q_* are scaling parameters for velocity, temperature, and humidity in the constant stress layer and are directly related to the fluxes:

D43762, A. PDMO Released: 2009-09-28 (VERIFY REVISION STATUS)
PDMO

$$H = -\rho_a C_p u_* t_*$$
$$E = -\rho_a L_e u_* q_*$$
$$\tau = -\rho_a u_*^2$$

where

ρ_a = density of air at the sea surface
C_p= specific heat of air at constant pressure
L_e = latent heat of evaporation
H = sensible heat flux
E = latent heat flux
τ = surface stress (momentum flux)

The surface roughness is given by (see section 4.1.1.2)

$$z_0 = \alpha u_*^2 / g + .11\nu / u_*$$

The kinematic roughnesses z_t and z_q are functions of the surface roughness Re and are found from empirical fits following the LKB approach (see section 3.1.1.2). Finally, the stability functions ψ_u, ψ_t, and ψ_q are a blending of two empirically derived sets, the standard Kansas-type functions and scalar profile functions valid in the free convection limit. The scalar profile functions ψ_t and ψ_q are assumed to be equal. The Kansas-type profiles are given for unstable conditions by:

$$\psi_{Ku} = -2\ln[(1+x)/2] - \ln[(1+x^2)/2] + 2\tan^{-1} - \pi/2$$

$$\psi_{Kt,q} = 2\ln[(1+x^2)/2],$$

where

$$x = [1 - 16(z/L)]^{1/4},$$

and for stable conditions by:

$$\psi_{Ku,t,q} = 4.7(z/L)$$

For the free convective limit, the following profile can be used:

$$\psi_c = 1.5\ln[(y^2 + y + 1)/3] - \sqrt{3}\tan^{-1}[(2y+1)/\sqrt{3}] + \pi/\sqrt{3},$$

where

D43762, A. PDMO Released: 2009-09-28 (VERIFY REVISION STATUS)
PDMO

$$y = \sqrt[3]{(1-12.87(z/L)}$$

The two types of profiles are then blended to yield a profile function that holds over a wide range of conditions:

$$\psi_x = \frac{1}{1+(z/L)^2}\psi_{xK} + \frac{(z/L)^2}{1+(z/L)^2}\psi_c$$

Note that in the free convective limit, L will tend to zero and the equation above will reduce to the second term on the right. Conversely, for smaller values of L, the equation will reduce to the first term on the right.

Given the above equation, the TOGA COARE code iteratively solves for u_*, t_* , and q_*, then uses theses values to calculate the sensible and latent heat fluxes.

The COARE latent and sensible heat flux algorithm is an iterative search for the parameters that describe the wind speed, temperature, and humidity profiles, given measurements of these variables at some predetermined height, and the surface temperature. These profiles are valid throughout the turbulent, or inertial, boundary layer, but do not apply in the thin layer next to the surface, where the flow is dominated by viscosity and is laminar.

One of the profile parameters is the aerodynamic surface roughness, z_0. z_0 is defined as the height at which the extrapolated turbulent wind speed profile becomes zero; the wind speed actually only reaches zero at the surface, due to the presence of the viscous boundary layer, but the aerodynamic surface roughness still has some physical content, as it is directly related to the neutral stability drag coefficient (Andreas, 1987). For profiles over water z_0 is determined as part of the solution for the wind speed profile, but over ice z_0 is fixed and is a function of the surface irregularities. Banke et al (1980) performed a series of measurements in the Beaufort Sea and derived the following empirical equation:

$$z_0 = -0.03 + 0.012\zeta,$$

where ζ is the rms of the surface elevation. The Beaufort Sea measurements over a wide range of ice types, yielded a range of z_0 from 0.001 cm to 0.2 cm, corresponding to smooth new ice and ridged, older ice, respectively. Similar results were found over snow (Kondo et Yamazawa, 1985), which extends the applicability of the equation above, since ice is often snow covered. Smaller values of z_0 (as low as 0.001 cm) have been observed by some researchers (Garbrecht et al, 2002) for very smooth ice.

In the absence of surface elevation statistics, the VIIRS heat flux over ice algorithm will use ice age estimates to determine z_0 as given in Table 3-1.

D43762, A. PDMO Released: 2009-09-28 (VERIFY REVISION STATUS)
PDMO

Table 3-1 – Aerodynamic Roughness as a Function of Ice Age

Ice Age	Aerodynamic Roughness (cm)
New	0.01
old type	0.075

3.2.3. Ocean Surface Albedo Mathematical Description

Ocean Surface Albedo is a boundary condition for the RRTM short-wave flux calculation and is a required intermediate product. The RRTM input is for an average over an aggregated horizontal cell. The Ocean Surface Albedo IP is produced at the VIIRS M-band pixel locations. The pixel level ocean surface albedo product is primarily a COART LUT-based product using pixel level input data.

For the final output pixel level Ocean Surface Albedo product, we compute a correction factor between the flux-based and the COART LUT aggregated albedos and apply this correction to the initial COART LUT pixel level albedo.

This approach ensures consistency between the ocean surface albedo product and the shortwave radiative fluxes computed by RRTM.

The ocean surface albedo is computed using a five-step process that is applied one aggregation cell at a time:

1. For each valid pixel in the aggregation cell, compute the broadband albedo (covering 0.4 to 4 μm) by multi-linear interpolation of the COART Look-up table over the values at each pixel of the four inputs: wind speed, aerosol optical depth, solar zenith angle, and chlorophyll concentration.
2. Compute the monochromatic ocean surface albedo using the COART LUT at the 14 standard wavelengths in the COART LUT from the average values over the aggregation cell of the four inputs noted in Step 1.
3. Linearly interpolate to the spectral grid used in RRTM from the 14 COART wavelengths (a single value is produced for each aggregation cell). Provide these values as input boundary conditions to RRTM-SW and use RRTM-SW to compute the down- and up-welling integrated shortwave fluxes at the ocean surface. Compute an RRTM-derived aggregation cell averaged ocean surface albedo from the net up- and down-welling fluxes.
4. Compute an albedo correction factor for each horizontal cell as the ratio of the albedo derived by RRTM in Step 3 and of the average broadband albedos over the horizontal cell output by Step 1.
5. For each pixel in an aggregation cell, multiply by the correction factor of Step 4 to derive the albedo estimate at each pixel. This is the final Ocean Surface Albedo IP at the VIIRS M-band pixel locations.

D43762, A. PDMO Released: 2009-09-28 (VERIFY REVISION STATUS)
PDMO

A valid pixel is a clear pixel (VIIRS M-band) for which all required input products are available and within valid range.

Step 1 employs a n-dimensional linear interpolation (with n = 4). First, one obtains the 2^4 (= 16) values of ocean spectral reflectivity stored in the LUT that bound the actual values of solar zenith angle, aerosol optical thickness, wind speed, and chlorophyll concentration (SZA, AOT, U, and CHL respectively). Values of i, j, k, and l are determined that satisfy:

$$SZA_i \leq SZA \leq SZA_{i+1}$$
$$AOT_j \leq AOT \leq AOT_{j+1}$$
$$CHL_l \leq CHL \leq CHL_{l+1}$$

Compute the interpolation coefficients as:

$$w_{sza} = (SZA - SZA_{i+1}) / ((SZA_i - SZA_{i+1})$$
$$w_{aot} = (AOT - AOT_{j+1}) / ((AOT_j - AOT_{j+1})$$
$$w_{UU} = (U - U_{k+1}) / ((U_k - U_{k+1})$$
$$w_{chl} = (CHL - CHL_{l+1}) / ((CHL_l - CHL_{l+1})$$

Compute the interpolated reflectivity ρ_n^{COART} from the 16 values of reflectivity stored in the LUT (at each monochromatic wavelength) for each pixel in the aggregation cell.

The LUT values are denoted as: $r_{i', j', k', l'}$ where i' member of {i, i+1}, j' member of {j, j+1}, where k' member of {k, k+1}, where l' member of {l, l+1}.

The m-dimensional linear interpolation is performed as:

$$\rho_n^{COART} = \sum_{I \in i'} \sum_{J \in j'} \sum_{K \in k'} \sum_{L \in l'} r_{I,J,K,L} \; w^*_{AOT}(I) \quad w^*_{SZA}(J) \quad w^*_{U}(K) \quad w^*_{CHL}(L)$$

$w^*_{AOT}(I)$ is w_{AOT} if I = i and $(1\text{-}w_{AOT})$ if I = i + 1

$w^*_{SZA}(J)$ is w_{SZA} if J = j and $(1\text{-}w_{SZA})$ if I = j + 1

$w^*_{U}(K)$ is w_{U} if K = k and $(1\text{-}w_{U})$ if k = k + 1

$w^*_{CHL}(L)$ is w_{CHL} if L = l and $(1\text{-}w_{CHL})$ if L = l + 1

This interpolation is applied to derive albedo estimates for each of the 14 COART short-wave wavelengths and for a broadband albedo covering 0.4- 4.0 μm.

In step 3, the albedo estimates at the COART wavelengths are linearly interpolated to the standard wavelengths used by RRTM-SW. This step outputs:

$\rho^{RRTM} = F^{\uparrow}_{SW} / F^{\downarrow}_{SW}$ the average alebdo over the cell

$R_{SW} = F^{\uparrow}_{SW} - F^{\downarrow}_{SW}$

The latter is the short-wave net heat flux over the aggregation cell (one of the four heat components of the Net Heat Flux).

Step 4 computes an albedo correction factor as:

$$\gamma = \rho^{RRTM} / \sum_{\{n \in \text{valid pixels in cell}\}} \rho_n^{COART}$$

D43762, A. PDMO Released: 2009-09-28 (VERIFY REVISION STATUS)
PDMO

Step 4 applies the correction factor from Step 3 to each of the individual albedo estimates for the pixels within each aggregation cell:

$$\rho_n^* = \gamma \ \rho_n^{COART}$$

where ρ_n^* is the final ocean alebdo estimate

This approach constrains average of the pixel albedos over the aggregation cell to be the same as the albedo value derived by RRTM for Net Heat Flux for the entire cell, making the products consistent.

3.3. Algorithm Processing Flow

The algorithm process is summarized below:

1. Divide the input VIIRS data (M-band resolution) into horizontal cells (HC) – also referred to as aggregation cells of approximately 12 km in size.
2. For each HC:
    a. Interpolate numerical weather prediction model inputs in time and space to the center of each HC (temperature profile, moisture profile, column ozone, ocean surface wind u- and v-components)
    b. Tag each M-band VIIRS input pixel as either clear-water, clear-ice or cloudy using land-water, cloud and ice mask inputs
    c. Compute average VIIRS input EDR values over clear water pixels (sea surface temperature, chlorophyll, aerosol optical thickness); determine predominate suspended matter (aerosol) type
    d. Compute average VIIRS input EDR values over clear ice pixels (ice surface temperature, sea ice age, aerosol optical thickness); determine predominate ice age of ice pixels in cell
    e. Compute the average albedo for clear water pixels over the HC using the primary inputs of chlorophyll concentration, wind speed, and aerosol optical thickness based on look-up tables generated by the COART model
    f. Compute an initial albedo estimate for each pixel in cell using the COART LUT using the values of the primary inputs at each VIIRS m-band pixel location [See Note A]
    g. Compute the average albedo for clear ice pixels over the HC by assigning an ice albedo based on ice age to each pixel and averaging of all clear ice pixels in the HC
    h. If number of clear water pixel with valid data is greater than a minimum threshold, compute the following:
        i. sensible and latent heat fluxes with the COARE-Water model
        ii. long-wave radiative flux with the RRTM-LW model
        iii. short-wave flux with the RRTM-SW model
        iv. RRTM-derived albedo over the HC from the ratio of the up- and down-welling shortwave fluxes at the surface
    i. If number of clear ice pixel with valid data is greater than a minimum threshold, compute the following:

D43762, A. PDMO Released: 2009-09-28 (VERIFY REVISION STATUS)
PDMO

i. sensible and latent heat fluxes with the COARE-Ice model
ii. long-wave radiative flux with the RRTM-LW model
iii. short-wave flux with the RRTM-SW model

j. Compute the weighted sum of all flux components to derive the Net Heat Flux EDR
k. Compute the ocean surface albedo correction factor as the ratio of the RRTM-derived HC-averaged albedo (Step 2-e-ii) and the average of the COART-derived pixel albedo estimates over valid clear ocean pixels (Step 2-f)
l. Multiply each COART-derived pixel level albedo estimate by the correction factor of Step 2-l
m. Compute quality control mask, insert fill values if Net Heat Flux could not be computed
n. Write output Net Heat Flux EDR (Step 2-j) and Ocean Surface Albedo (Step 2-l)
o. Write other diagnostic output data including individual flux components

3. Proceed with the next HC (Step 2)

NOTE A – Solar zenith angle, optical depth and chlorophyll input at the VIIRS moderate resolution pixel locations. For NPP, wind speed is obtained from the NWP model and set for each pixel in the cell to the interpolated value at the center of the HC. During NPOESS era, wind speed is derived from MIS when available. It is envisioned that when available this will be interpolated from MIS inputs to each pixel.

The NHF Algorithm functional flow is illustrated in Figure 3-1.

D43762, A. PDMO Released: 2009-09-28 (VERIFY REVISION STATUS)
PDMO

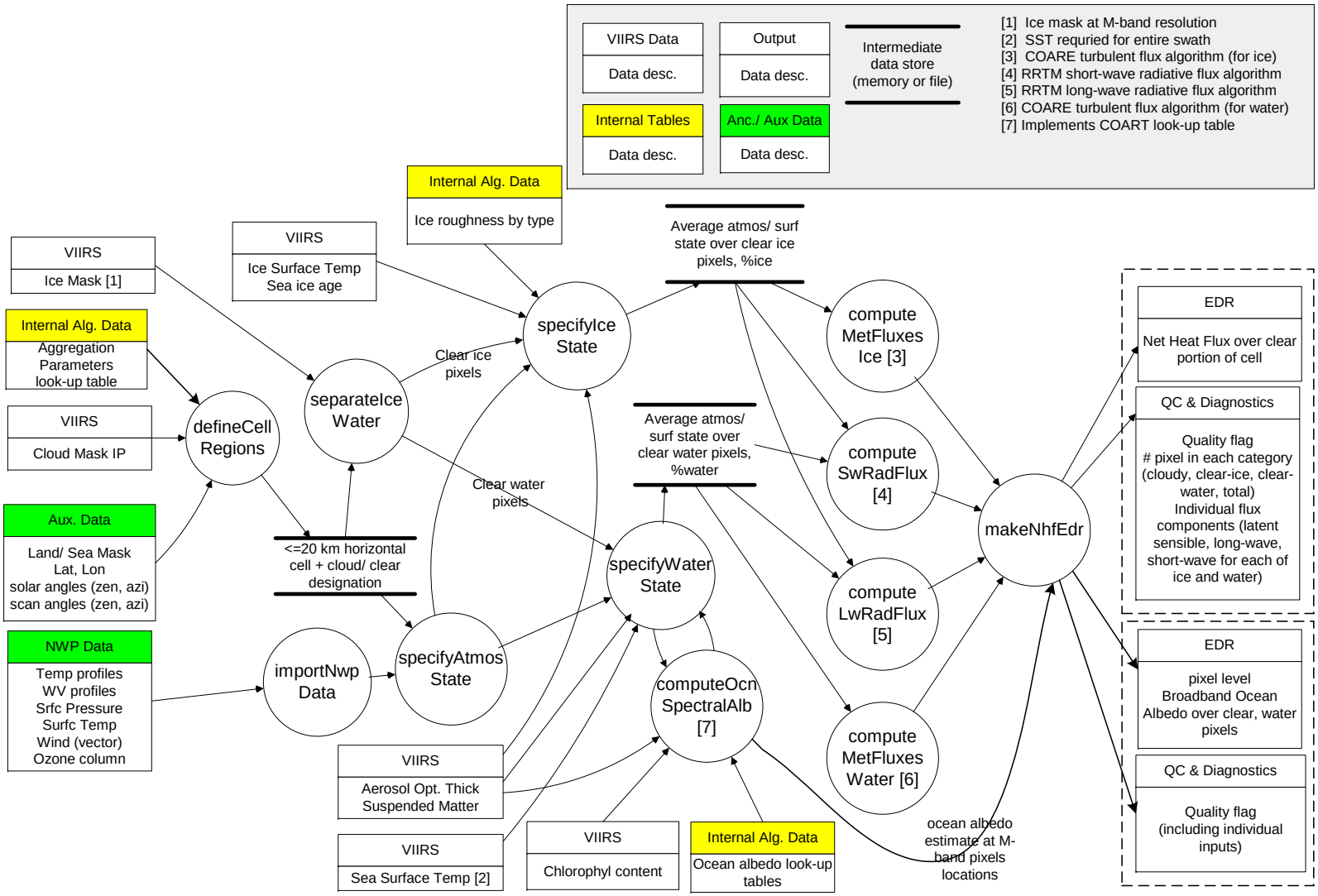

Figure 3-1 – Net Heat Flux Algorithm Functional Flow

3.3.1. Input Data

The approach is to estimate the atmospheric/surface state variables relevant for each process from NPOESS sensor data, ancillary data sources. Table 3-2 lists the key input parameters and their application to each process and for the surface types (water or ice) they are used.

The "METHOD" column indicates the approach to computing the state variables used in the model computations for each horizontal cell. Several methods are used:

- AGG ("aggregate and average"): aggregate individual VIIRS EDR values over selected subset of pixels (clear-ice or clear-water)
- INT ("interpolate"): interpolate to center of horizontal cell; for the NWP input data the interpolation is in both time and space and assumes input NWP data for times surrounding the time of the pixel observation; for MIS data, the interpolation is only in space.
- SEL ("select"): indicates a variable used to select or identify which processing how to process each pixel

Table 3-2 – Summary of Atmospheric/Surface State Variables Relevant to NHF EDR Their Sources and Applicability to Ice or Water Conditions

	Process/ Module					Sensor/ Other Source				Surface	
Parameter	LW	SW	SEN	LAT	METHOD	VIIRS	MIS	CrIMSS	NWP	Water	Ice
Sea surface temperature	X		X	X	AGG	P				X	
Ice surface temperature	X		X	X	AGG	P					X
Ocean wind speed (water/ ice)		X	X	X	INT		P/ none [B]		S/ P [B]	X	X
Surface air temp.	[A]	[A]	X	X	INT			P3I	P	X	X
Surface humidity	[A]	[A]	X	X	INT			P3I	P	X	X
Atmos. temperature profile	X	X			INT			P3I	P	X	X
Atmos. moisture profile	X	X			INT			P3I	P	X	X
Aerosol type and optical depth	-	X			AGG	P				X	X
Ozone	X	X			INT				P [C]		
Cloud mask	X	X	X	X	SEL	P				X	X
Ice mask	X	X	X	X	SEL	P				X	X
Ice age	X	X	X	X	SEL	P					X

D43762, A. PDMO Released: 2009-09-28 (VERIFY REVISION STATUS)
PDMO

Parameter	Process/ Module				METHOD	Sensor/ Other Source				Surface	
	LW	SW	SEN	LAT		VIIRS	MIS	CrIMSS	NWP	Water	Ice
Chlorophyll		X			AGG	P				X	
Solar zenith angle		X			AGG	[D]				X	X

Key: LW = long-wave radiative flux; SW = short-wave radiative flux; SEN = sensible heat flux; LAT = latent heat flux; EXEC = needed for algorithm executive to control execution

Process/Module denotes which inputs are relevant to each flux process: X denotes primary input;

METHOD denotes how the quantities are computed for the HCs: AGG == aggregate and average VIIRS EDRs over appropriate pixel subsets; INT = interpolate in time and space the NWP data to center of horizontal

Sensor/Other Source denotes sources of the data: P = primary source; S = secondary source; P3I = possible future P3I source

Surface denotes which inputs are relevant to ice or water surface conditions: X = input used

Notes: [A] The surface humidity, air temperature is treated as part of the profile for the radiative fluxes. [B] MIS is the preferred source over water, but is not available for NPP and NPOESS C1. NWP will be the primary NPP source. Only NWP can determine wind speed over ice. [C] NWP model ozone is the primary source, but OMPS could be P3I. [D] Solar zenith angle is taken from VIIRS auxiliary file.

During the NPP and NPOESS C1 Era, wind speed data is provided exclusively from numerical weather prediction model input (NWP). As this parameter is a key driver of EDR accuracy/ precision, the most timely model data should be used. We have performed our testing with the NCEP Global Forecast Model (GFS).

During the NPOESS Era, the primary source of ocean wind speed is from the available microwave imager. It is recommended that a fallback mode be developed that uses NWP data when no MIS data is available even for the NPOESS era.

3.3.2. Output Data

Table 3-3 and Table 3-4 list the key output products from the NHF and Ocean Surface Albedo algorithms. They data are divided into three categories:

- EDR is a required EDR parameter
- QC is a quality control value recommended for delivery at all times
- DIAG is a diagnostic value that will be required during Cal/Val, algorithm tuning, and operational trouble shooting

The DIAG values listed below may be strongly desired by many operational users as well, although we note they are not explicitly listed as EDR requirements.

Table 3-3 – Net Heat Flux Output Product Summary

D43762, A. PDMO Released: 2009-09-28 (VERIFY REVISION STATUS)
PDMO

Product	Units	Type	Description
Net heat flux total	W/ m^2	EDR	Net heat flux (positive means transfer of heat from surface to atmosphere) from water and ice surfaces
Ocean surface albedo	Unitless (fraction)	IP	Integrated albedo over solar spectrum at ocean water surface based on F_{up} / F_{down} where F_{up} and F_{down} are the net solar fluxes at the water surface, fill if no clear water pixels in cell
Latitude	Deg.	EDR	At center of horizontal cell (positive direction is East and North)
Longitude	Deg.	EDR	
Quality bit mask	N/A	QC	See software documentation for details
Total # of VIIRS M-band pixels in horizontal cell		DIAG	Can be used to determine fraction of cell in each category
# of clear pixels in cell		DIAG	
# of clear pixels with ice surface		DIAG	
# of clear pixels with water surface	N/A	DIAG	
Latent flux over water	W/ m^2	DIAG	Individual flux components. When no pixels of either water or ice are present the appropriate flux values are replaced with fill values. Short-wave flux is fill value at nighttime.
Sensible flux over water	W/ m^2	DIAG	
Long-wave flux over water	W/ m^2	DIAG	
Short-wave flux over water	W/ m^2	DIAG	
Latent flux over ice	W/ m^2	DIAG	
Sensible flux over ice	W/ m^2	DIAG	
Long-wave flux over ice	W/ m^2	DIAG	
Short-wave flux over ice	W/ m^2	DIAG	

D43762, A. PDMO Released: 2009-09-28 (VERIFY REVISION STATUS)
PDMO

Table 3-4 – Ocean Surface Albedo Output Product Summary

Product	Units	Type	Description
Ocean surface albedo	Unitless (fraction)	IP	Obtained via the COART LUT using pixel level parameters of solar zenith angle, optical depth, ocean color/chlorophyll, and wind speed, and adjusted susing flux-derived aggregated albedo, fill if not a valid clear water pixel
Latitude	Deg.	EDR	(positive direction is East and North)
Longitude	Deg.	EDR	
Quality bit mask	N/A	QC	See software documentation for details

3.3.3. Internal Data, Look-up Tables, Etc.

The following are the key internal data are used by the various algorithm components.

Table 3-5 – Summary of Key Internal Data (Static) Used by the Algorithm

Data	Used by	Desc.
Ice roughness by ice age	Driver for COARE	Standard algorithm external configuration file
Ice albedo by age	Driver for RRTM-SW	Standard algorithm external configuration file
Horizontal cell aggregation tables	HC construction function	Standard algorithm external configuration file
Ocean surface albedo look up tables	Ocean surface albedo interpolation code	External binary files (data and weights)
RRTM shortware gas absorption characteristics	RRTM-SW	External text file, also available as FORTRAN BLOCK DATA statements in code
RRTM longwave gas absorption characteristics	RRTM-LW	External text file, also available as FORTRAN BLOCK DATA statements in code
RRTM aerosol models	RRTM-SW	FORTRAN BLOCK DATA statements in code

D43762, A. PDMO Released: 2009-09-28 (VERIFY REVISION STATUS)
PDMO

4. Algorithm Testing and Performance

4.1. Overall Approach

We performed two types of testing (in additional to algorithm sensitivity analysis) of the algorithm:

- Testing with real data from EOS
- Testing with simulated data

The real data testing is designed to demonstrate functional and physically reasonable operation of the algorithm. Since ground truth data are not available it is not possible to derive quantitative accuracy and precision values for the NHF algorithm using this testing method.

For this reason, we also employ testing with simulated scenes. Using simulated testing a more complete range of atmospheric conditions can be evaluated and complete control over all error sources is obtained. Most importantly, the truth is known and so complete performance (accuracy and precision) can be determined. We explicitly budget for model uncertainties based on validation of the two physical models employed by the algorithm (RRTM and COARE) and so these sources of error are not neglected.

4.2. Real Data Scene-Based Testing with Proxy Sensor/Product Input Data

We performed testing with the scenes listed in Table 4-1. The input parameters were derived from the data sources listed in Table 4-2.

Table 4-1 – Test Scenes for Real Data Testing

Scene #	Location	Time	Day/ Night	Scene and Derived EDR	Scatter Plot
R1	Indian Ocean	October 2003	Day	Figure 4-1	Figure 4-2
R2	Tropical Pacific	December 2003	Day	Figure 4-3	Figure 4-4
R3	North Atlantic	August 2003	Day	Figure 4-5	Figure 4-6
R4	Tropical Atlantic	July 2003	Night	Figure 4-7	Figure 4-8
R5	Hudson Bay	May 2003	Night	Figure 4-9	Figure 4-10

Table 4-2 – Data Sources of Key Input Variables for Real data Testing

Input	Source
SST	MODIS SST product
Cloud mask	MODIS cloud mask
Ice mask	From MODIS cloud mask

D43762, A. PDMO Released: 2009-09-28 (VERIFY REVISION STATUS)
PDMO

IST	MODIS IST product
Aerosols	MODIS aerosol product
Ocean surface wind speed	NCEP Global Forecast Model (GFS)
Temperature/ moisture profiles	NCEP Global Forecast Model (GFS)
Ozone	NCEP Global Forecast Model (GFS)
Chlorophyll	MODIS Ocean Color product (not all scenes)

The data for each scene are presented as a pair of figures. The first figure of each pair has six images 2 across by 3 down: upper left shows the SST (a primary input); upper right shows the Net Heat Flux (final EDR) and the bottom four images show the individual flux components (short-wave, long-wave latent and sensible). The second figure of each pair presents a set of scatter plots showing the derived fluxes versus key input variables.

Scene R1 (Figure 4-1 and Figure 4-2) is a very clear scene of the Indian Ocean partially observing the Indian subcontinent. The Net Heat Flux ranges mostly between -500 and +500 W/m^2 with some values higher than 500 W/m^2. Consistent with the generally clear conditions and low aerosols, there is a high negative shortwave flux. As expected, the long-wave and sensible fluxes show a moderate positive correlation with SST. The latent and sensible fluxes show a negative correlation with air-sea temperature difference and a positive correlation with wind speed, as expected. The correlation with aerosol optical thickness is not as clear, but indicates a small positive correlation at lower optical thicknesses and little or no correlation for the higher. This is probably due to the association of the aerosol conditions with other meteorological variables that drive the fluxes.

Inspection of the results for the other scenes likewise indicates physically consistent behavior with reasonable output values for both total flux and the individual flux components.

A set of tools were developed for this portion of the testing that create the NHF input data sets from HDF-EOS files from the EOS DAC for Aqua or Terra satellites. These tools could facilitate more extensive testing.

Figure 4-11presents Ocean Surface Albedo for the September 2003 North Atlantic Scene, R3. The top two panels are for the full scene (the Ocean Surface Albedo IP on the left and chlorophyll input on the right), with the bottom a zoom of the lower right corner. In the chlorophyll image black pixels, including the dark swath running down the center, are fill values that were replaced by a default chlorophyll value of 0.1 mg/ cm^3. Figure 4-12 shows scatter plots of key variables.

D43762, A. PDMO Released: 2009-09-28 (VERIFY REVISION STATUS)
PDMO

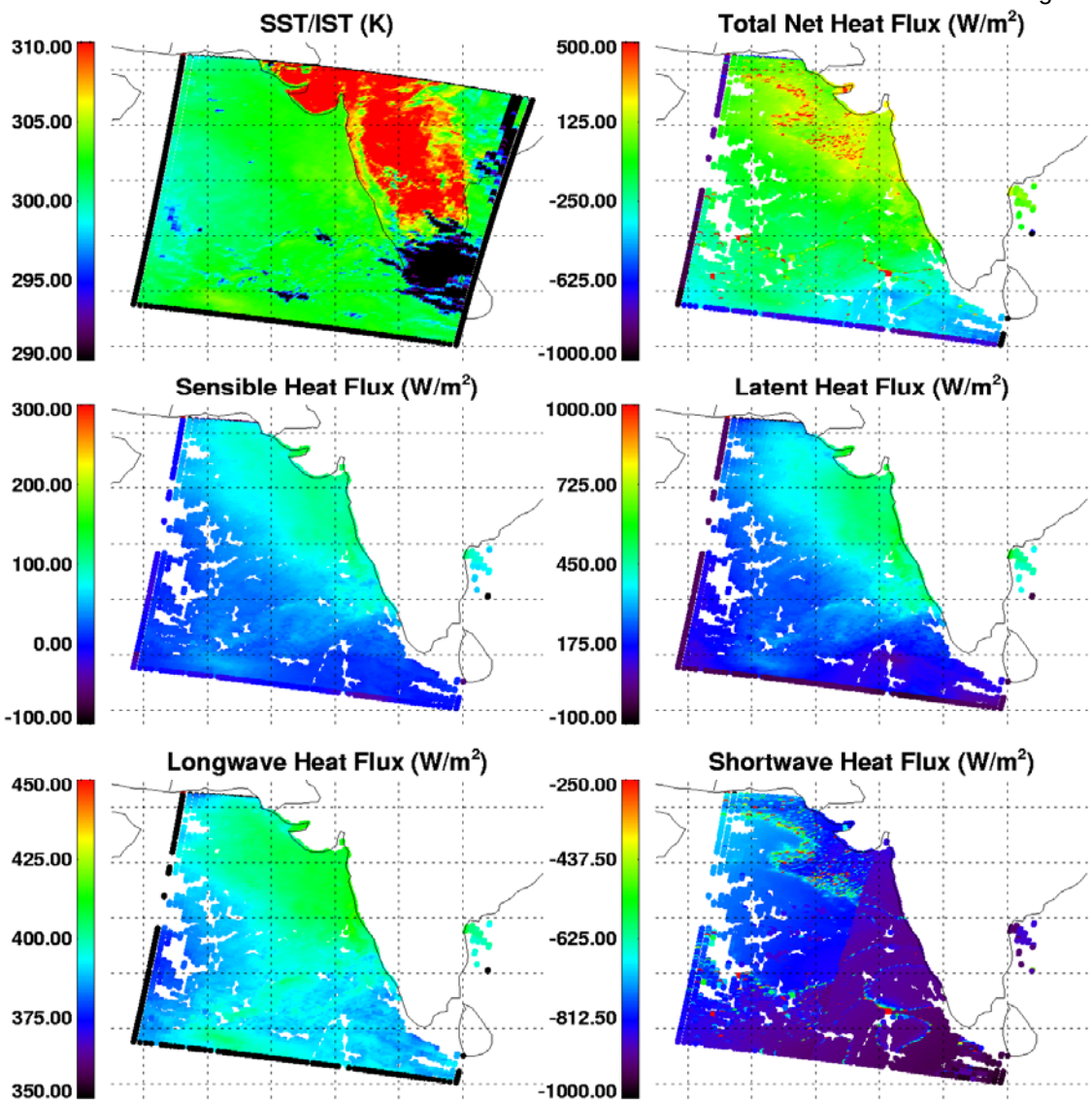

Figure 4-1 – Fluxes and SST over the Indian Ocean (October 2003)

D43762, A. PDMO Released: 2009-09-28 (VERIFY REVISION STATUS)
PDMO

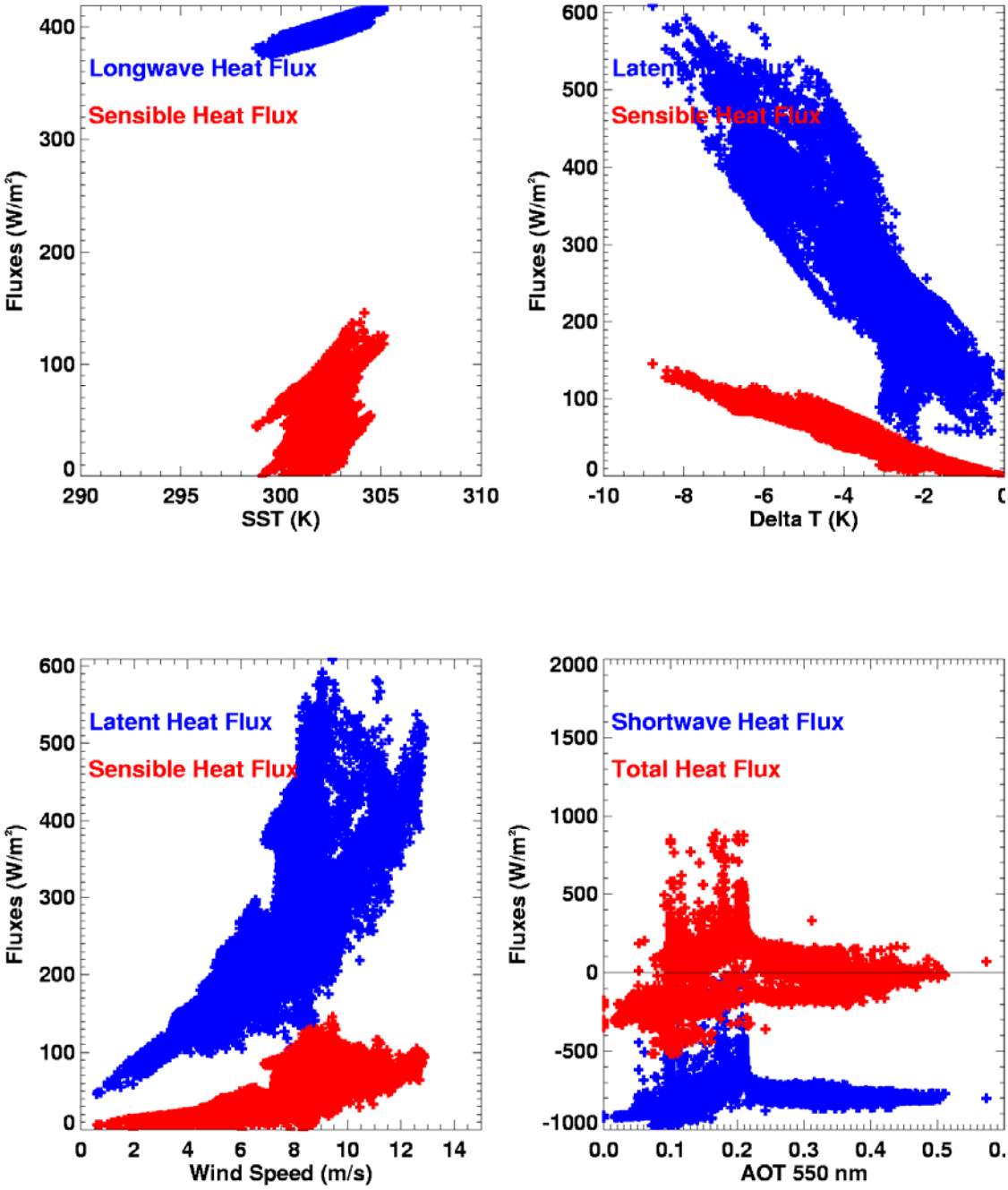

Figure 4-2 – Fluxes vs input parameters over the Indian Ocean (October 2003)

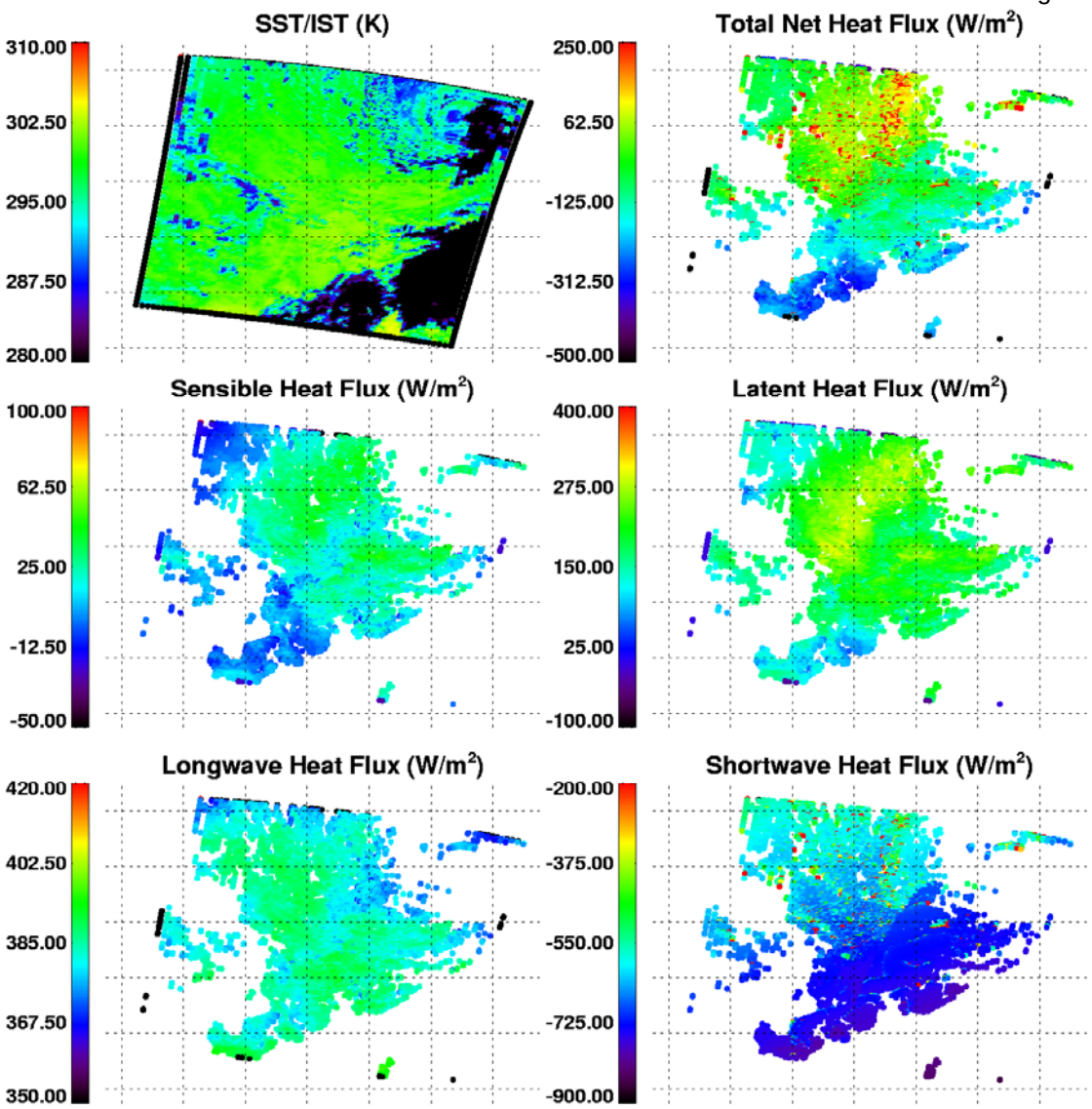

Figure 4-3 – SST and Heat Fluxes over the Tropical Pacific (December 2003)

D43762, A. PDMO Released: 2009-09-28 (VERIFY REVISION STATUS)
PDMO

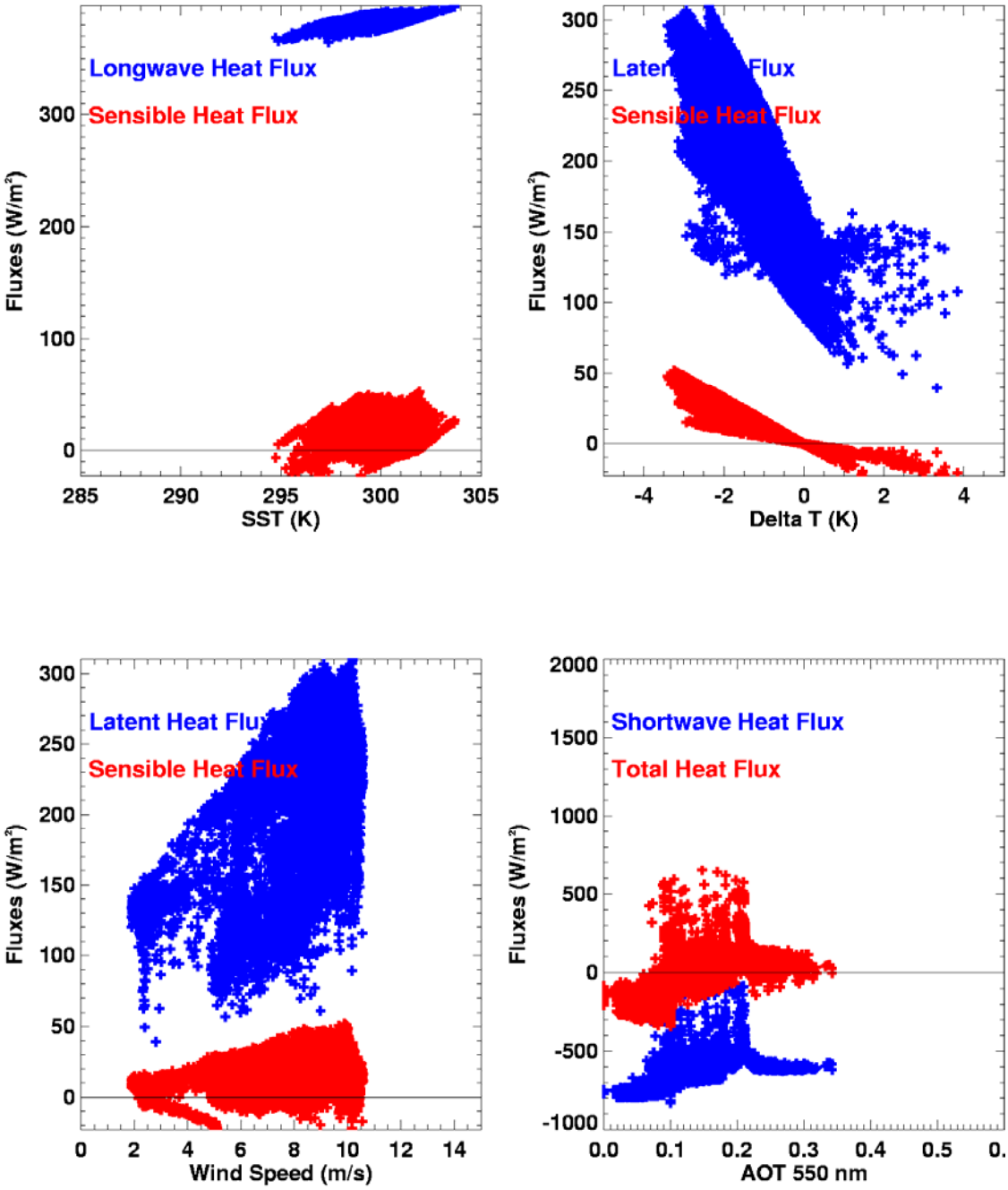

Figure 4-4 – Input Parameters and Heat Fluxes over the Tropical Pacific (December 2003)

D43762, A. PDMO Released: 2009-09-28 (VERIFY REVISION STATUS)
PDMO

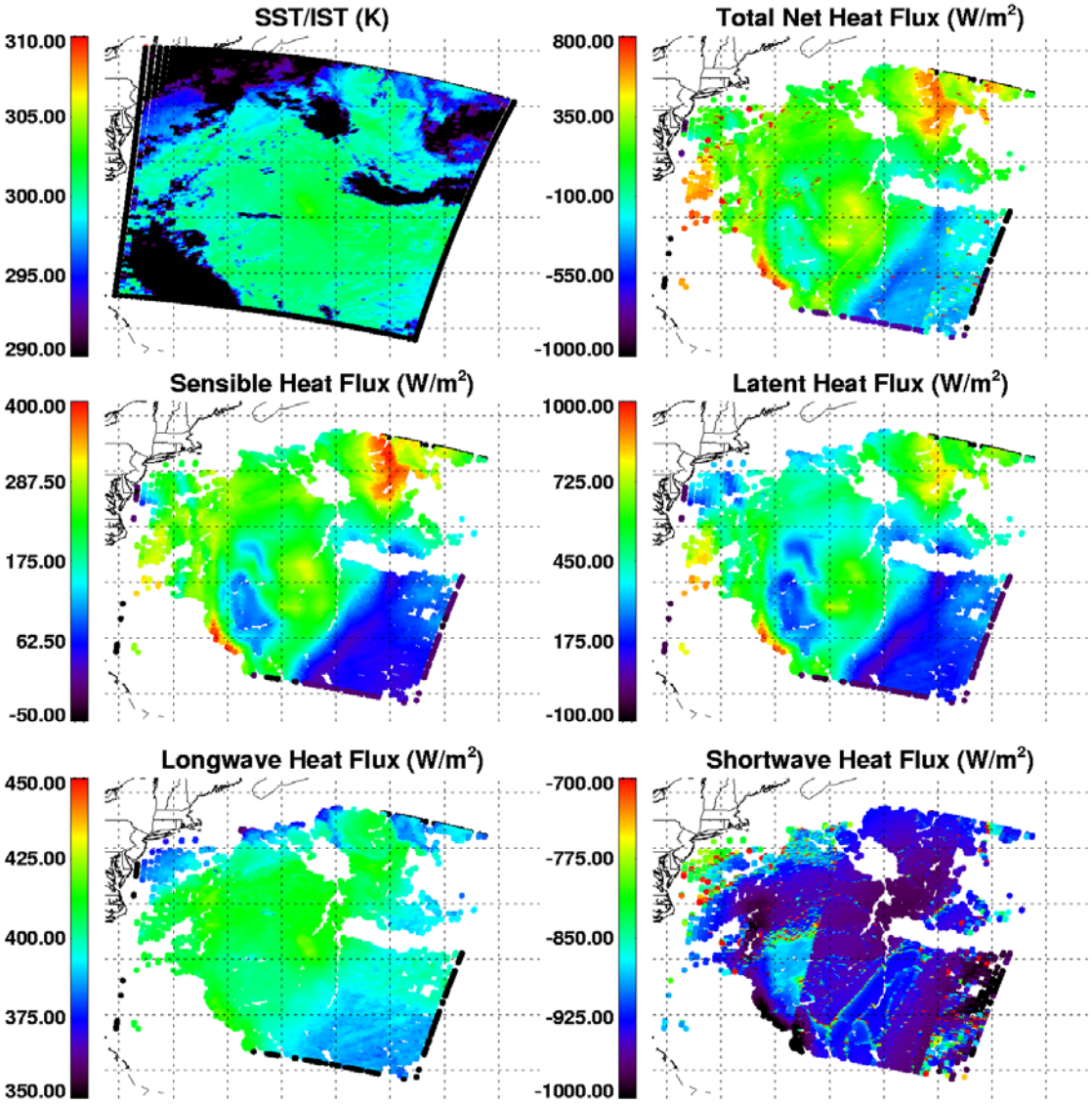

Figure 4-5 – SST and Heat Fluxes over the North Atlantic (August 2003)

D43762, A. PDMO Released: 2009-09-28 (VERIFY REVISION STATUS)
PDMO

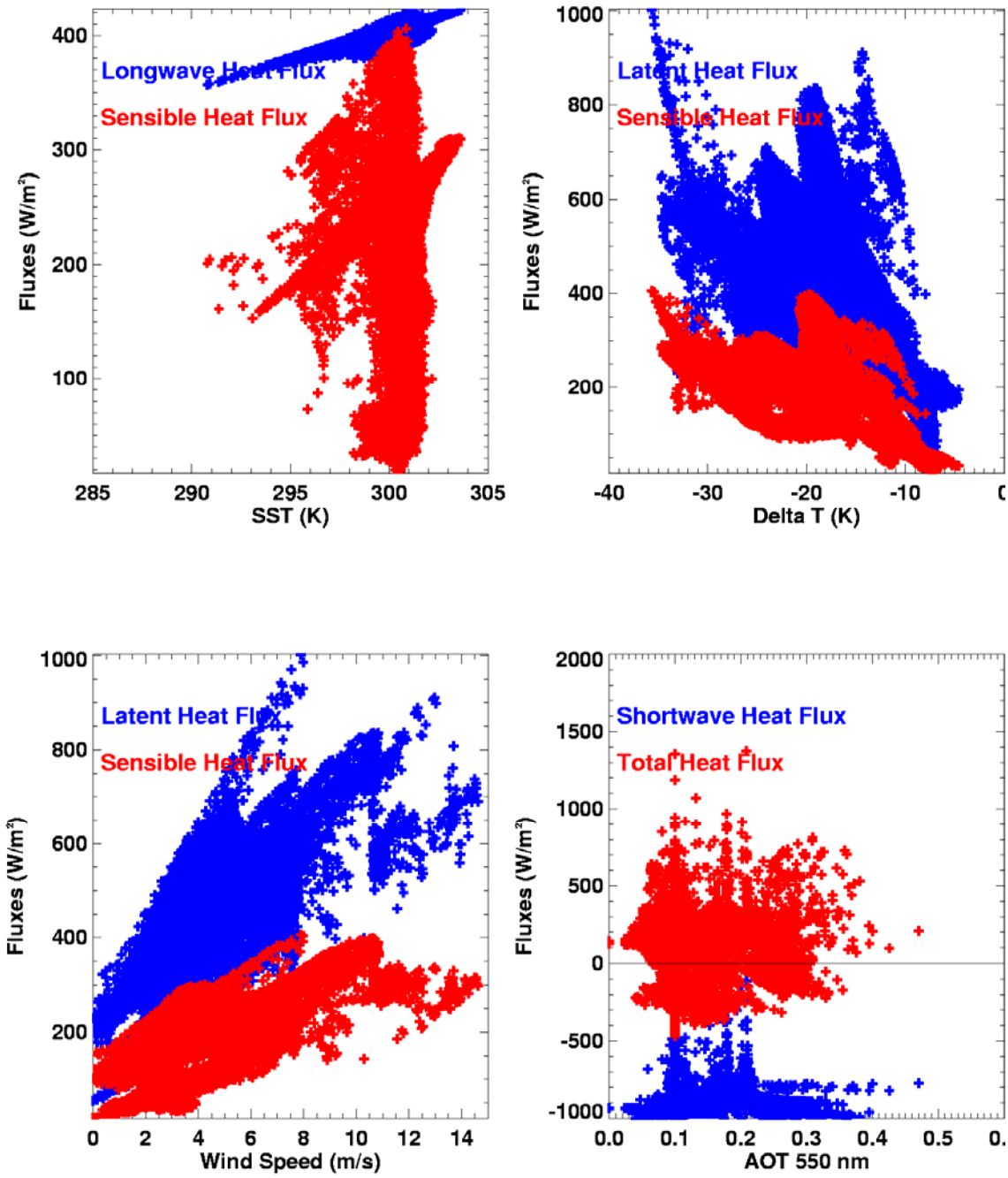

Figure 4-6 – Input Parameters and Heat Fluxes over the North Atlantic (August 2003)

D43762, A. PDMO Released: 2009-09-28 (VERIFY REVISION STATUS)
PDMO

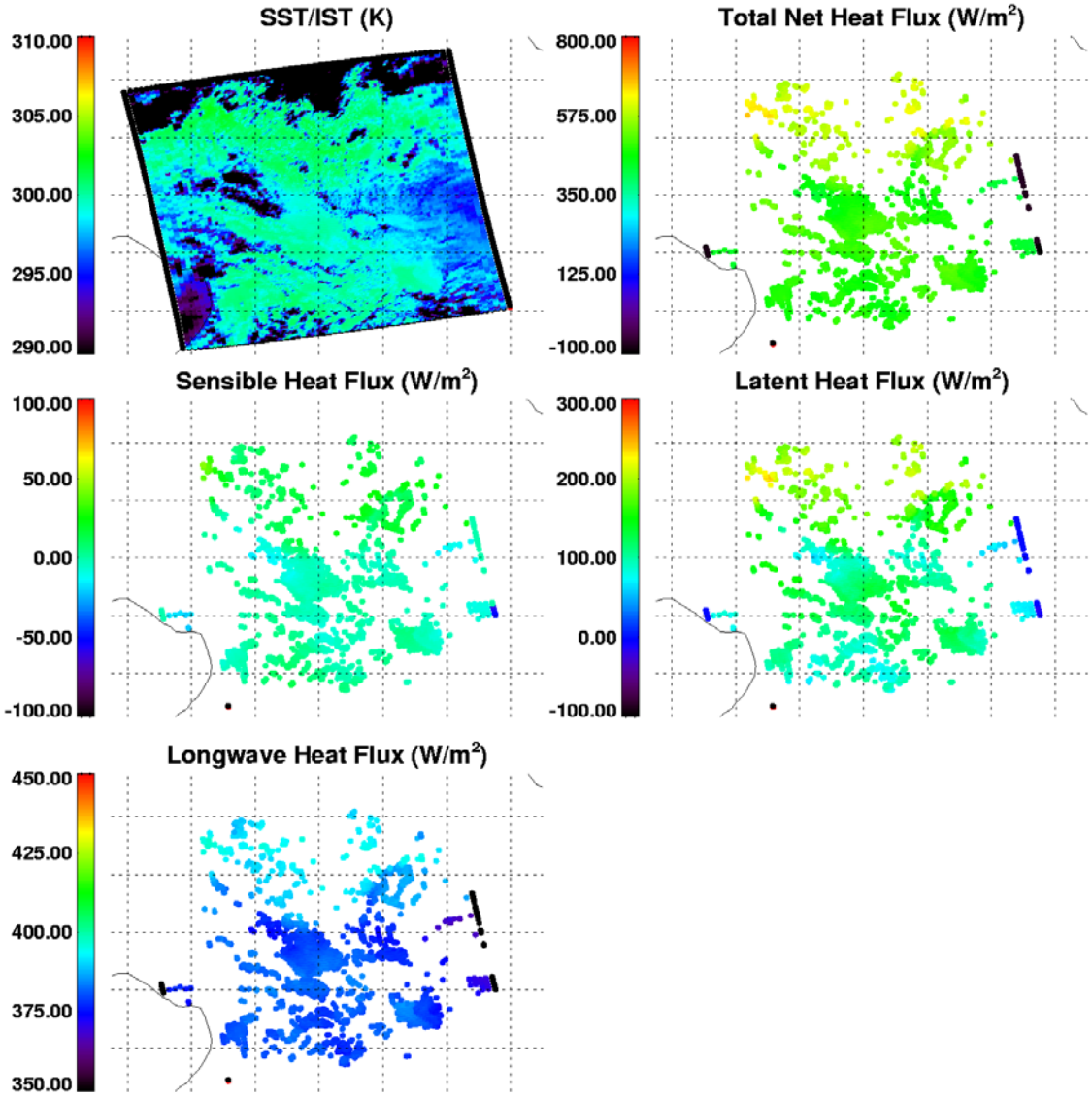

Figure 4-7 – Nighttime SST and Fluxes over the Tropical Atlantic (July 2003)

D43762, A. PDMO Released: 2009-09-28 (VERIFY REVISION STATUS)
PDMO

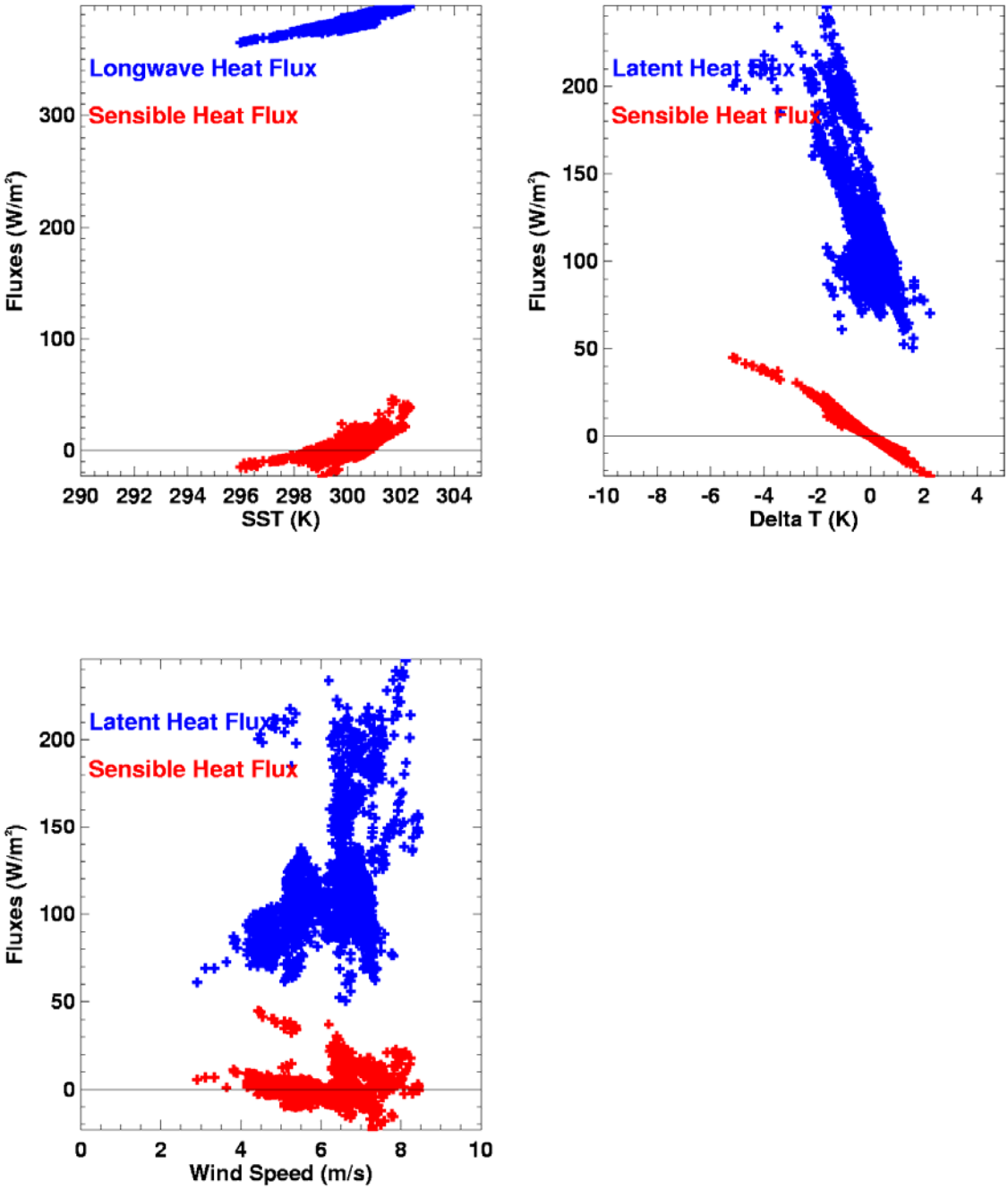

Figure 4-8 – Nighttime Input Parameters and Heat Fluxes over the Tropical Atlantic (July 2003)

D43762, A. PDMO Released: 2009-09-28 (VERIFY REVISION STATUS)
PDMO

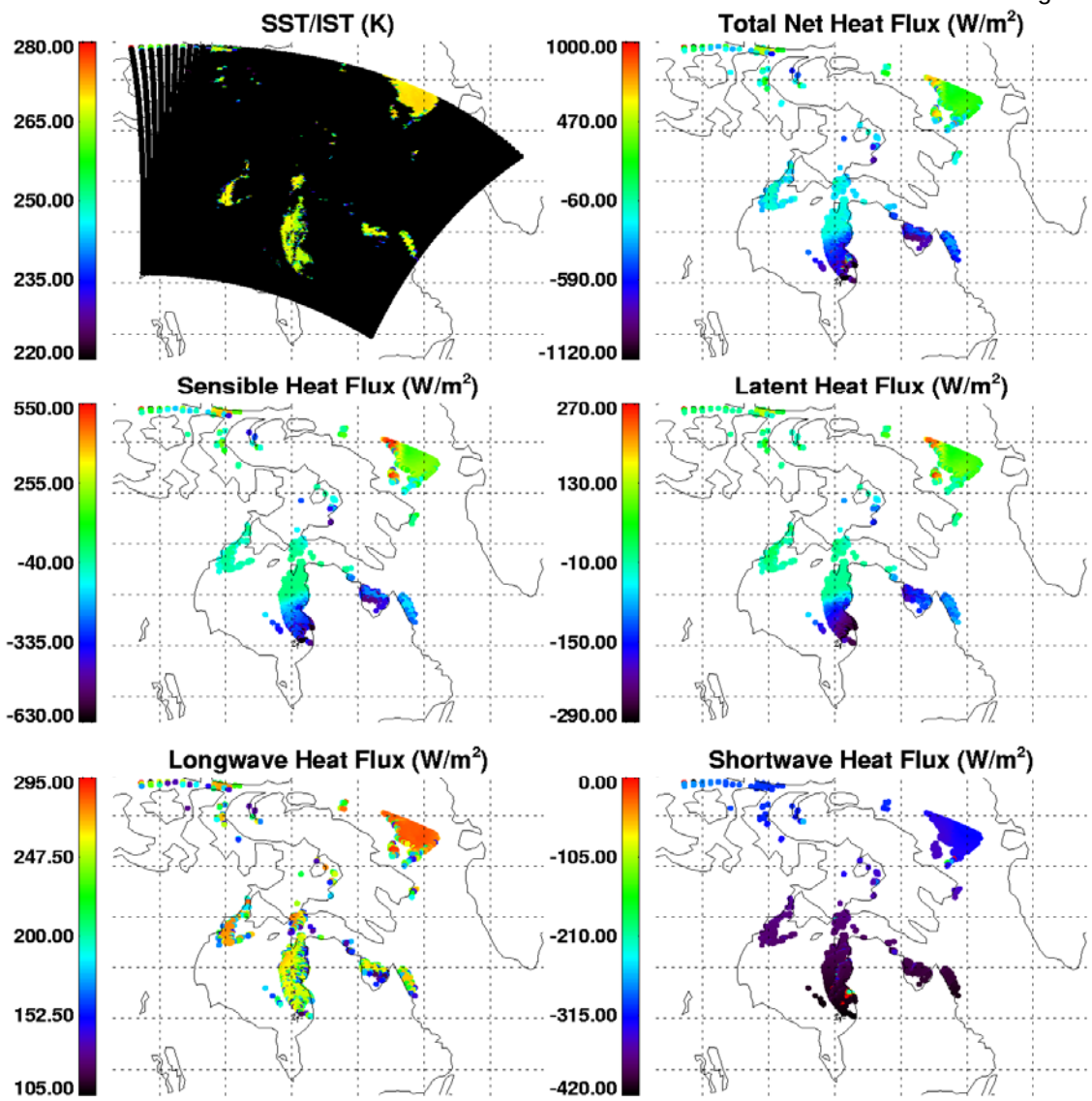

Figure 4-9 – IST and Heat Fluxes in the Hudson Bay Area (May 2003)

D43762, A. PDMO Released: 2009-09-28 (VERIFY REVISION STATUS)
PDMO

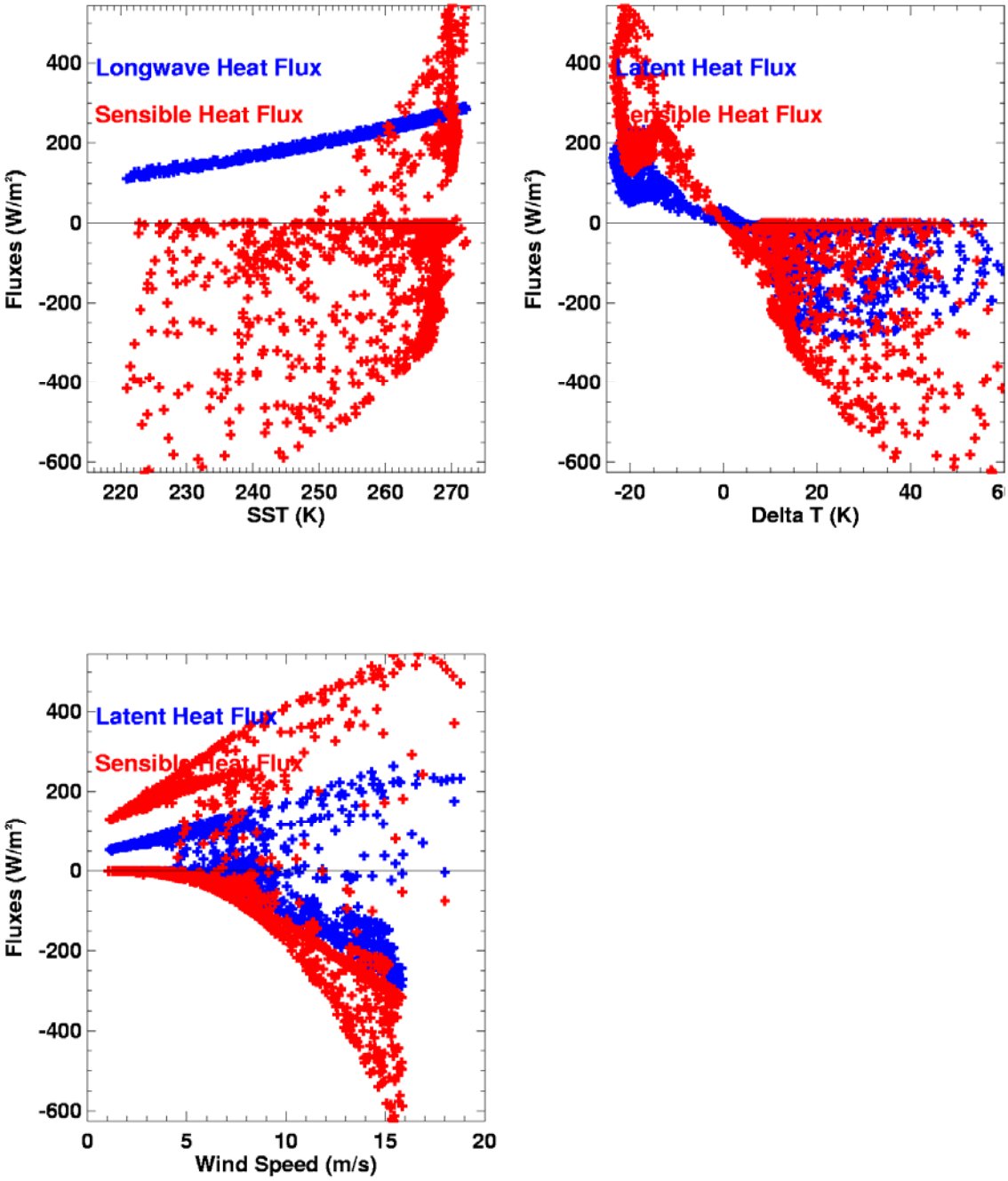

Figure 4-10 – Heat Fluxes vs Input Parameters in the Hudson Bay Area (May 2003)

D43762, A. PDMO Released: 2009-09-28 (VERIFY REVISION STATUS)
PDMO

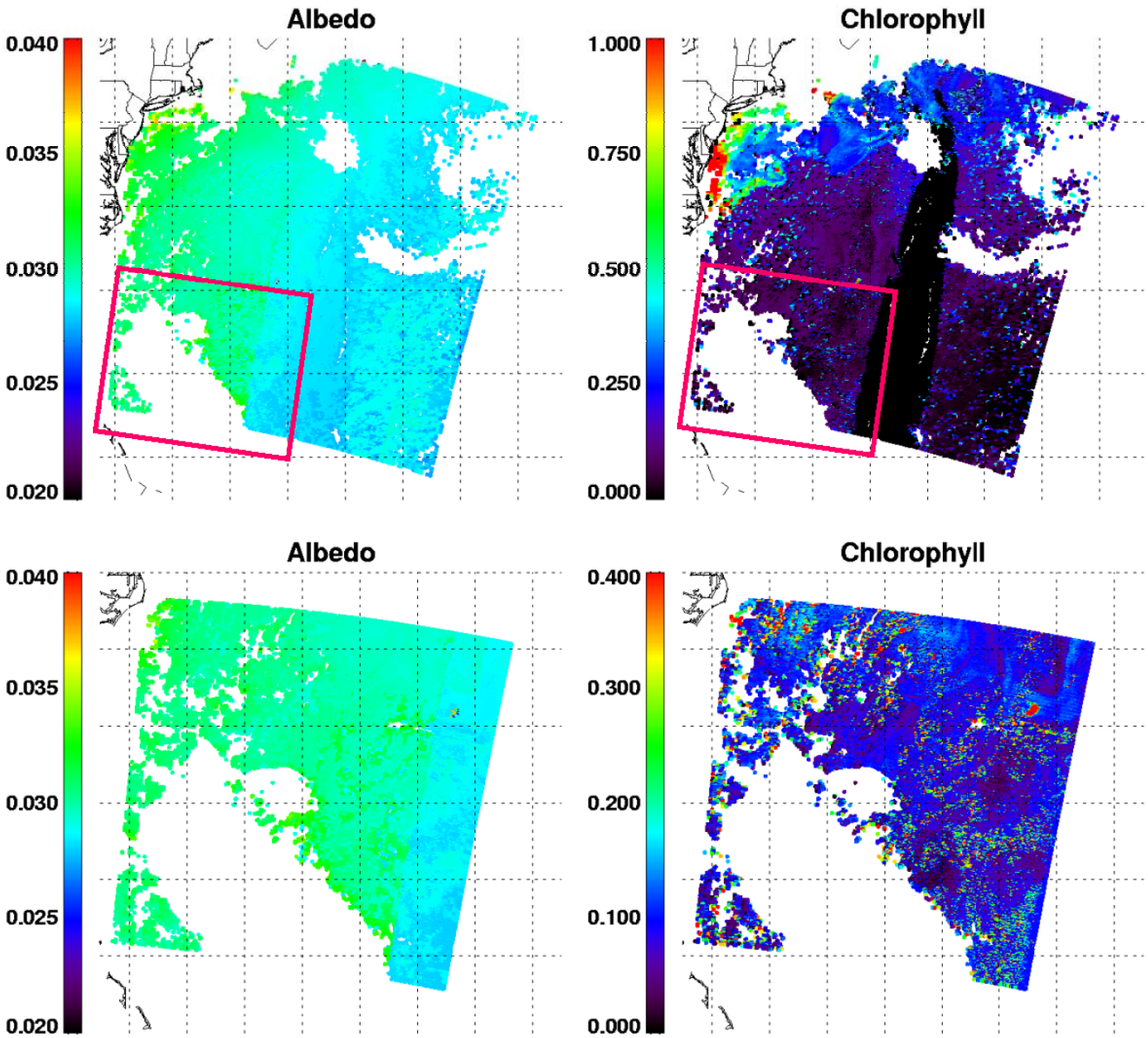

Figure 4-11 – Ocean Surface Albedo Product (left) and Chlorophyll Input (right). Upper two images are entire North Atlantic Scene (R3); lower two images are zooms of area marked in red. Albedo units are fraction. Chlorophyll units are mg/cm^3.

D43762, A. PDMO Released: 2009-09-28 (VERIFY REVISION STATUS)
PDMO

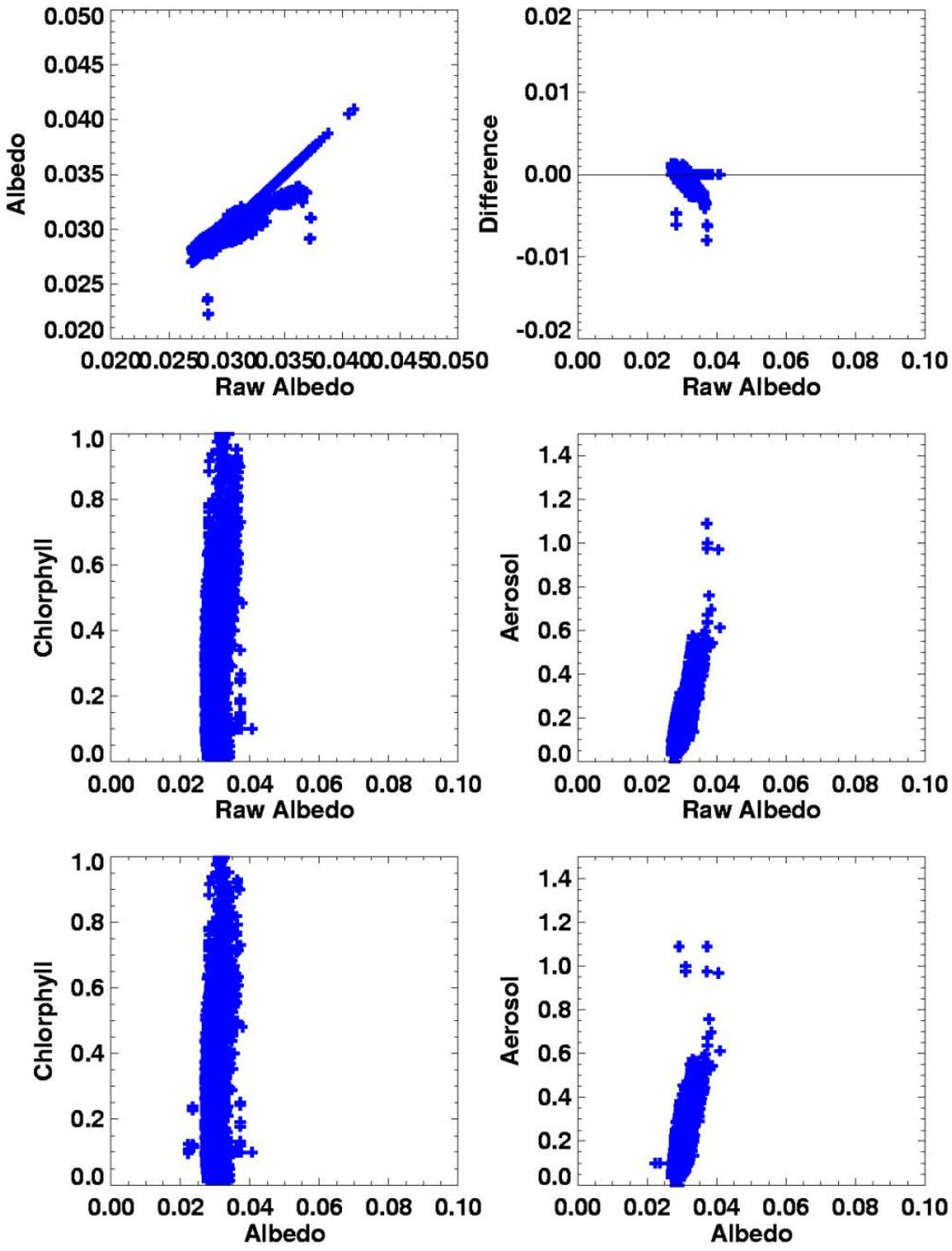

Figure 4-12 – Scatter plots corresponding to Figure 4-11. Albedo is the final corrected product that is the deliver IP. Raw albedo is the direct output of the COART LUTs. Chlorophyll units are g/cm^3. Aerosol is the optical depth (unitless).

D43762, A. PDMO Released: 2009-09-28 (VERIFY REVISION STATUS)
PDMO

4.3. Performance Testing with Simulated Data

Net heat flux is a derived EDR; it is calculated from retrieved values of several NPOESS EDRs, both from VIIRS and other NPOESS sensors, or from NWP model results, when some or all of the required inputs parameters are not available from measurements. Thus the error in net heat flux may often be driven mainly by errors in non-VIIRS inputs. Previous studies (AIPT-36) have indicated that the significant uncertainties in many of the necessary input parameters (e.g., air temperature and water vapor content, aerosol model) lead to large uncertainties in net heat flux. This analysis attempts to quantify the magnitudes and sources of both VIIRS and non-VIIRS errors by examining the retrieval errors in a synthetic scene with known "truth" values. Three different error "scenarios" are analyzed:

- VIIRS only: includes only errors from VIIRS parameters (e.g., SST, AOT)
- Reduced: includes errors from all input parameters, reduced from the baseline estimate by 50%
- Baseline: includes errors from all input parameters, estimated from current sensor and model capabilities

The "Baseline" case represents expected performance on a Horizontal Cell basis for current estimated NPOESS capabilities. The "Reduced" cases indicate a range of potential improvement for future reduction in errors of contributing EDRs and NWP model inputs. Finally since most errors are from other than VIIRS-derived inputs, the "VIIRS-only" case indicates that portion of the error due to the VIIRS sensor.

4.3.1. Methodology

In order to create the synthetic scene, a significant number of ECMWF profiles were selected; these profiles covered a wide range of physical conditions, from tropical to Arctic. They contained most of the necessary inputs for heat flux calculations; aerosol model optical depth, chlorophyll concentration, and solar zenith angle. Inputs required by the shortwave flux algorithm, were generated separately for each profile by random selection from uniformly distributed values over physically meaningful ranges. Two subsets were created: one for heat flux calculations over water, with 200 profiles, and another, with colder, drier profiles (85), for heat flux over ice. Each profile was then perturbed 100 times, by adding a randomly generated bias and error to each input parameter. Both the bias and the error obeyed Gaussian distributions with zero means and standard deviations listed in Table 4-3.

D43762, A. PDMO Released: 2009-09-28 (VERIFY REVISION STATUS)
PDMO

Table 4-3 – Input parameter error specification for synthetic scenes

Parameter	Truth Variable Selection		Applied Errors					
	Source	**Range**	**Error model**	**Units**	**BIAS**	**SD**	**Src**	**Notes**
Surface skin temp, ice	ECMWF-PROF	[Note A]	Gaussian	K	0.20	0.6	VIIRS	
Surface skin temp, sea	ECMWF-PROF	[Note A]	Gaussian	K	0.10	0.27	VIIRS	
SZA	uniform-random	0-85 deg,	none	deg	N/A	N/A	VIIRS	day only
Wind speed	ECMWF-PROF	[Note A]	Gaussian	m/s	0.4	1.00	CMIS	
Atmos temp	ECMWF-PROF	[Note A]	Gaussian	K	0.30	1.00	NWP	
Atmos/moisture	ECMWF-PROF	[Note A]	Gaussian	%	5.0%	10.0%	NWP	
Ozone (from NWP) -- baseline	ECMWF-PROF	total column	Gaussian		10	10	NWP	O3'(p) = O3(p) + O3(p) * O3err/ O3col
AOT (over ice)	uniform-random	0.05 to 1.0	Gaussian	unitless	0	0.05+.2* tau	VIIRS	
AOT (over water)	uniform-random	0.05 to 1.0	Gaussian	unitless	max(0.02,0.07-0.015* tau)	0.3	VIIRS	
Aerosol Model	random	70%: maritime	Gaussian	n/a	n/a	85%	VIIRS	[Note B]
		6%: Dust	Gaussian	n/a	n/a	85%	VIIRS	[Note B]
		6%: Sand	Gaussian	n/a	n/a	85%	VIIRS	[Note B]
		6%: Volcanic ash	Gaussian	n/a	n/a	85%	VIIRS	[Note B]
		6%: Smoke	Gaussian	n/a	n/a	85%	VIIRS	[Note B]
		6%: SO2	Gaussian	n/a	n/a	85%	VIIRS	[Note B]
Chlorophyll	random (select class), uniform-random within class	60%: 0.1-1 mg/m3	Gaussian	mg/m^3	15%	20%	VIIRS	
		30%: 1.0-10.mg/m3	Gaussian	mg/m^3	30%	30%	VIIRS	
		10%: 10-50 mg/m3	Gaussian	mg/m^3	50%	50%	VIIRS	

Note A - Atmospheric variables are taken from the subset of ECMWF profiles applicable to water or ice

Note B – Std. Dev. in this case indicates the probability of correctly classifying the aerosol type (85%). When incorrect (15%) another type is randomly selected.

D43762, A. PDMO Released: 2009-09-28 (VERIFY REVISION STATUS)
PDMO

4.3.2. Specification Errors

Our first objective was to evaluate the impact on the net heat flux retrievals of errors in VIIRS parameters alone. This was accomplished by perturbing the input parameters obtained from VIIRS: SST and aerosol optical depth and model (VIIRS only scenario). The results of the nighttime case over water can be seen in Figure 4-13 through Figure 4-18, which display the error as a function of the "true" (unperturbed) flux and the accuracy, precision and uncertainty binned by the flux value. Longwave, latent, sensible and net heat fluxes are plotted, with the convention that upward fluxes are positive.

Slight errors in the longwave fluxes and moderate errors in the latent and sensible heat fluxes lead to errors in net heat flux well within the specified requirements for accuracy, precision and uncertainty. These results also illustrate two aspects of the error analysis that will recur repeatedly: the longwave flux can be obtained within 2 W/m^2 of "truth", and the latent heat flux error will drive the uncertainty in net heat flux over water, especially where the latent heat flux is strong.

Daytime fluxes require a shortwave flux calculation (Figure 4-17). The new total (Figure 4-18) is the sum of the longwave, latent, and sensible fluxes from the nighttime case and the shortwave flux. Even with the added uncertainty due to errors in the aerosol model and optical depth, the daytime net heat flux uncertainty assuming only errors in VIIRS parameters remains within the requirements.

Next we examined the error in net heat flux with reduced hypothetical values for the input errors. The standard deviations of the input errors were reduced by half and the synthetic scenes were recreated (Baseline Reduced). Figure 4-19 through Figure 4-24 (similar to Figure Figure 4-13 through Figure 4-18) present the results of this exercise: the requirements are met or nearly met for all values of net heat flux, day or night, and the average over the entire scene yields an uncertainty below the required threshold. This result suggests that significant progress needs to be made in the retrieval algorithms for the net heat flux input parameters before the requirements can be met.

Finally, we added perturbations to all input parameters using the current baseline specification errors (Baseline). The results appear in Figure 4-25 through Figure 4-30. The uncertainty estimates confirm the conclusions of earlier studies: given the current uncertainties in the required input parameters it is not possible to meet the net heat flux requirements. While this is discouraging, it must be kept in mind that in this analysis the errors have been allowed to vary independently, while in reality they are all somewhat correlated; thus we have probably determined an upper limit for net heat flux uncertainty, rather than a true estimate.

Table 4-4 summarizes the results from the three error scenarios.

D43762, A. PDMO Released: 2009-09-28 (VERIFY REVISION STATUS)
PDMO

Table 4-4 – Uncertainties in net heat flux and its components for each error scenario

	VIIRS Only	Reduced Baseline	Baseline
Longwave (W/m^2)	1.5	0.8	1.6
Latent (W/m^2)	8.3	22.8	45.5
Sensible (W/m^2)	3.5	6.7	13.4
Night Net (W/m^2)	13.0	27.1	53.9
Shortwave (W/m^2)	10.3	6.4	10.5
Day Net (W/m^2)	16.6	28.2	55.8

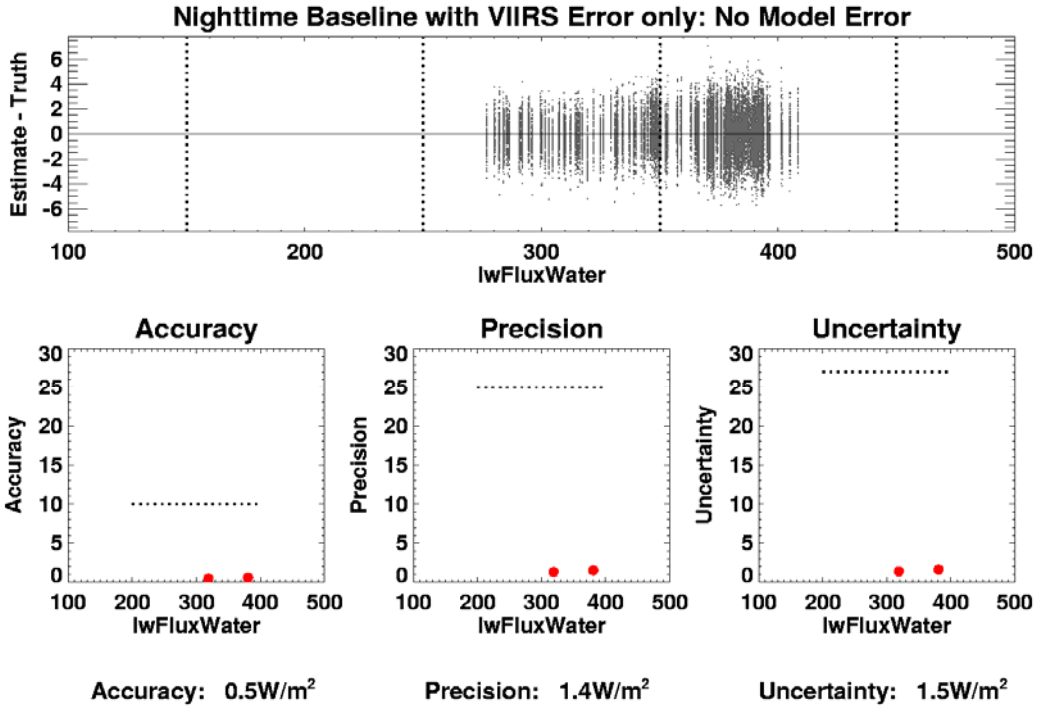

Figure 4-13 – Errors in Longwave Flux Due to Errors in VIIRS Parameters Only (SST).

D43762, A. PDMO Released: 2009-09-28 (VERIFY REVISION STATUS)
PDMO

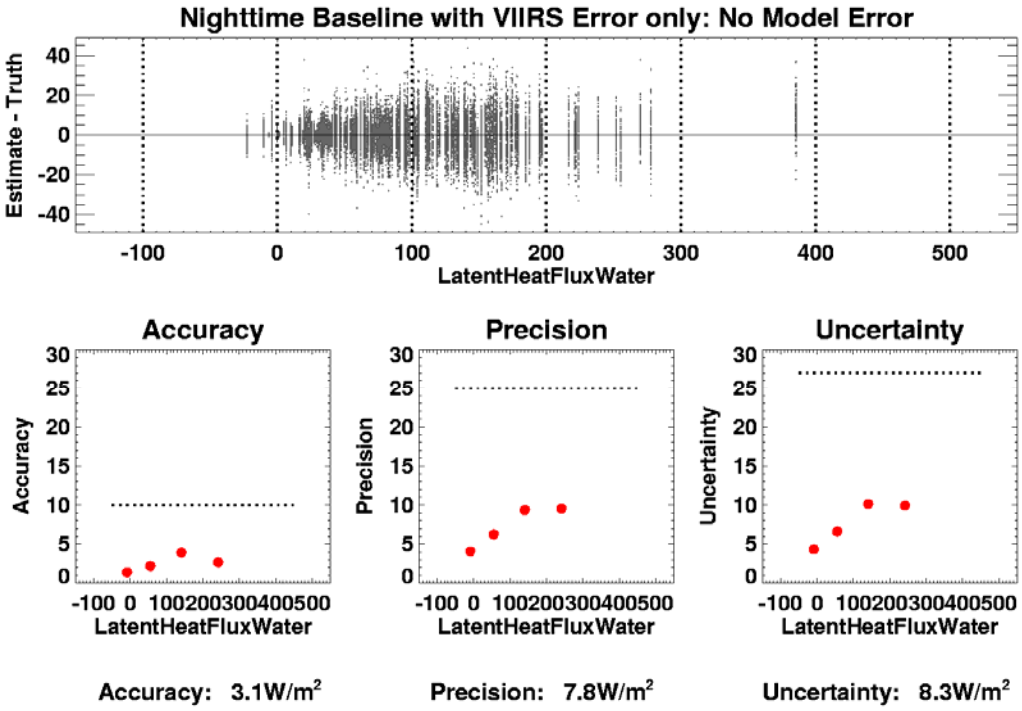

Figure 4-14 – Errors in Latent Heat Flux Due to Errors in VIIRS Parameters Only (SST).

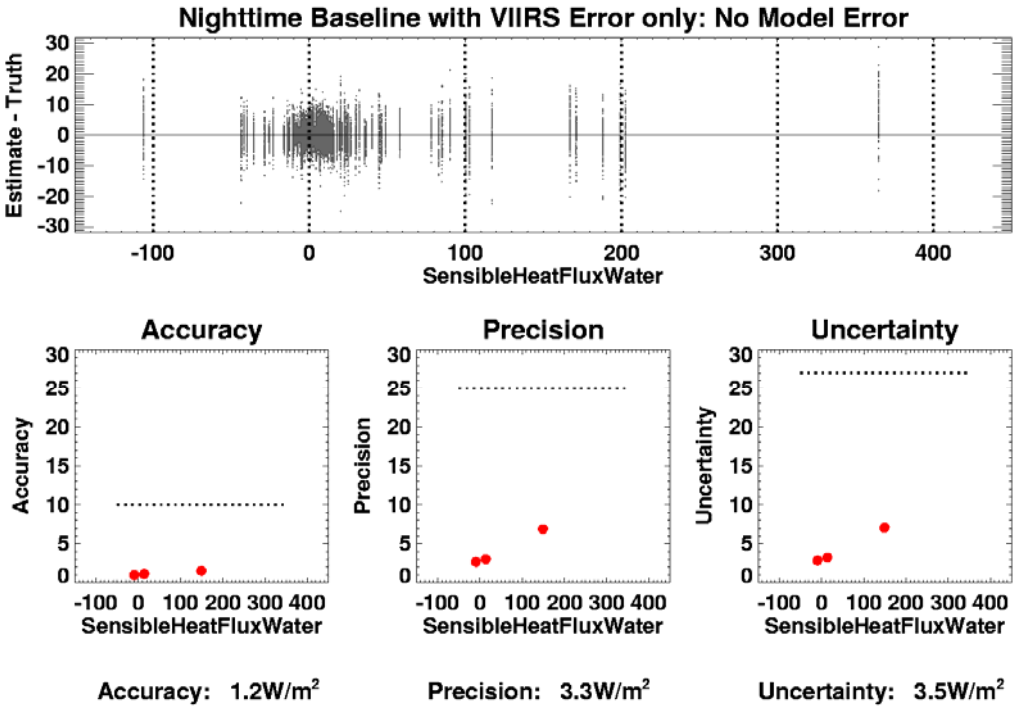

Figure 4-15 – Errors in Sensible Heat Flux Due to Errors in VIIRS Parameters Only (SST).

D43762, A. PDMO Released: 2009-09-28 (VERIFY REVISION STATUS)
PDMO

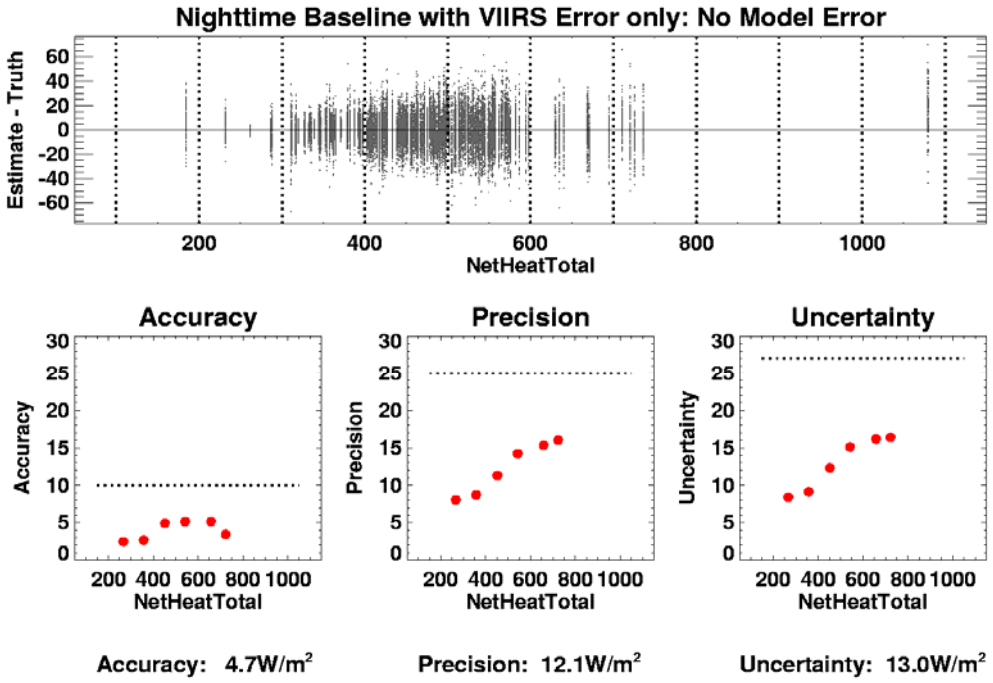

Figure 4-16 – Errors in Net Heat Flux Due to Errors in VIIRS Parameters Only (SST).

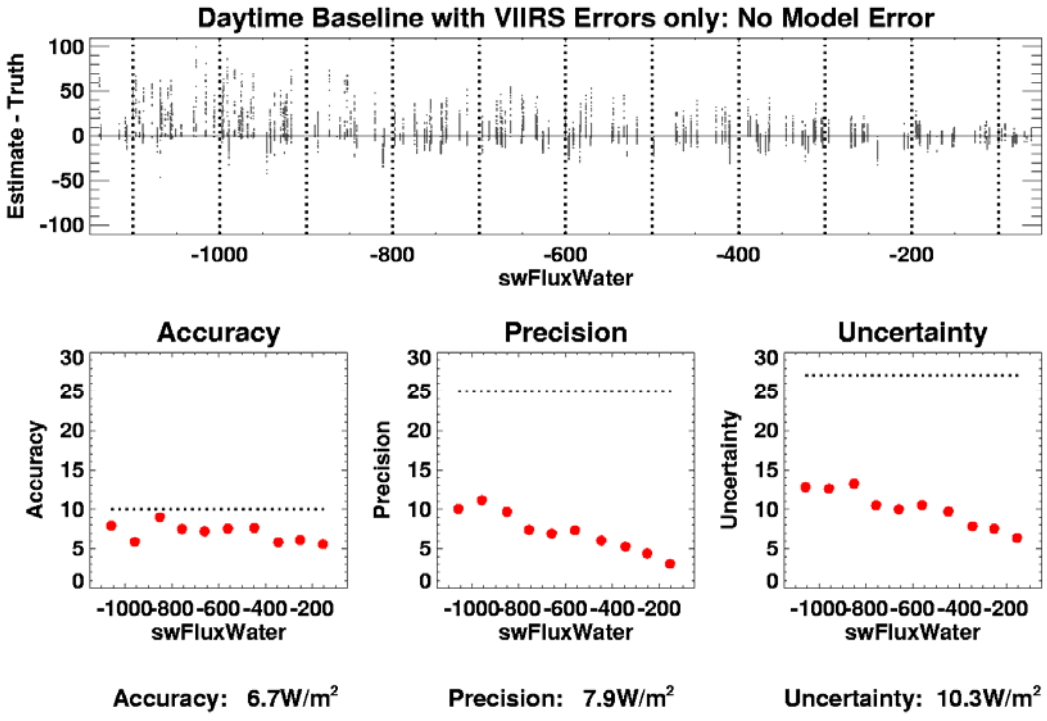

Figure 4-17 – Error in Shortwave Flux over Water Due to Aerosol Error (AOT and Model).

D43762, A. PDMO Released: 2009-09-28 (VERIFY REVISION STATUS)
PDMO

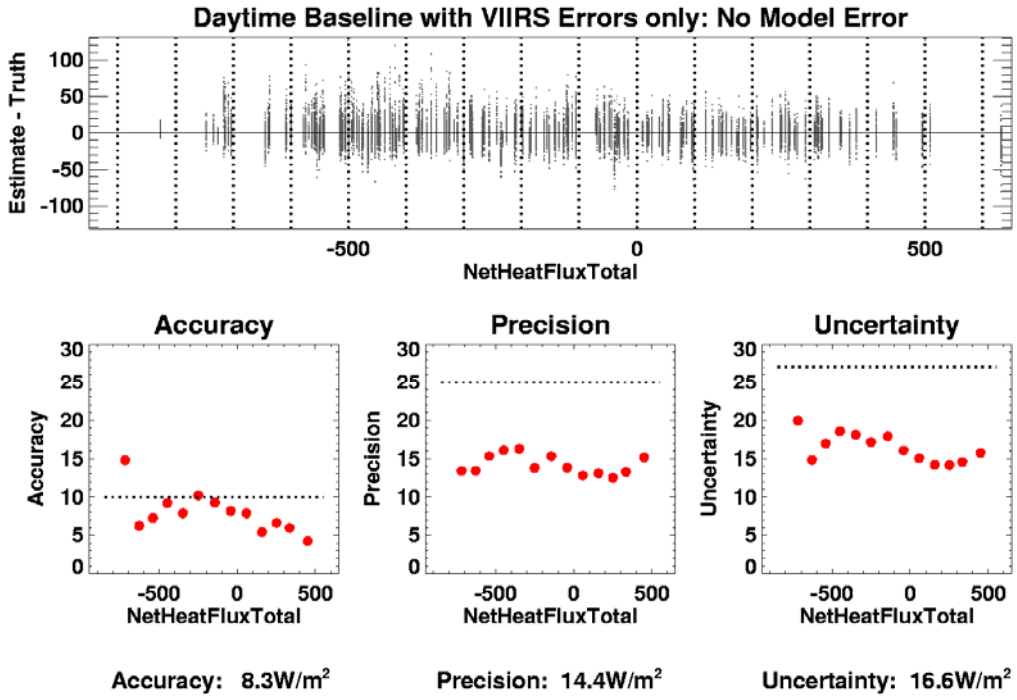

Figure 4-18 – Errors in Daytime Net Heat Flux Due to VIIRS Input Errors (SST and Aerosol AOT and Model).

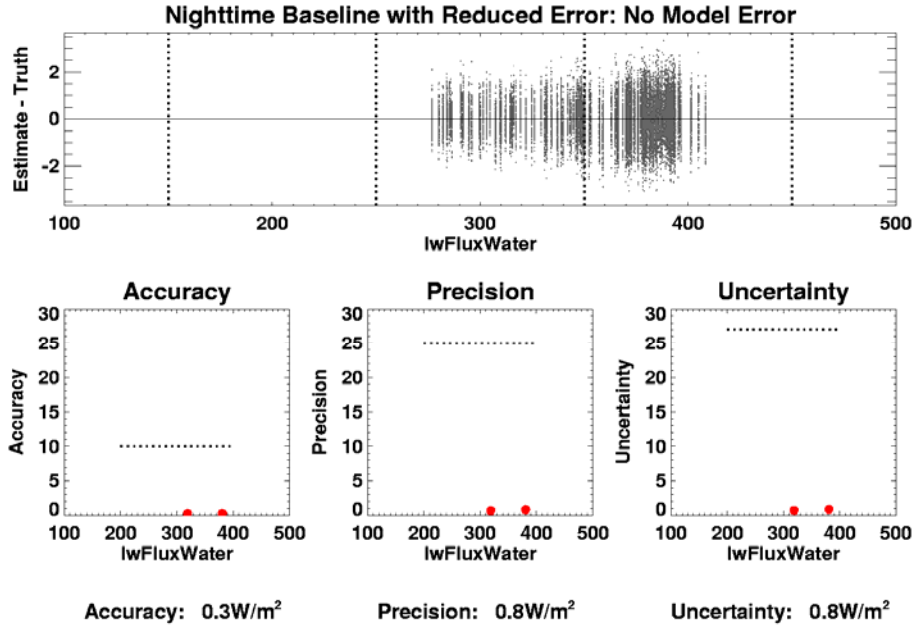

Figure 4-19 – Errors in Nighttime Longwave Flux Due to Reduced Errors in All Input Parameters.

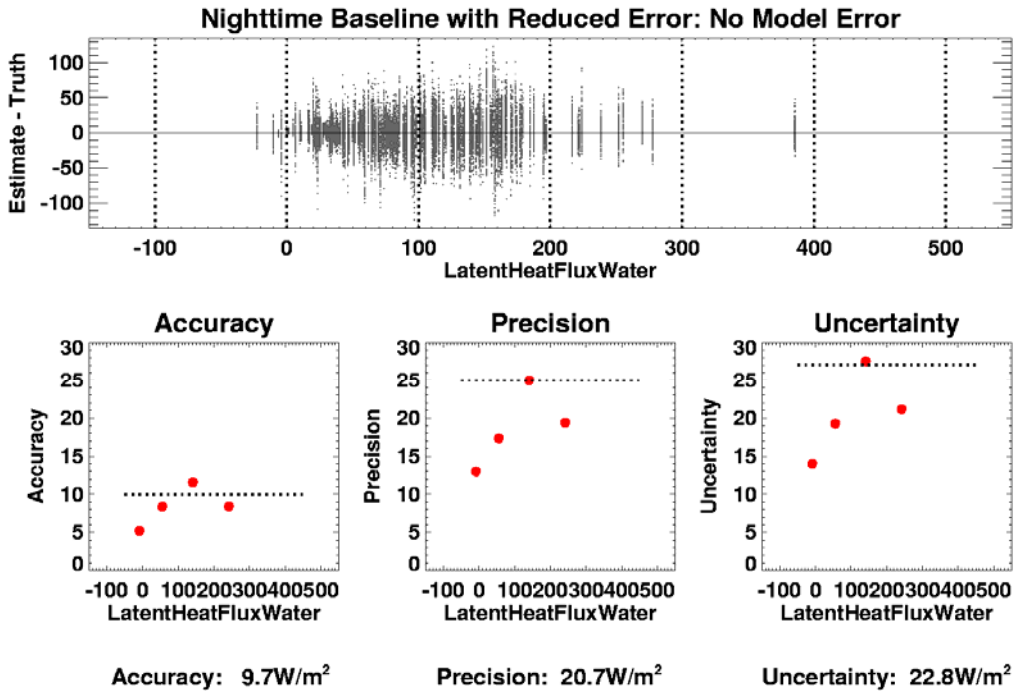

Figure 4-20 – Errors in Nighttime Latent Heat Flux Due to Reduced Errors in All Input Parameters.

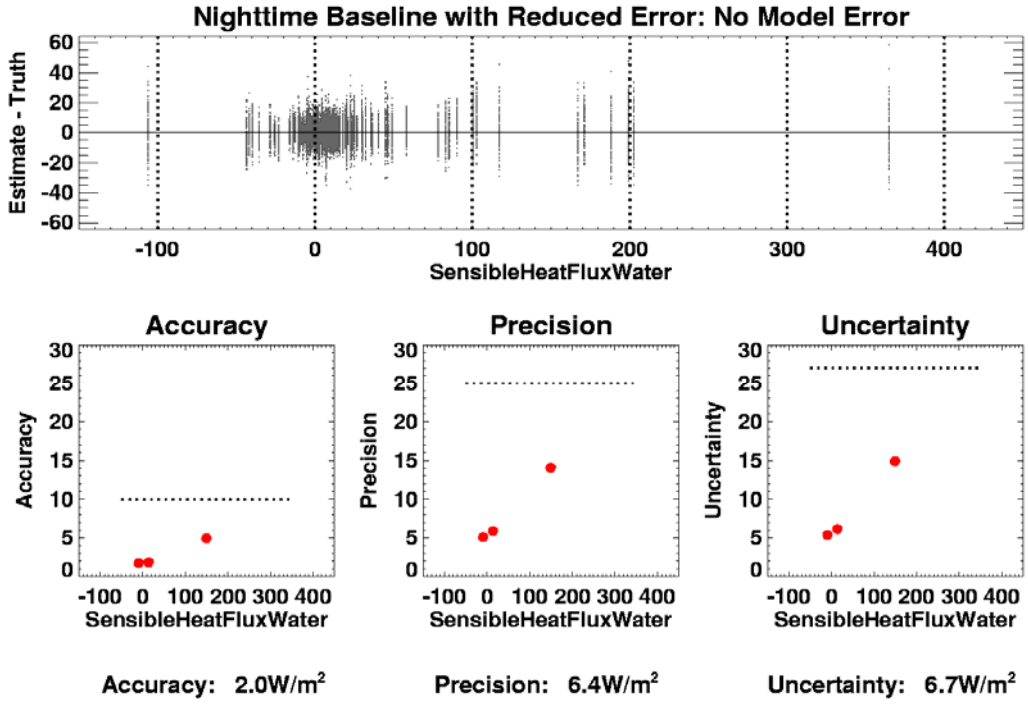

Figure 4-21 – Errors in Nighttime Sensible Heat Flux Due to Reduced Errors in All Input Parameters

D43762, A. PDMO Released: 2009-09-28 (VERIFY REVISION STATUS)
PDMO

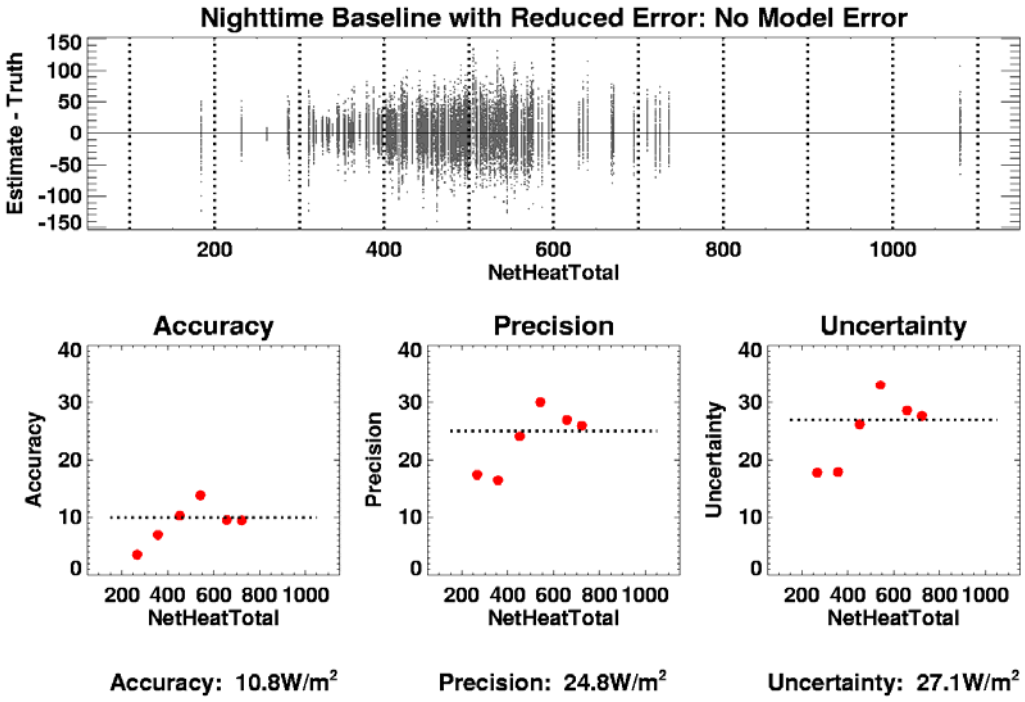

Figure 4-22 – Errors in Nighttime Net Heat Flux Due to Reduced Errors in All Input Parameters

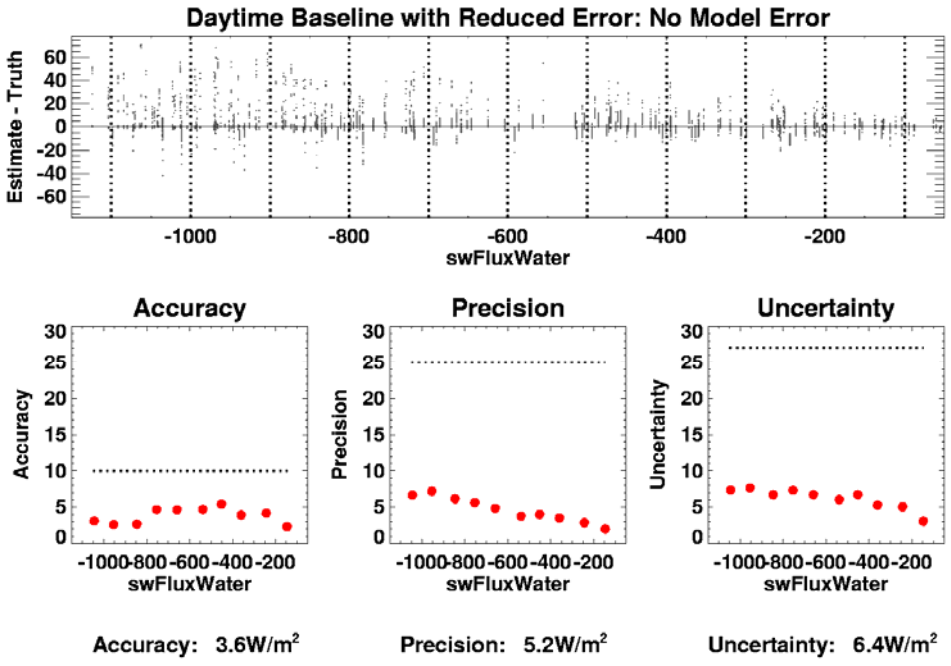

Figure 4-23 – Errors in Shortwave Flux Due to Reduced Errors in All Input Parameters.

D43762, A. PDMO Released: 2009-09-28 (VERIFY REVISION STATUS)
PDMO

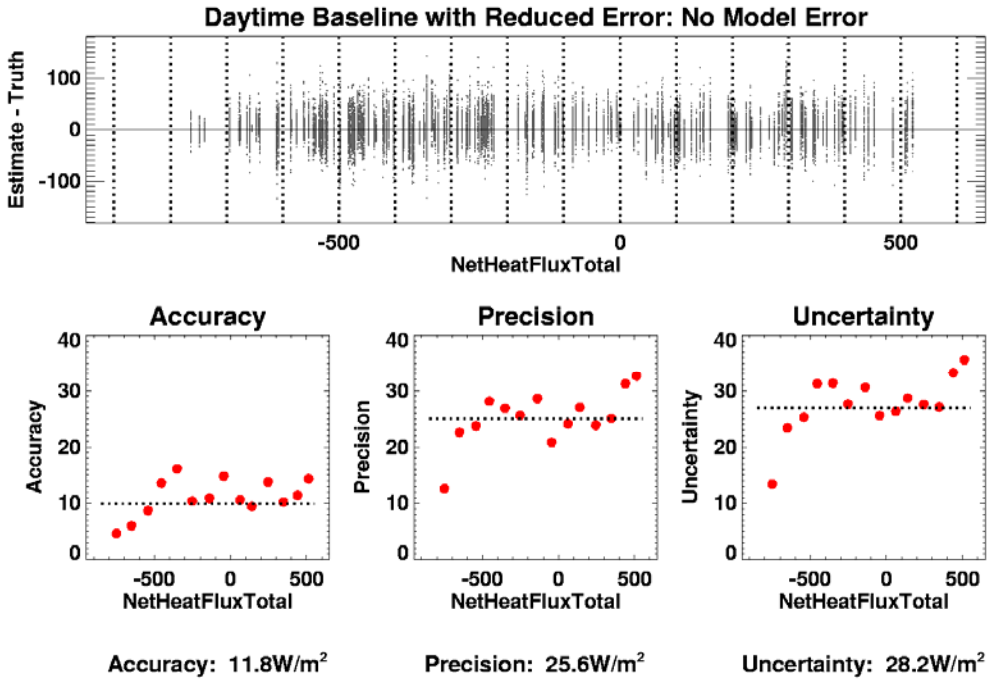

Figure 4-24 – Errors in Daytime Net Heat Flux Due to Reduced Errors in All Input Parameters.

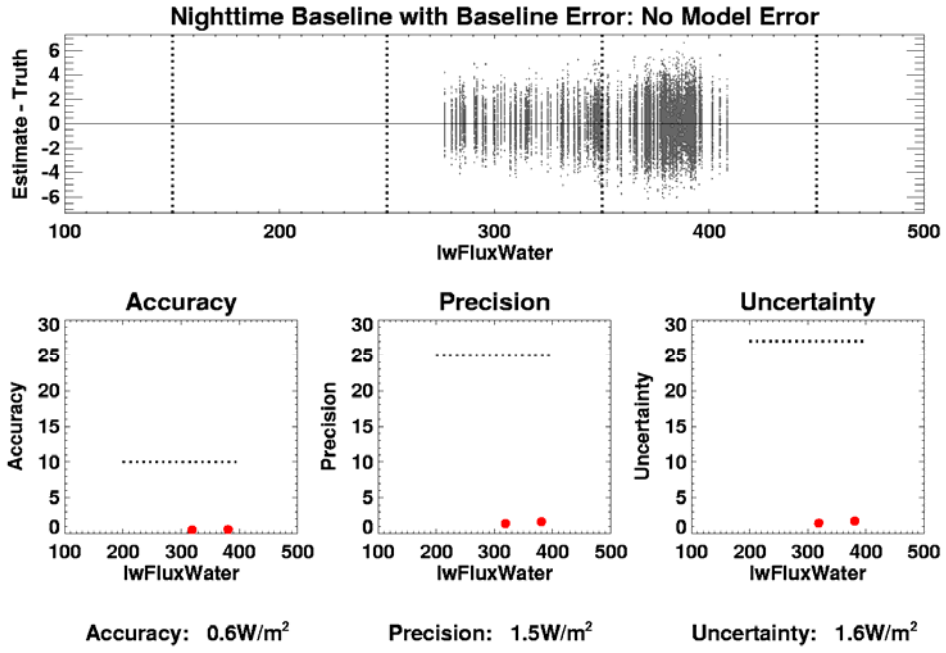

Figure 4-25 – Errors in Nighttime Longwave Flux over Water Due to Baseline Errors in All Input Parameters.

D43762, A. PDMO Released: 2009-09-28 (VERIFY REVISION STATUS)
PDMO

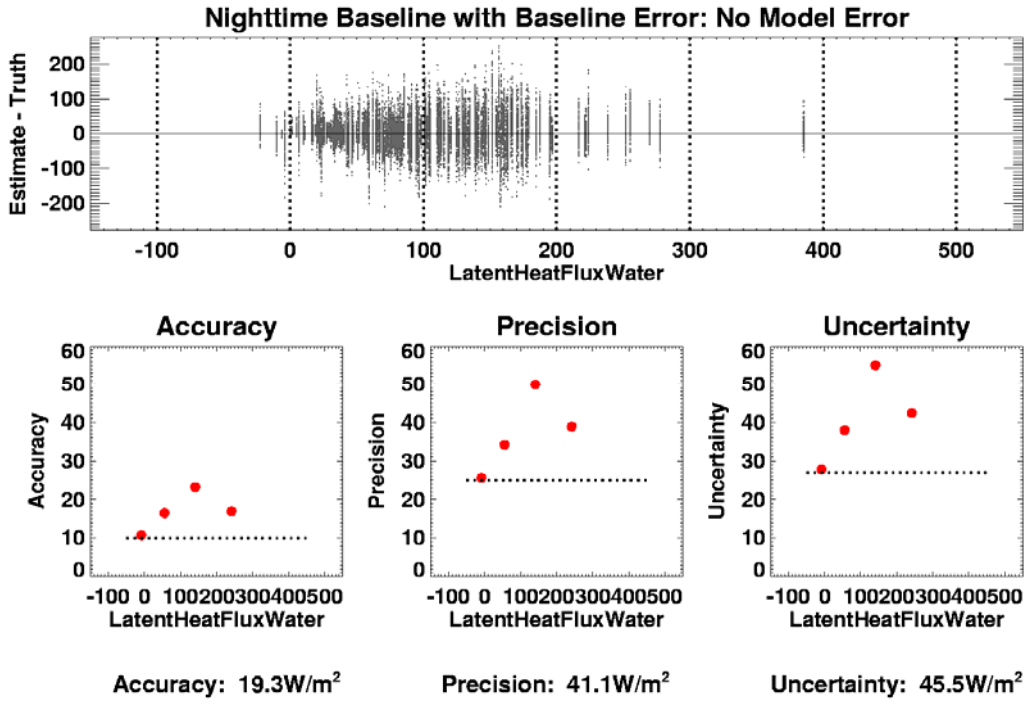

Figure 4-26 – Errors in Nighttime Latent Heat Flux Due to Baseline Errors in All Input Parameters.

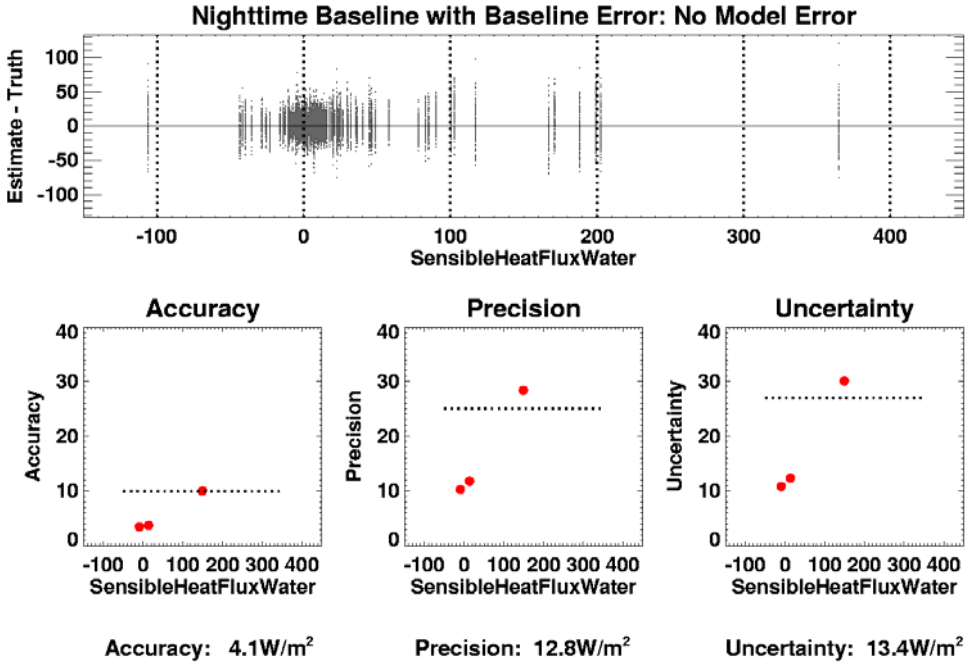

Figure 4-27 – Errors in Nighttime Sensible Heat Flux over Water Due to Baseline Errors in All Input Parameters.

D43762, A. PDMO Released: 2009-09-28 (VERIFY REVISION STATUS)
PDMO

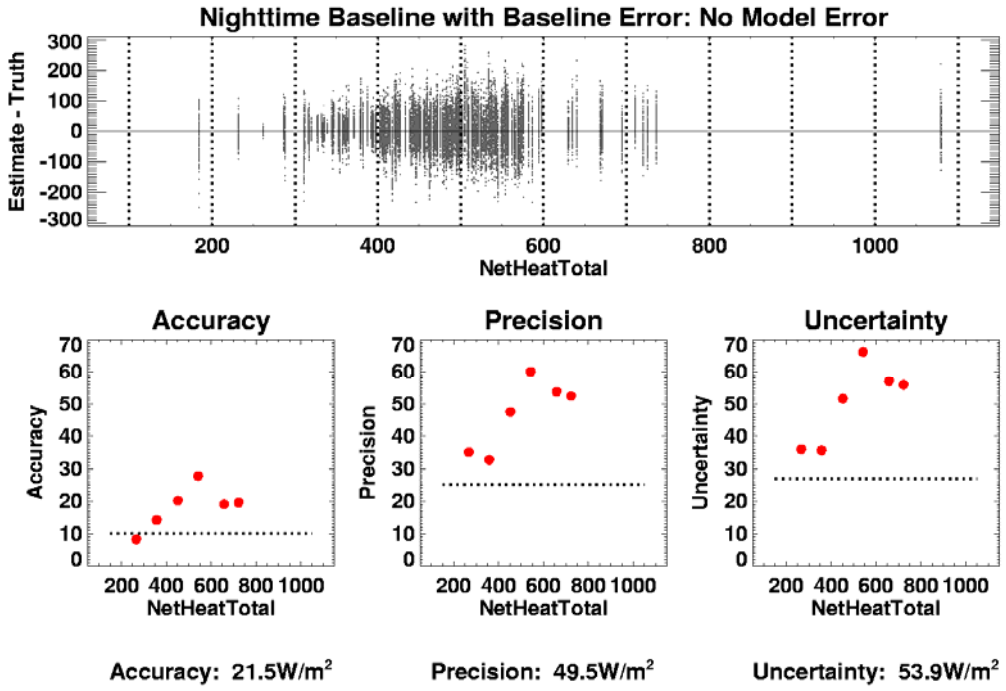

Figure 4-28 – Errors in Nighttime Net Heat Flux Due to Baseline Errors in All Input Parameters.

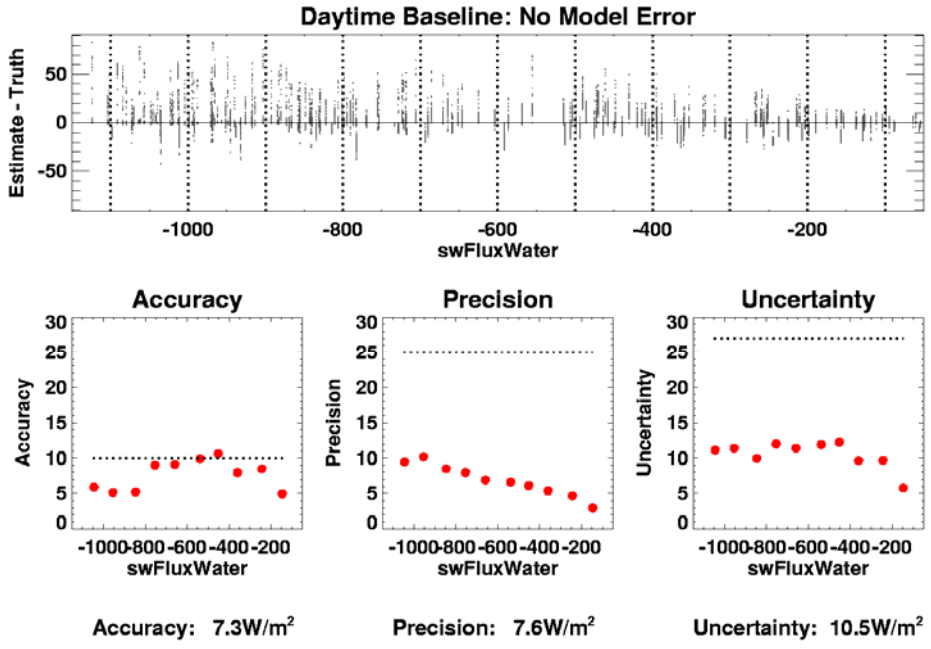

Figure 4-29 – Error in Shortwave Flux Due to Baseline Errors in All Input Parameters.

D43762, A. PDMO Released: 2009-09-28 (VERIFY REVISION STATUS)
PDMO

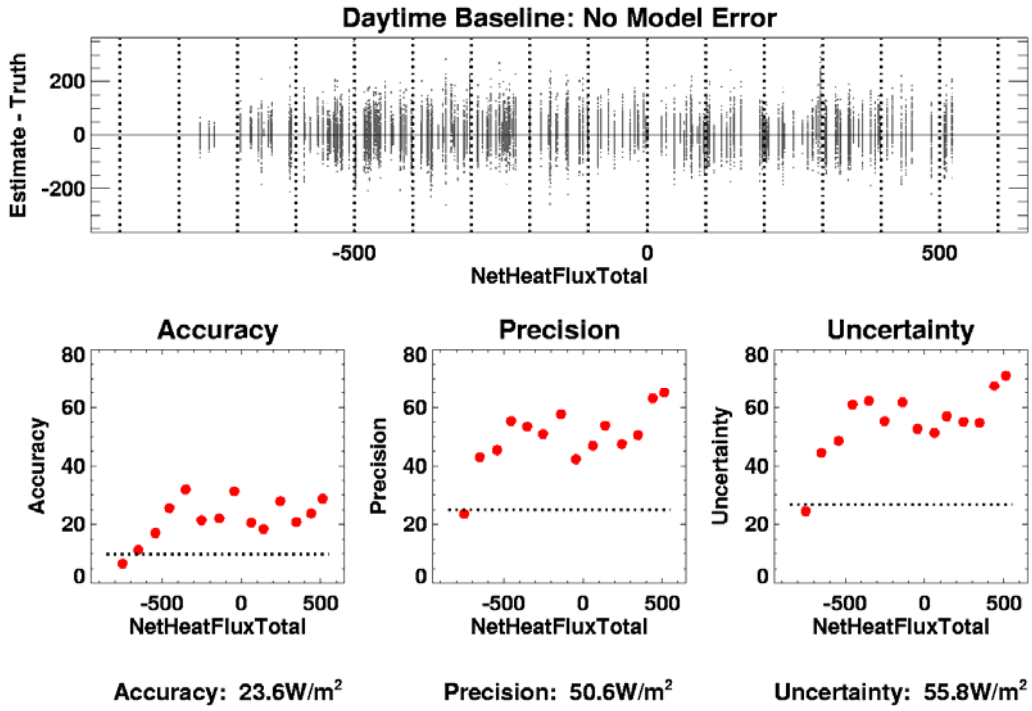

Figure 4-30 – Errors in Daytime Net Heat Flux Due to Baseline Errors in All Input Parameters.

4.3.3. Sensitivity Analysis

In order to evaluate the contribution of the error in each input parameter to the uncertainty in net heat flux, scenes were created in which only one input parameter at a time was perturbed, using the error model parameters specified in Table 4-3. A summary of the results is shown in Table 4-5. Note that some input parameters have little or no effect on some components and these columns have been left blank (e.g, air temperature and shortwave flux, optical depth and longwave flux). The largest sources of error are the uncertainties in air temperature and water vapor, which lead to significant errors in sensible and especially in the latent heat flux. Wind speed errors also impact the latent and sensible heat fluxes.

Table 4-5: Uncertainty in heat flux components due to error in input parameters

	Error due to Air Temperature (W/m^2)	Error due to Water Vapor Mixing Ratio (W/m^2)	Error due to Sea Surface Temperature (W/m^2)	Error due to Wind Speed (W/m^2)	Error due to Aerosol Model and Optical Thickness (W/m^2)
Longwave	0.6		1.5		
Latent	23.2	34.8	8.4	13.3	
Sensible	15.8	0.1	4.3	4.5	
Shortwave					10.3

D43762, A. PDMO Released: 2009-09-28 (VERIFY REVISION STATUS)
PDMO

These results confirm the previous section the largest errors are in the latent heat component and the two largest error contributors to this error are the air temperature at the surface and the surface water vapor.

All the uncertainty values discussed previously are aggregate values, calculated over the entire synthetic scene or over flux bins. It is worthwhile examining single rows of the synthetic scene in order to evaluate the range in flux values obtained when a single parameter is varied within the specifications. In Figure 4-31 through Figure 4-41 we show the impact of varying a single parameter.

Air temperature variability leads to approximately a 1 W/m^2 per 1K change for the longwave flux (Figure 4-31); the variability in latent and sensible heat fluxes is much larger (Figure 4-32 and Figure 4-33) as much as 200 W/m^2 for latent heat flux, highlighting the importance of reducing the uncertainty in air temperature measurements. Note that for small flux values the flux is not linear in air temperature, due to the link between air temperature and transfer coefficients.

Water vapor mixing ratio variability also has a large impact on latent heat flux (Figure 4-34), but a much smaller effect on sensible heat flux (Figure 4-35), the latter due mainly to changes in density. The flat plateaus or valleys at high water vapor indicate that the randomly generated mixing ratio surpassed saturation and was reset in the model calculations.

Longwave flux is driven principally by surface emission; thus, though the errors in SST are smaller than the errors in air temperature, they lead to larger errors in longwave flux (Figure 4-36). Latent and especially sensible heat flux, on the other hand, have smaller errors due to SST errors (Figure 4-37 and Figure 4-38) than to air temperature errors, since they are about equally sensitive to both, but the SST errors are smaller.

Wind speed variability has a smaller impact on latent and sensible heat flux than air temperature or water vapor, but slighty greater than SST (Figure 4-39 and Figure 4-40). Finally Figure 4-41 shows while errors in AOT can lead to significant uncertainties in the shortwave flux, selecting the wrong model for the flux calculation leads to often greater errors.

D43762, A. PDMO Released: 2009-09-28 (VERIFY REVISION STATUS)
PDMO

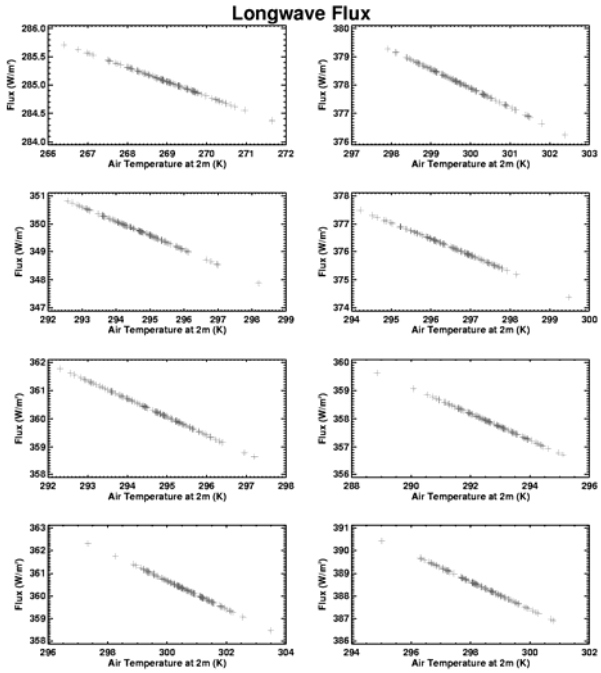

Figure 4-31 – Longwave Flux vs Air Temperature at 2m

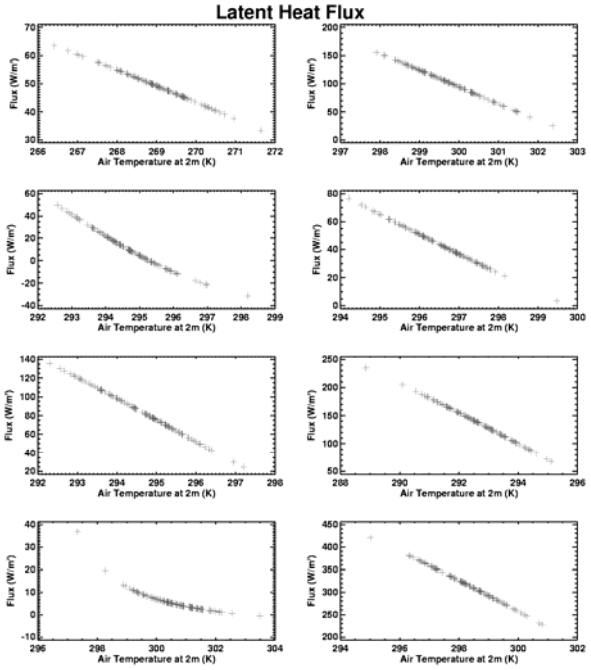

Figure 4-32 – Latent Heat Flux vs Air Temperature at 2m

D43762, A. PDMO Released: 2009-09-28 (VERIFY REVISION STATUS)
PDMO

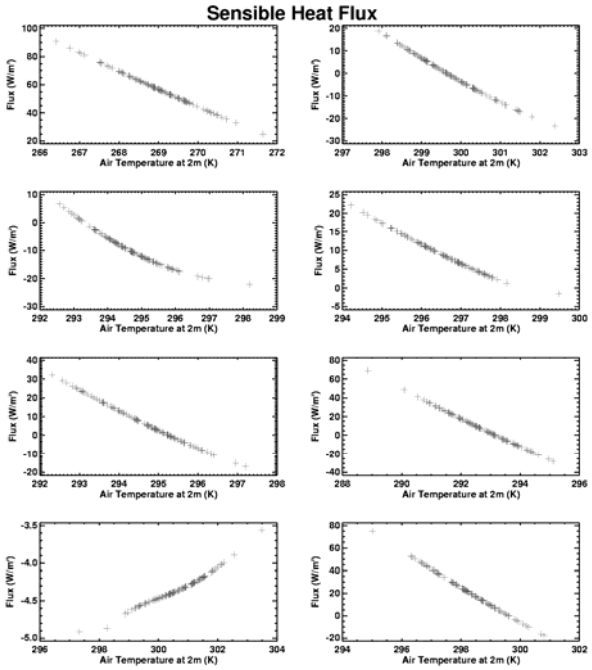

Figure 4-33 – Sensible Heat Flux vs Air Temperature at 2m

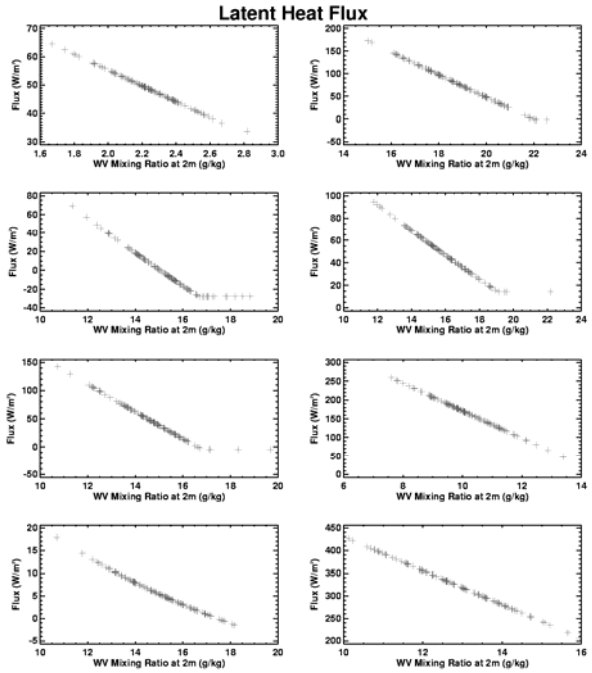

Figure 4-34 – Latent Heat Flux vs Water Mixing Ratio at 2m

D43762, A. PDMO Released: 2009-09-28 (VERIFY REVISION STATUS)
PDMO

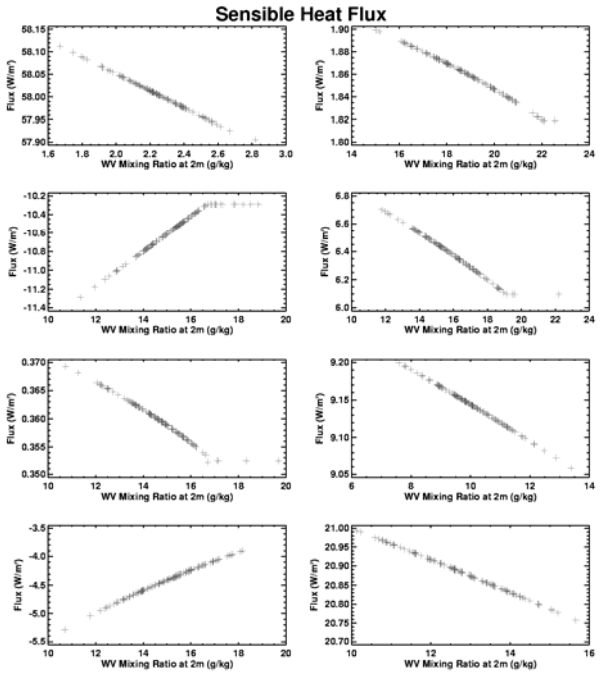

Figure 4-35 – Sensible Heat Flux vs Water Mixing Ratio at 2m

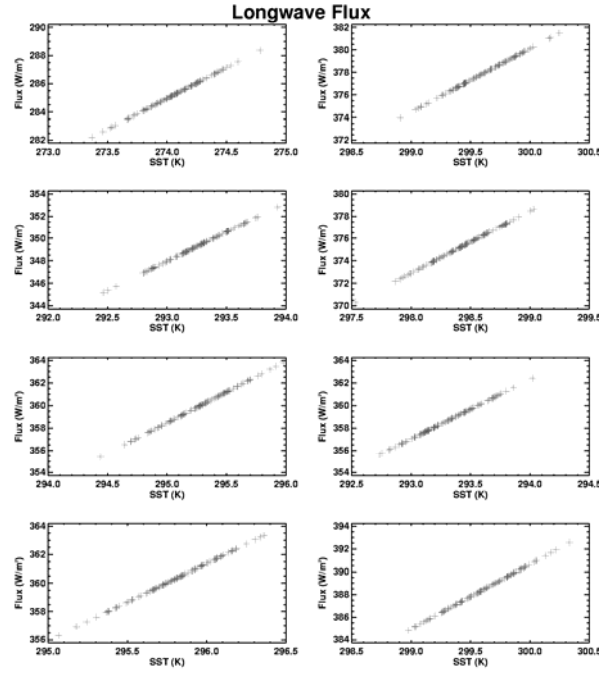

Figure 4-36 – Longwave Flux vs SST

D43762, A. PDMO Released: 2009-09-28 (VERIFY REVISION STATUS)
PDMO

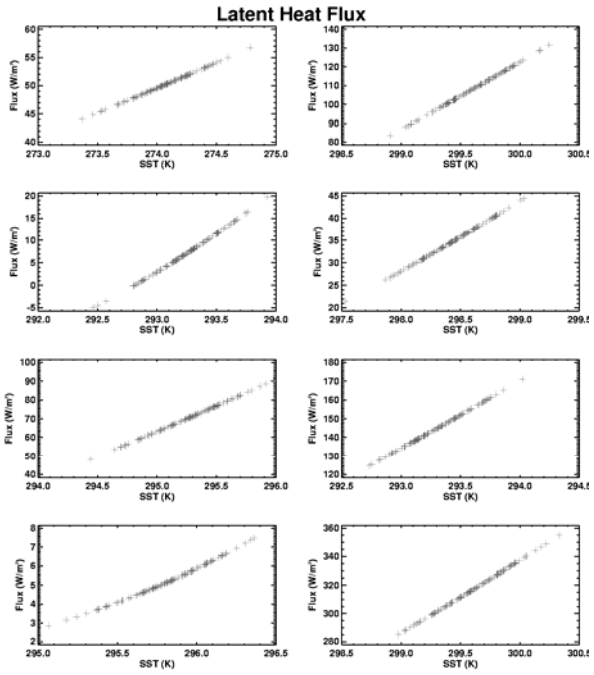

Figure 4-37 – Latent Heat Flux vs SST

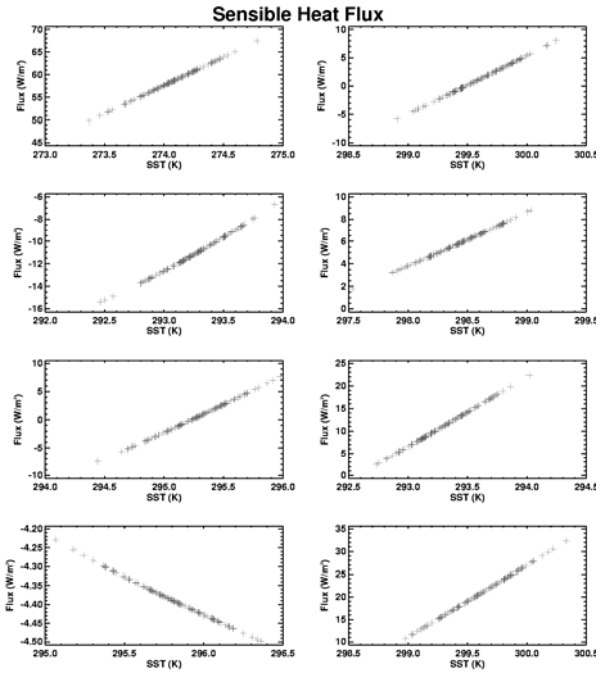

Figure 4-38 – Sensible Heat Flux vs SST

D43762, A. PDMO Released: 2009-09-28 (VERIFY REVISION STATUS)
PDMO

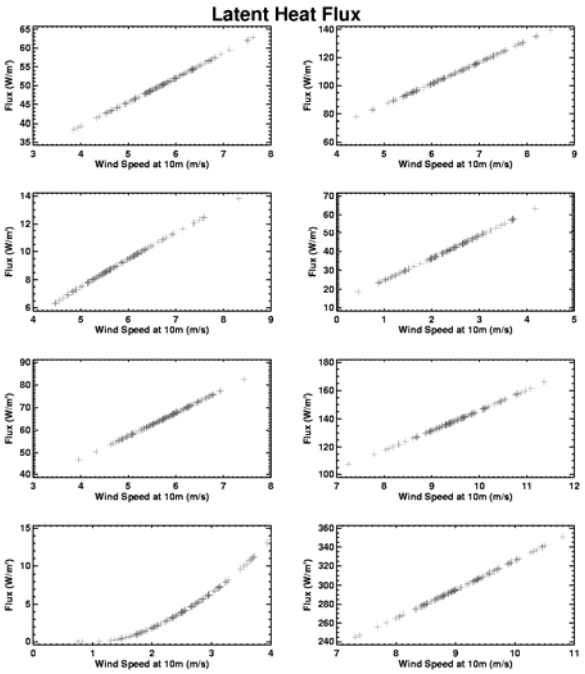

Figure 4-39 – Latent Heat Flux vs Wind Speed at 10 m

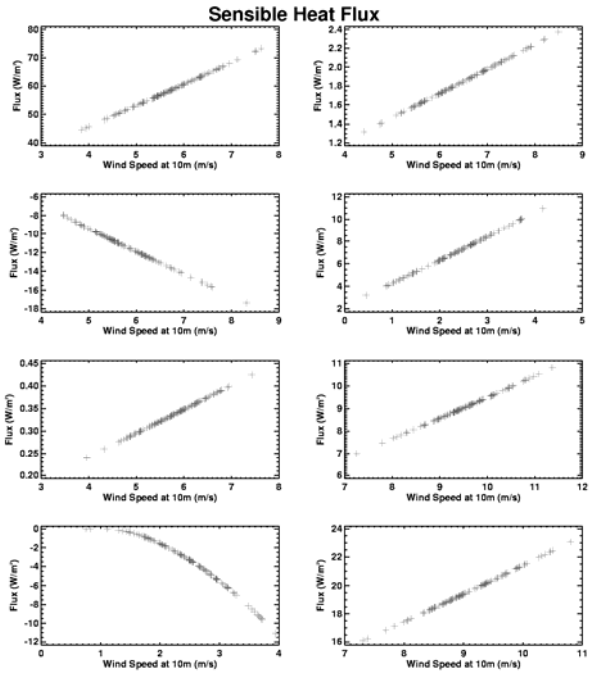

Figure 4-40 – Sensible Heat Flux vs Wind Speed at 10 m

D43762, A. PDMO Released: 2009-09-28 (VERIFY REVISION STATUS)
PDMO

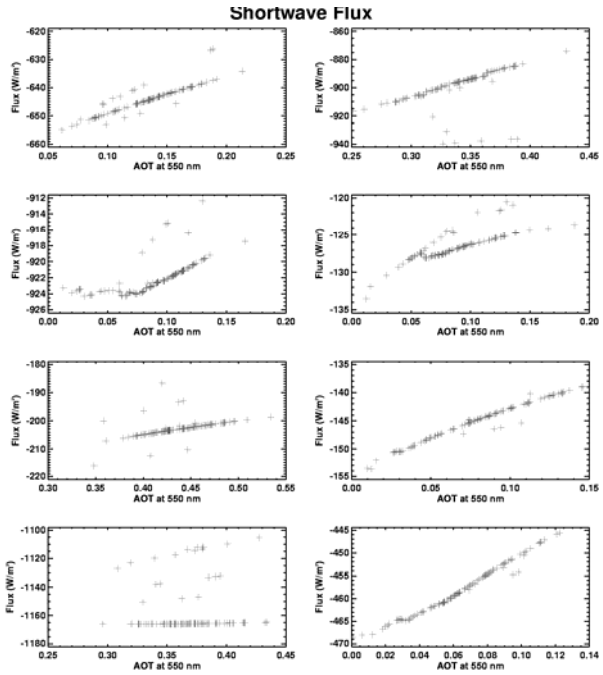

Figure 4-41 – Shortwave Flux vs AOT at 550 nm (Aerosol Model Also Varied)

4.3.4. Ocean Surface Albedo Errors

The same methodology and data set was used to estimate the errors in the ocean surface albedo product. The results are shown in Figure 4-42. This section includes specification errors (i.e., errors in the input parameters) only.

D43762, A. PDMO Released: 2009-09-28 (VERIFY REVISION STATUS)
PDMO

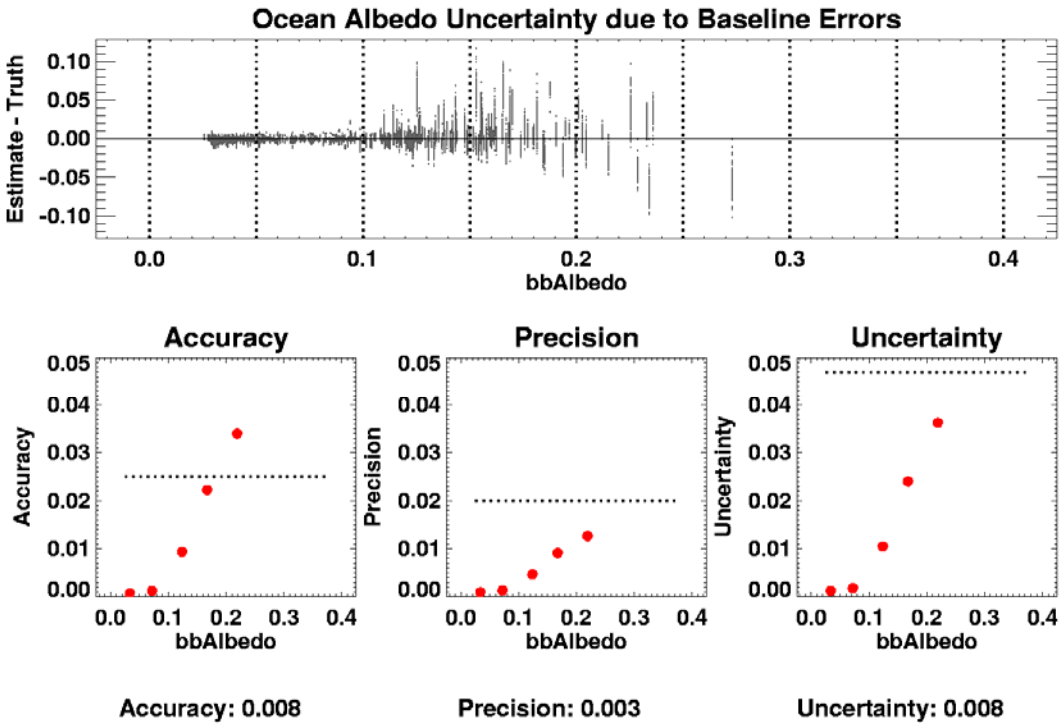

Figure 4-42 – Ocean Surface Albedo Errors

Jin, Charlock and Rutledge (2002) present several observation studies with model versus observed values of ocean surface albedo are less than 0.01 with the bias (accuracy) and standard deviation (precision) being approximately equal in most cases. They furthermore find that uncertainties in water vapor, chlorophyll, and aerosols are not the drivers of the observed differences. They believe many differences are due to un-modeled scattering in the water, notably from air bubbles suspended in the water or from other particulates. Errors larger than these could possibly occur in areas of high water turbidity such as major river outflow areas especially after heavy rains.

4.3.5. Model Error

Up to this point only specification errors, i.e, errors in the input parameters, have been considered. While the models adopted for net heat flux have excellent validation records, even perfect inputs will still lead to minor errors in net heat flux results. Table 4-6 presents a summary of the estimates of the errors associated with each model. RRTM_LW has been extensively validated against LBLRTM, which is considered the community standard for line-by-line radiative transfer calculations. RRTM_SW has been validated to within less than 1 W/m^2 to CHARTS (Code for High Resolution Accelerated Transfer), which in turn agrees to within 2 W/m^2 with clear sky RSS (Rotating Shadowband Spectroradiometer) measurements taken at the ARM SGP (Southern Great Plains) site. The COARE code used to determine latent and sensible heat fluxes has been used in TOGA COARE and SHEBA to compare measured with calculated turbulent fluxes.

D43762, A. PDMO Released: 2009-09-28 (VERIFY REVISION STATUS)
PDMO

Adding model error only slightly increases the total uncertainty in net heat flux (see Table 4-7, Figure 4-43, Figure 4-44, and Figure 4-45). The difficulty of meeting the heat flux uncertainty requirements lies not in the models, which are state of the art and very accurate, especially the radiative flux models, but in the large errors in some of the input parameters, namely air temperature, water vapor, and wind speed, and to some extent aerosol properties. This circumstance allows for easy upgrading of the net heat flux algorithm: as the retrievals of the input parameters improve, the uncertainty in the net heat flux calculations will decrease, without any significant software changes.

Given the expected large uncertainties, the usefulness of the net heat flux EDR may be questioned. As part of the NPOESS VIIRS program the net heat flux algorithm will generate global, continuous, and self consistent flux values, in effect creating the largest net heat flux database to date.

Table 4-6 – Heat Flux Model Component Errors

Heat Flux Component	Model Error	Reference
Shortwave	3 W/m^2	Mlawer et al, 2000 and Iacono (personal communication)
Longwave	1 W/m^2	Mlawer et al, 1997
Latent	2 W/m^2	Fairall et al, 1996
Sensible	2 W/m^2	Fairall et al, 1996

Table 4-7 – Daytime net heat flux errors due input specification errors with and without model error

	VIIRS Only Errors (W/m^2)	Reduced Baseline Errors (W/m^2)	Baseline Errors (W/m^2)
Specification Errors	16.6	28.2	55.8
Specification and Model Errors	17.2	28.5	56.0

D43762, A. PDMO Released: 2009-09-28 (VERIFY REVISION STATUS)
PDMO

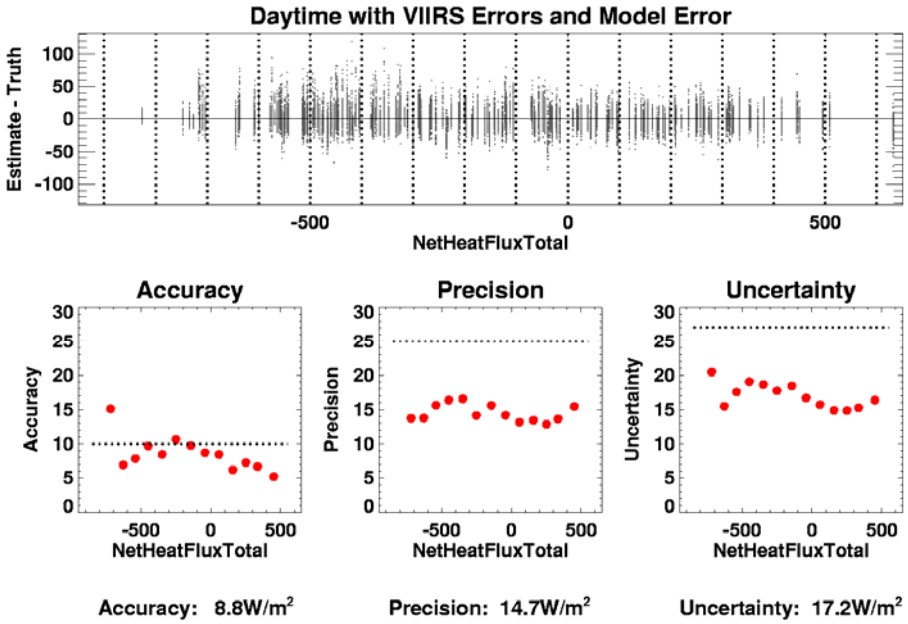

Figure 4-43 – Specification and Model Error in Net Heat Flux Due to VIIRS Input Errors Only

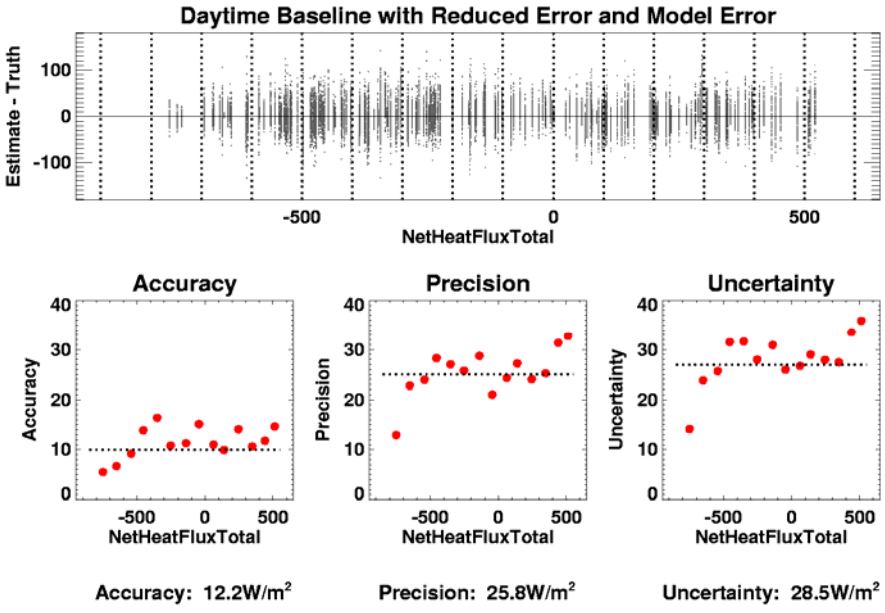

Figure 4-44 – Specification and Model Error in Net Heat Flux Due to Reduced Baseline Input Errors

D43762, A. PDMO Released: 2009-09-28 (VERIFY REVISION STATUS)
PDMO

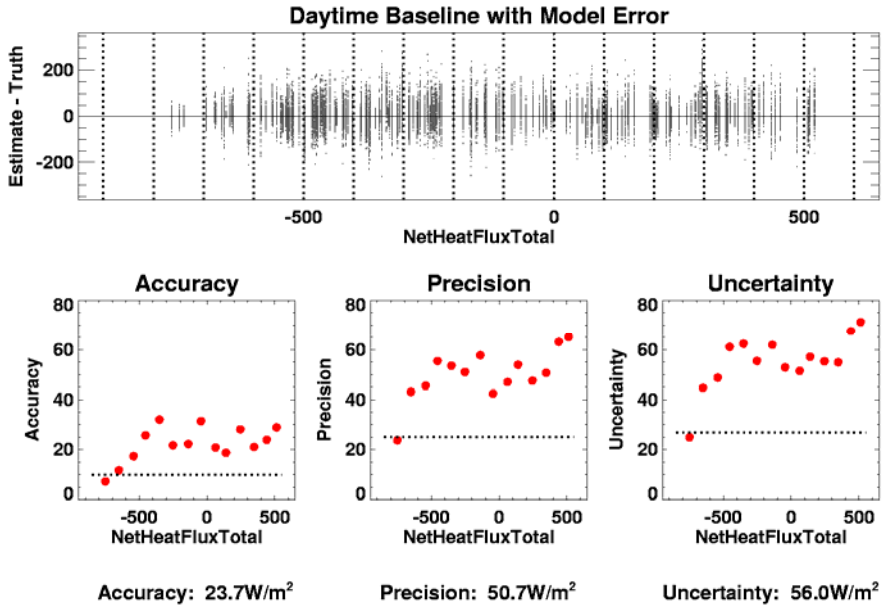

Figure 4-45 – Specification and Model Error in Net Heat Flux Due to Baseline Input Errors

4.4. EDR Performance Summary for Net Heat Flux

First simplicity the previous discussion referred to the total error or measurement uncertainty. Table 4-8 lists separately accuracy and precision for the three different sets of inputs errors (with model error included).

Table 4-8 – Accuracy and Precision: Requirement versus simulated performance for three cases including model errors

Item	Accuracy (W/m^2)	Precision (W/m^2)
Baseline error performance	23.7	50.7
Reduced error performance	12.2	25.8
VIIRS only error performance	8.8	14.7

The errors estimated for our previous version of the algorithm (Cady-Periera, 2000), were between the Baseline and Reduced Error cases, which is reasonable as the input error for that study were between the two also.

We emphasize the following:

- the physical models employed are state of the art and widely used in the community (RRTM, COARE, COART)

D43762, A. PDMO Released: 2009-09-28 (VERIFY REVISION STATUS)
PDMO

- the inherent algorithm errors contribute negligibly to the overall accuracy and precision values
- VIIRS derived EDR inputs have only a modest contribution to total errors
- the most significant drivers of the error are air temperature and surface level moisture
- reduced input errors ("Reduced" case) reduce measurement accuracy to within 10 W/m^2 and precision to within 25 W/m^2

The "Reduced" case is also relevant to one of the most wide applications of Heat Flux data: analysis of resolution fluxes for time averages for climate analysis. This performance can be reasonably approach for monthly averages over moderate resolution cells (~2.5x2.5 degrees), although additional analysis would be required to verify this.

In conclusion, we believe this NHF algorithm can provide good quality data on both total flux and individual flux components to users. As it is based on state of the art physical models, it can improved in the future through either upgrades to the models themselves or through improvements to the input parameters.

4.4.1. EDR Performance Summary for Ocean Surface Albedo

Table 4-9 presents the ocean surface albedo required versus predicted performance. The predicted performance includes both the errors due to propagation of errors in input parameters and a 0.01 error contributor for the inherent model error.

Table 4-9 – Ocean Surface Albedo IP Performance Summary

Parameter	SZA	Accuracy	Precision	Uncertainty
Requirement	< 70 deg.	0.025	0.020	0.03
Predicted		0.020	0.010	0.022
Requirement	70-85 deg. [Note A]	0.040	0.040	N/S
Predicted		0.036	0.018	0.041
NOTE A – This is given as a degraded performance condition.				

These results show that the Ocean Surface Albedo output meets the requirements in the NPOESS System Specification.

5. Practical Considerations

5.1. Numerical Computing Considerations

The physical model calculations are performed in FORTRAN-90 codes primarily using 32-bit single precision computations. The code has been tested on both 32-bit and 64-bit architectures. Testing of the algorithm has not revealed any numerical instabilities in the underlying algorithms over the range of conditions evaluated.

D43762, A. PDMO Released: 2009-09-28 (VERIFY REVISION STATUS)
PDMO

5.2. Programming Considerations

The software delivered implementing the NHF algorithm should present no special programming or compatibility problems. It is written in ANSI standard C++ and FORTRAN. It employs standard data formats (netCDF and GRIB) and uses standard libraries for accessing these data. It has been tested on multiple platforms.

The program executive is coded in ANSI C++. The executive handles input of all required data sources, determines the appropriate processing paths, performs basic error checking, and prepares the data for use by the COART LUTs and for input to the COARE and RRTM models. It then outputs the EDR and IP, quality flags, and other diagnostic data.

Interfaces to sensor and other data are through an object oriented standard application programmer's interface (API). Current sensor inputs and output EDRs are in netCDF format. The numerical weather prediction data are input in GRIB format (Version 1, Table 2). The API is flexible and can be easily adapted to other target environments.

The COARE and RRTM models are written in FORTRAN and compile under ANSI compliant FORTRAN-90[1] compilers. The COARE and RRTM Short-wave models employ FORTRAN 90 language features. The RRTM Long-wave model is basically a FORTRAN-77 application that has been slightly revised to compile under FORTRAN-90.

5.3. Computer Hardware/Software Requirements

The software has been tested with several computer architectures including LINUX (ix86 architecture) processors, Solaris (Sparc 32-bit architecture), and SGI/IRIX (RISC-10K 64-bit architecture). See the software design documentation for details.

Table 5-1 presents computational speed benchmarks for the NHF algorithm. The times include the computation of the Ocean Surface Albedo IP. These are processing times for each clear horizontal cell with all valid input data. The number of horizontal cells per VIIRS scan depends on the final details of the horizontal cell construction (see Appendix B). For the recommended square cell option, there is 102 HCs per scan with a scan period of 1.7 seconds. The number of clear cells will vary greatly depending on scene characteristics. Only a very small number of mixed pixels have been observed in the test data, a few percent of total in the worst-case and none for most cases.

Table 5-1 – NHF Processing Time Benchmark

Day/Night	Scene Type	Processing time per HC (ms)
Day	all water or all ice	19.0
	mixed water/ ice	35.0
Night	all water or all ice	8.5
	mixed water/ ice	16.0

[1] We have not tested with fully compliant FORTRAN-95 compilers, but there are no known compatibility issues.

D43762, A. PDMO Released: 2009-09-28 (VERIFY REVISION STATUS)
PDMO

The hardware/environmental conditions for the timing tests are:

- AMD Athalon 2000MP, 1.67 GHz processor (single processor used on 2 processor node) with 2GB RAM (596 SPECfp-2000 and 662 SPECint-2000)
- Linux Red Hat 8 OS
- PGI FORTRAN-90 compiler, optimization level 3

This is a moderate speed processor based on 2001 technology.

5.4. Quality Control and Diagnostics

Quality control and diagnostic information output includes:

- flags denoting source and quality of input data are listed in Table 5-2
- number of pixels within each cell that are: cloudy, cloud free & water covered, cloud free and ice covered
- individual flux contributors separately for the ice and water portions: short-wave, long-wave, sensible heat and latent heat fluxes

For detailed content of the quality control information see the software documentation.

5.5. Exception and Error Handling

The algorithm tests and flags for missing or bad input data. Bad input data are flagged based on range checking. Range checking is also performed on the output data.

For any case that valid data for all required inputs are provided and the output passes the range checking tests, a valid output EDR is produced, otherwise a flag is set and a fill value is inserted into the output.

5.6. Special Database Requirements

A variety of look-up tables and algorithm coefficients is being used by the NHF and Ocean Surface Albedo algorithms. These include:

- correlated-k absorption coefficients
- aerosol model optical depth and phase function tables
- parameters related to the turbulent fluxes
- tables relating ocean surface albedo to chlorophyll, wind speed, etc.

These tables are subjected to revision based on scientific advances in the underlying community algorithms or NPOESS testing and validation. They should be reviewed prior to launch and periodically during operations to determine if updated tables should be incorporated.

5.7. Archival Requirements

The only required products to be archived by the System Specification are the total heat flux, the four individual heat flux contributors (latent sensible, long-wave and short-wave fluxes), and ocean surface albedo for each cell plus the associated quality control flags. These variables are very valuable in monitoring algorithm performance.

D43762, A. PDMO Released: 2009-09-28 (VERIFY REVISION STATUS)
PDMO

6. List of References

AER, Inc., VIIRS Cloud Cover/ Layers Algorithm Thoeretical Basis Document, Version 6, December 2004 (AER Doc # P1187-TR-I-006)

Cady-Pereira, K. 2000: VIIRS Algorithm Theoretical Basis Document for the Net Heat Flux EDR," Version 1.3, May 2000, AER, Inc. [Prepared for the NPOESS Risk Reduction Phase of the Visible and Infrared Imaging Radiometer Suite and delivered to the government as part of the ITT contract.]

Andreas, E.L, 1987.: A theory for the scalar roughness and the scalar transfer coefficients over snow and sea ice, *Boundary Layer Meteo*., **38**, 159-184

Businger, J.A., J.C. Wyngaard, Y.Izumi and E.F. Bradley, 1971: Flux profile relationships in the atmospheric surface layer, *J. Atmos. Sci.,* **28**, 181-189, 1971

Charnock, H., 1955: Wind stress on a water surface, *Q.J.R. Meteorolo. Soc.,* **81**, 639

Clough, S.A. and M.J. Iacono, 1995: Line-by-line calculation of atmospheric fluxes and cooling rates, 2, Application to carbon dioxide, ozone, methane, nitrous oxide and the halocarbons, *J. Geophys. Res.,* **100**, 16,519-16,535

Fairall, C. W., E. F. Bradley, D. P. Rogers, J. B. Edson and G. S. Young, 1996: Bulk parameterization of air-sea fluxes for Tropical Ocean-Global Atmosphere Coupled-Ocean Atmosphere Response Experiment. *J. Geophys. Res*., **101**, 3747-3764

Guest, P.S. and K.L. Davidson, 1991: The aerodynamic roughness of different types of sea ice, J. Geophys. Res, C3, **96**, 4709-4721

Gosnell, R.C., W. Fairall and P.J. Webster, 1995: The sensible heat of rainfall in the open ocean, *J. Geophys. Res.*, **100**, 18,437-18,442

Iacono, M.J., E.J. Mlawer, and S.A. Clough, 1999: Impact of an improved longwave radiation model, RRTM, on the energy budget and thermodynamic properties of the NCAR Community Climate Model, CCM3, submitted to *JGR-Atmospheres*

Jones, C., P. Peterson and C. Gautier, 1999: A New Method for Deriving Ocean Surface Specific Humidity and Air Temperature: An Artificial Neural Network Approach, *Journal of Applied Meteorology*, **38**, 1229-1245

Kraus, E.B. and J.A. Businger, 1994: *Atmosphere-Ocean Interaction*, 352 pp, Oxford Univ. Press, New York

Large, W. G. and S. Pond, 1982: Sensible and Latent Heat Flux Measurements over the Ocean. *J. Phys. Oceano*., **12**, 464-482

Li, Z. and H.G. Leighton, 1993: Estimation of SW flux absorbed at the surface from TOA reflected flux, *Journal of Climate*, **6**, 317-330

Liu, W. T., K. B. Katsaros and J. A. Businger, 1979: Bulk parameterization of air-sea exchange of heat and water vapor including the molecular constraints at the interface. *J. Atmos. Sci*, **36**, 1722-1735

Masuda, K., T. Takashima and Y. Takayama, 1988: Emissivity of pure and sea waters for the model sea surface in the infrared window regions. *Remote Sensing Environ.*, **24**, 313-329

D43762, A. PDMO Released: 2009-09-28 (VERIFY REVISION STATUS)
PDMO

Mlawer, E.J., S.J. Taubman, P.D. Brown, M.J. Iacono and S.A. Clough, 1997 : Radiative transfer for inhomogeneous atmospheres: RRTM, a validated correlated-k model for the longwave, *J. Geophys. Res,* **102**, 16,663- 16,682

Stokes, G.E. and S.E. Schwartz, 1994: The Atmospheric Radiation Measurement (ARM) Program: Programmatic background and design of the cloud and radiation test bed, *Bull. Am. Meteorolo. Soc,* **75**, 1201-1221

Webb, E.K., G.I. Pearman and R.Leunig, 1980: Correction of flux measurements for density effects due to heat and water vapor transport, *Q.J.R. Meteoro. Soc.,* **108**, 85-100

Wu, X. and W.L. Smith, 1997: Emissivity of rough sea surface for 8-13 μm: modeling and verification, *Applied Optics*, **36**, 2609-2619.

Andreas, E.L. (1987) A theory for the scalar roughness and the scalar transfer coefficients over snow and sea ice, *Boundary-Layer Meteorology* **38**, 159-184.

Banke, E.G., S.D. Smith and R.J. Anderson (1980) Drag coefficients at AIDJEX from sonic Aanemometer measurements. In *Sea Ice Processes and Models* (R.S. Pritchard, Ed.). Seattle: University of Washington Press, p. 430–442.

Garbrecht, T., C. Lüpkes, J. Hartmann and M. Wolff (2002) Atmospheric drag coefficients over sea ice - validation of a parameterisation concept, *Tellus* **54A**, 205-219.

Kondo, J. and H. Yamazawa (1986) Bulk transfer coefficient over a snow surface, *Boundary Layer Meteorology* **34**, 123-135.

T. Charlock, F. Rose, D. Rutan, T. Alberta, L. Coleman, G. Smith, N. Manolo-Smith, T. Bess, CERES Subsystem 5.0: Compute Surface and Atmospheric Fluxes, ATBD-CER-15, June 1997

Z. Jin, T. P. Charlock, K. Rutledge, 2002: Analysis of Broadband Solar Radiation and Albedo over the Ocean Surface at COVE, J. Atmos. Oceanic Tech.,Vol. 19, pp. 1585-1601.

Z. Jin and T. Charlock, 2001: Radiative Transfer Modeling of the Ocean Surface Albedo for CERES SARB, Co-investigator Report at the 23rd CERES SCience TEam Meeting, Williamsburg, VA, 23-25 January 2001

Jin, Z., T. Charlock, W. Smith Jr., K. Rutledge (2004), A Parameterization of Ocean Surface Albedo, Geophys. Res. Lett., 31, L22301, doi:10.1029/2004GL021180.

D43762, A. PDMO Released: 2009-09-28 (VERIFY REVISION STATUS)
PDMO

7. Appendix A – Sea Surface Emissivity in the Long-Wave Infrared

Sea surface emissivity is a strongly varying function of wavelength and emission angle (Wu and Smith, 1997) (Figure 7-1), yet in most ocean heat flux modeling efforts it is assumed constant with a value around 0.97 (e.g., Fairall et al, 1997). This study shows that 0.97 is very close to the effective emissivity for an average oceanic wind speed.

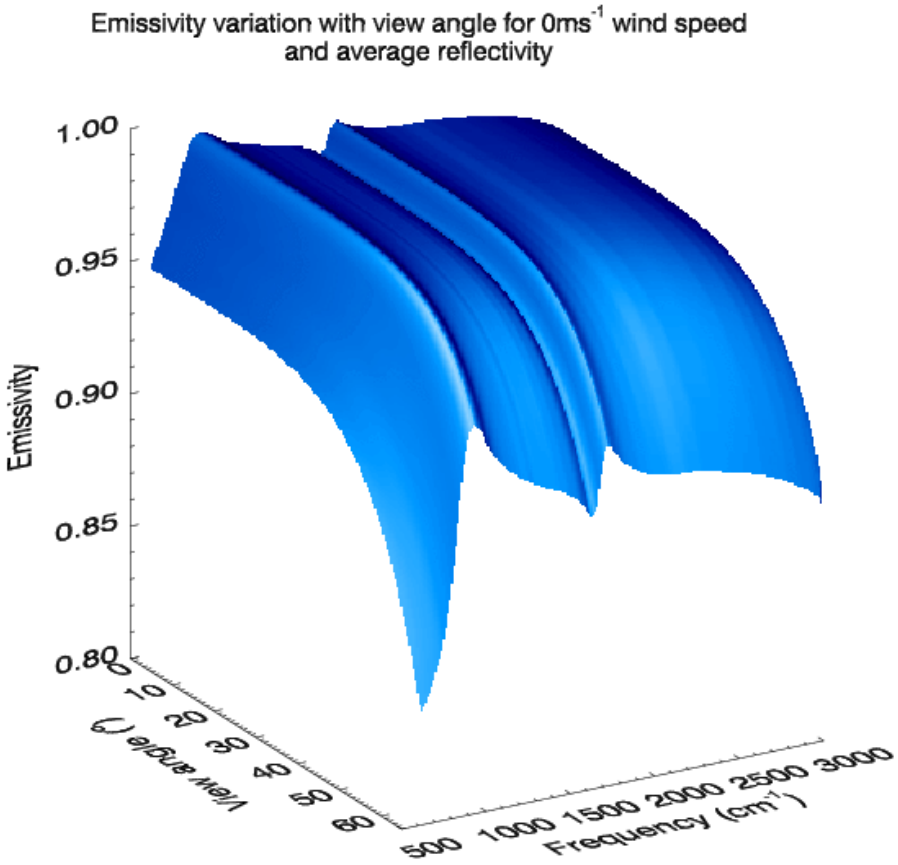

Figure 7-1: Sea Surface Emissivity

In order to get an estimate of the size of the error, in the net long-wave flux, due to neglecting the angular dependence of the emissivity, MODTRAN was run at a number of angles to obtain values for the down-welling radiation; the up-welling radiation at each angle was then calculated by using Planck's function to determine the Earth's blackbody radiation, and the approach detailed in the attached appendix to estimate the surface emissivity and thus the reflectance. The values at each angle were integrated to give the total flux H (see equation below, where L is the down-welling radiation).

.

$$H = -\iint L \sin\theta \cos\theta d\phi d\theta + \iint (1-\varepsilon(\theta)) L \sin\theta \cos\theta d\phi d\theta + \iint \varepsilon(\theta) B(T) \sin\theta \cos\theta d\phi d\theta$$

Emissivity was treated in two different ways: an angular dependent emissivity, as in the equation above, and a hemispherically averaged emissivity that could be pulled out of the integral.

D43762, A. PDMO Released: 2009-09-28 (VERIFY REVISION STATUS)
PDMO

The results can be found in Table 7-1, and can be summarized as follows: neglecting the angular dependence of emissivity leads to underestimation in the total flux over the five bands investigated ranging from 0.5 to 1.5 W/m^2. While these bands are the major contributors to the total flux (approximately 90% of the total flux), there are contributions from other bands, especially in the sub-arctic winter profile, which could add a 0.2 W/m^2 error.

Table 7-1 – LW Fluxes Calculated with Hemispherically Varying Emissivity (No Averaging) and a Hemispherically Averaged Emissivity

	TRO			MLS			SAW		
Band (cm-1)	No average	Hem. averaged	Error	No average	Hem. averaged	Error	No average	Hem. averaged	Error
700-820	5.73	5.52	0.21	8.57	8.28	0.30	12.38	12.17	0.21
820-980	21.50	21.02	0.48	27.92	27.38	0.54	25.36	25.17	0.19
980-1080	13.57	13.27	0.29	14.47	14.19	0.27	9.14	9.04	0.10
1080-1180	11.53	11.29	0.24	12.53	12.31	0.22	7.97	7.89	0.08
1180-1390	5.22	5.10	0.13	5.94	5.80	0.13	4.87	4.79	0.08
Total	57.55	56.20	1.35	69.42	67.96	1.46	59.72	59.07	0.65

In conclusion, using a hemispherically averaged sea surface emissivity will slightly (~2%) underestimate the net long-wave surface flux. This suggests that a slightly better value would be 1.02 times the hemispherically averaged value.

The next question is the determination of a reasonable single value for the longwave sea surface emissivity, for use in modeling efforts that do not want to explicitly include spectral and wind speed dependence. The hemispherically averaged emissivities calculated for Table 7-1 were weighted by the RRTM bandwidths to yield spectrally averaged emissivities at six different wind speeds. Once again only the five principal bands were considered. Table 7-2 shows that the average emissivity increases slightly with increasing wind speed. The effective emissivity in the table is 1.02 times the averaged value.

Table 7-2 – Hemispherically and Spectrally Averaged Emissivities as a Function of Wind Speed

Wind speed (m/s)	Averaged-Emissivity	Effective Emissivity
0	0.943	0.962
1	0.945	0.964
3	0.948	0.967
5	0.950	0.969
10	0.954	0.973
15	0.957	0.976

D43762, A. PDMO Released: 2009-09-28 (VERIFY REVISION STATUS)
PDMO

Examination of Table 7-2 indicates that the often cited value of 0.97 for sea surface emissivity is very close to emissivity for an average oceanic wind speed of ~7 m/s. Thus, 0.97 is a good value if a fixed wind-speed-independent emissivity value is used.

A modest variation of ~ 0.1 over a wind speed range of 10 m/s is observed (this corresponds to about10 W/m^2). It is estaimted that this contributes an root mean squared error of ~ 4 W/m^2. A future improvement could incorporate a windspeed dependence to the effective emissivity determination.

We note that for wind speeds above ~15 m/s, the effects of foam should also be considered.

The emissivity calculations were performed as described next.

Define:

θ_n = zenith angle of the normal to a facet of the sea surface

θ_e = zenith angle of emitted radiance

φ = azimuthal angle of the normal to a facet

η = complex refractive index of sea water = f(λ)

w = surface wind (m/s)

ρ = reflectivity of the sea surface

X = zenith angle of incidence or reflection relative to the facet normal

X' = angle of refraction

Fresnel formulas for the reflectivity of polarized waves:

$$\rho_{\text{II}} = \frac{\eta \cos \text{X} - \cos \text{X}'}{\eta \cos \text{X} + \cos \text{X}'} \qquad \textbf{Equation A-1}$$

$$\rho_{\perp} = \frac{\cos \text{X} - \eta \cos \text{X}'}{\cos \text{X} + \eta \cos \text{X}'} \qquad \textbf{Equation A-2}$$

$$\sin \text{X}' = \frac{(\sin \text{X})}{\eta} \qquad \textbf{Equation A-3}$$

Given that most infrared sensors are unpolarized, a total reflectivity can be defined:

$$\rho(\eta, \text{X}) = \frac{\left|\rho_{\text{II}}\right|^2 + \left|\rho_{\perp}\right|^2}{2} \qquad \textbf{Equation A-4}$$

From conservation of energy and Kirchoff's law:

$$\varepsilon(\eta, \text{X}) = 1 - \rho(\eta, \text{X}) \qquad \textbf{Equation A-5}$$

D43762, A. PDMO Released: 2009-09-28 (VERIFY REVISION STATUS)
PDMO

From spherical trigonometry:

$$\cos \mathrm{X} = \cos\theta_e \cos\theta_\eta + \sin\theta_e \sin\theta_\eta \cos\varphi$$
$$= \mu_e \mu_\eta + \left(1-\mu_e^2\right)^{\frac{1}{2}} \left(1-\mu_\eta^2\right)^{\frac{1}{2}} \cos\phi \qquad \textbf{Equation A-6}$$

Cox and Munk (1954) found that the facet slope distribution of the rough sea surface was approximately normal and isotropic, with a variance linearly proportional to the wind speed:

$$2\sigma^2 = 0.003 + 0.00512w \qquad \textbf{Equation A-7}$$

Following Masuda et al (1988) the mean emissivity for a given wavelength and direction can be found by integrating the contributions in that direction from all the normally distributed facets:

$$\overline{\varepsilon'}(\eta, \mu_e) = \frac{1}{\pi\sigma^2\mu_e} \int_0^1 \int_0^\pi \varepsilon(\eta, \mathrm{X}) \cos \mathrm{X} \quad e^{-\left(\frac{\tan^2\theta_\eta}{2\sigma^2}\right)} \mu_\eta^{-4} d\varphi d\mu_\eta, \quad when \quad \cos \mathrm{X} > 0$$

Equation A-8

Wave shadowing is taken into account by normalizing the equation above by the same integral evaluated for ε(η,X) = 1 :

$$\Sigma = \frac{1}{\pi\sigma\mu_e} \int_0^1 \int_0^\pi \cos \mathrm{X} \quad e^{-\left(\frac{\tan^2\theta_\eta}{2\sigma^2}\right)} \mu_\eta^{-4} d\varphi d\mu_\eta, \quad when \quad \cos \mathrm{X} > 0 \qquad \textbf{Equation A-9}$$

Thus we obtain:

$$\bar{\varepsilon} = \frac{\overline{\varepsilon'}}{\Sigma} \qquad \textbf{Equation A-10}$$

The integrals above were carried out using the DTWODQ IMSL routine, which uses a globally adaptive scheme to reduce the absolute error.

Wu and Smith (1997) show that the lower limit of the first integral can be set to μ_n^*

$$Note: \int_0^1 .....d\mu_n \sim \int_{\mu_n^*}^1 .....d\mu_n, \quad when \quad \mu_n^* = \left(1 - 2\sigma^2 \ln\delta\right)^{-\frac{1}{2}}$$

where δ is the required accuracy. This can considerably reduce the time required for integration.

D43762, A. PDMO Released: 2009-09-28 (VERIFY REVISION STATUS)
PDMO

In order to take into account the reflection of emitted radiation by the sea surface, which enhances the emissivity, $\varepsilon(\eta,X)$ in the integrals above needs to be replaced by:

$$\tilde{\varepsilon}(\eta, X) = \varepsilon(\eta, X) + [1 - \varepsilon(\eta, X)]P(\theta_\eta)\bar{\varepsilon}(\eta, \mu_r) \qquad \textbf{Equation A-11}$$

where $P(\theta_r)$ is the probability that the radiance arriving at a given point originated from the sea surface instead of the sky, given by:

$$P(\theta_r) = \begin{cases} 1, & \theta_r \geq 90° \\ 1 - (\theta_r - 85°)/25, & 85° \leq \theta_r \leq 90° \\ 0, & \theta_r \leq 85° \end{cases}$$

and θ_r is the zenith angle of the reflected radiance at that point, given by:

$$\cos\theta_r = 2\cos X - \cos\theta_e$$

Use of the expression for the emissivity with reflected emission (Equation A-11) entails a quadruple integral. This is very difficult to do numerically. Thus the integrals in Equations A-8 and A-9 were carried out for 951 angles, with emissivity given by Equation A-5. Then the resulting emissivity values were fit as a function of angles by a cubic spline (IMSL routine CSINT). The integrals were next recalculated for 11 selected view angles, ranging from 0° to 85°, using the emissivity given by Equation A-11, where $\varepsilon(\eta,\mu_r)$ was obtained from the cubic spline fit.

D43762, A. PDMO Released: 2009-09-28 (VERIFY REVISION STATUS)
PDMO

8. Appendix B – Construction of Net Heat Flux Horizontal Cells (HCs)

The VIIRS input data products SST and aerosols are assumed provided on the medium resolution sensor grid. This is illustrated in Figure B-1.

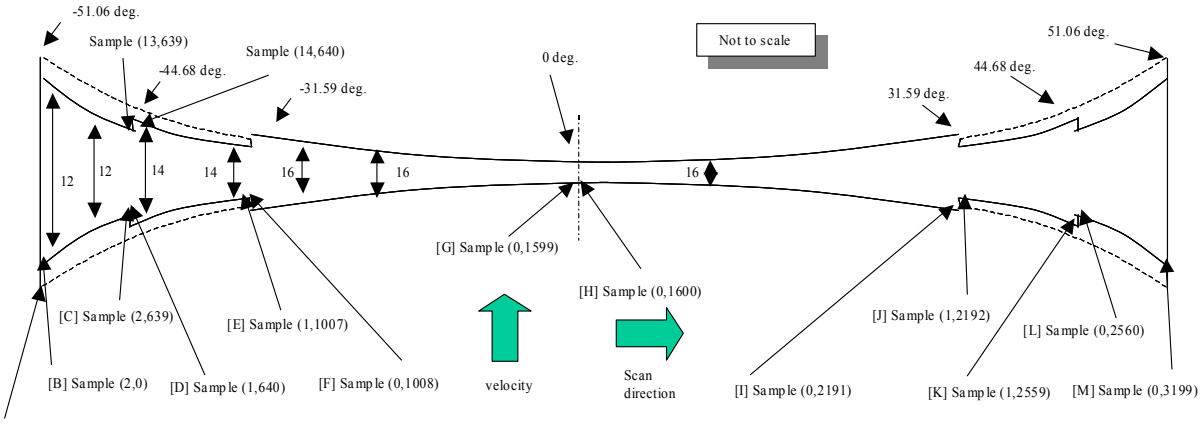

Figure B-1 – VIIRS scan geometry with bow-tie pixel deletion indicated

The Net Heat Flux EDR has a horizontal cell size requirement of 20 km, a worst-case value across the VIIRS scan. A detailed explanation of the scheme used for aggregating scan sensor data into horizontal cells can be found in the VIIRS Cloud Cover/Layers (CC/L) ATBD, Version 1.6 (AER Document #: P1187-TR-I-006). See section 2.5: Retrieval Strategy – Horizontal Cells.

Net Heat Flux produces aggregated data of nominally 12 km instead of the 6 km used by CC/L. The plots shown here are updated for the net heat flux aggregation of horizontal cells.

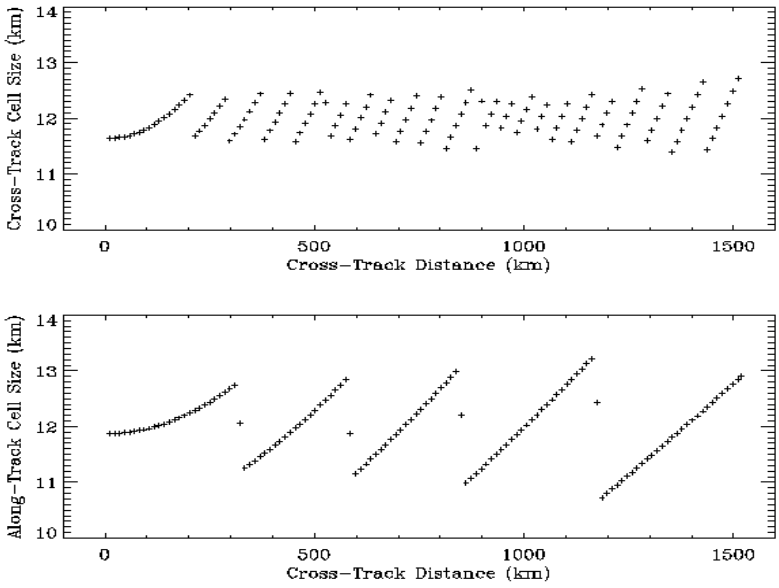

Figure B-2 – Horizintal cell size for Net Heat Flux EDR as function of distance from nadir along scan. Top plot is cross-track and bottom is along-track dimension.

D43762, A. PDMO Released: 2009-09-28 (VERIFY REVISION STATUS)
PDMO

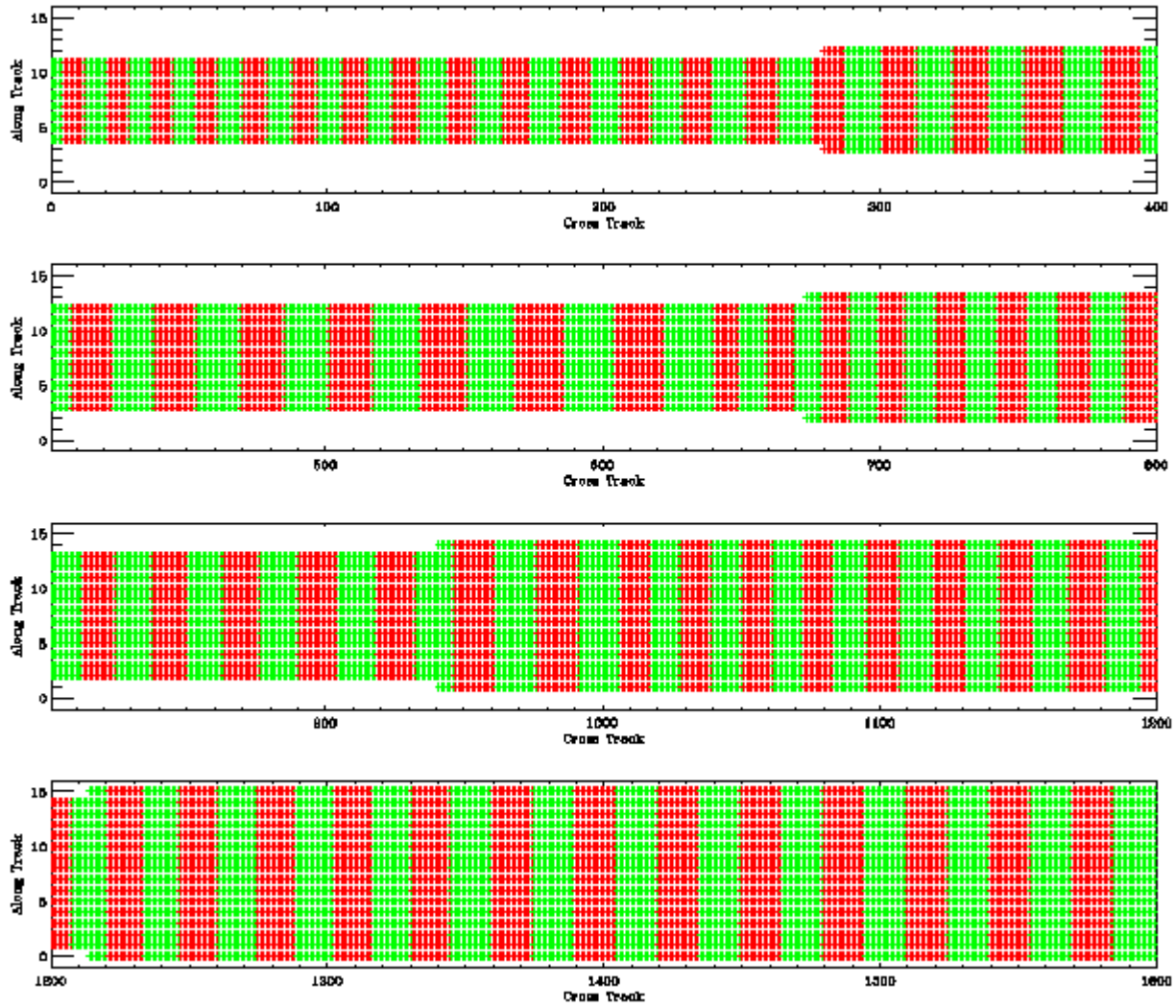

Figure B-3 – Illustration of horizontal cells for Net Heat Flux. Note: Cells are actually nearly square; the rectangular appearance is a plotting artifact.

D43762, A. PDMO Released: 2009-09-28 (VERIFY REVISION STATUS)
PDMO